The University of
Nottingham

RADIONUCLIDE TRANSPORT AT THE GEOSPHERE-BIOSPHERE INTERFACE- A COMBINED MEASUREMENTS AND MODELLING STUDY

by

Talal Waddah Mahayni
B.Sc., M.Sc.

Thesis submitted to the University of Nottingham for the degree of Doctor of Philosophy in Environmental Sciences

January 2012

The University of Nottingham

Ethos – Thesis for digitisation

Redactions

Thesis details:

Title: Radionuclide transport at the geosphere-biosphere interface: a combined measurements and modelling study.

Author: Mahaini, Talal Waddah

(Please note the spelling of Mahaini)

Please exclude the following sections/pages:

Page 12 Fig 2.1

Map of soil sampling area at Sutton Bonington

Dedication

سنوات من الجهد و العمل

لحظات من اليأس والأمل

والدي الغالي، إلى روحك

Years of hard work

Moments of desperation and hope

My beloved father, to you

Acknowledgements

I would like to thank my supervisors Dr. Elizabeth Bailey, Prof. George Shaw and Prof. Neil Crout for their guidance, support and patience throughout my PhD study and beyond. Thanks are due to Dr. Scott Young for his academic advice, John Corrie and Darren Hepworth for their technical assistance, Sue Grainger and Emma Hooley for their administrative assistance. I would like also to thank my colleagues in the division, in particular Ezzat Marzouk, who have always helped and supported me during the PhD hardships. In terms of non-academic support, I would like to thank Osama Chahrour for his nice companionship and useful advice (at times!). My gratitude is to my beloved mother for her sincere supplication, boundless support and encouragement at all times.

I would like to gratefully acknowledge the support of the Atomic Energy Commission of Syria and Director General Prof. Ibrahim Othman for providing the financial support during the course of this study.

Contents

List of Figures

List of Tables

List of Symbols

a	=	Suspended solid load in water (kg m^{-3})
α_L	=	Longitudinal dispersivity of the soil (m)
A	=	van Genuchten's scaling and curvature parameters
B_i	=	Soil pore size distribution index (m^{-1})
b_1	=	Empirical parameter (-)
b_2	=	Empirical parameter (-)
B	=	Dimensionless adjustable parameter (-)
$C_{porewater}$	=	Concentration in porewater (kg m^{-1})
C_{soil}	=	Total concentration in soil (solid + porewater) (kg kg^{-1} soil)
CR	=	Soil-to-plant concentration ratio (Bq kg^{-1} dw plant)/(Bq kg^{-1} dw soil))
D_m	=	Molecular diffusion (m^2 day^{-1})
D_{num}	=	Numerical dispersion (m^2 day^{-1})
D_w	=	Distance from the water table towards surface (m)
ΔH_r^0	=	Reaction standard enthalpy change (kJ mol^{-1})
δ	=	Water use distribution parameter (-)
E_h	=	Redox potential relative to a reference hydrogen electrode (volts)
E_a	=	Total actual evaporation rate (m day^{-1})
$E_{a,i}$	=	Maximum, actual evaporation rate from the i^{th} layer (m day^{-1})
E_p	=	Total potential evaporation rate (m day^{-1})
$E_{p,i}$	=	Potential evaporation rate from the i^{th} layer (m day^{-1})
ε_i	=	Porosity of the i^{th} layer (-)
F	=	Faraday constant (kJ $volt^{-1}$ mol^{-1})
$F_{i,j}$	=	Water flux (liquid phase transport) from the i^{th} layer to j^{th} receptor layer (m day^{-1})
G_i	=	Capillary flux in the i^{th} layer (m day^{-1})
G_{max}	=	Maximum capillary flux (m day^{-1})
h_1, h_2, h_3, h_4	=	Parameters for Feddes water stress reduction function (m)

$h(\theta)$	=	Soil matric potential (m)
$K_{d,i}$	=	Solid-liquid distribution coefficient (L kg^{-1})
K_{eq}	=	Equilibrium constant
K_s	=	Soil saturated hydraulic conductivity (m day^{-1})
K^0_{SO}	=	Solubility product at T = 298.15 °K
K_{SO}	=	Solubility product at T °K
$K(\theta_i)$	=	Soil hydraulic conductivity as a function of water content (m day^{-1})
κb	=	An extinction coefficient of radiation by the canopy (-)
ℓ	=	Pore connectivity parameter
LAI	=	Leaf area index (-)
$\lambda_{i,j}$	=	Transfer rate constant between the i^{th} and j^{th} layers (m^{-1})
$\lambda^k_{i,j}$	=	Transfer rate constant between the i^{th} and j^{th} for process k (m^{-1})
λ_N	=	Decay constant of radionuclide N (day^{-1})
m	=	van Genuchten's parameter
$M_{i,j}$	=	Soil flux from the i^{th} layer to j^{th} layer (kg m^{-3})
n	=	van Genuchten's curvature parameter
N_i	=	Activity of radionuclide N in the i^{th} soil layer (Bq)
ω_c	=	Critical stress index
pe	=	Electron activity (-)
$u^E_{f,i}$	=	Evaporation fraction from the i^{th} layer (-)
$u^T_{f,i}$	=	Transpiration fraction from the i^{th} layer (-)
R	=	Gas constant (J $°K^{-1}$ mol^{-1})
R_i	=	Retardation factor of N radionuclide in the i^{th} layer (-)
ρ	=	Soil bulk density (kg m^{-3})
S_e	=	Soil effective saturation
$S_i(t)$	=	External source term of radionuclide N into the i^{th} layer (Bq day^{-1})
S(t,z)	=	Sink term: water removed by roots (m^3 m^{-3} day^{-1})
T	=	Absolute temperature (°K)
$T_{a,i}$	=	Maximum transpiration rate from the i^{th} layer (m day^{-1})
T_p	=	Total potential transpiration rate (m day^{-1})

$T_{p,i}$	=	Potential transpiration from the i^{th} layer (m day^{-1})
$\frac{\Delta\theta_i}{\Delta t}$	=	Rate of change in moisture content in the i^{th} layer ($m^3\ m^{-3}\ day^{-1}$)
θ_i	=	Volumetric moisture content in the i^{th} layer ($m^3\ m^{-3}$)
$\theta_{critical}$	=	Threshold to initiate capillary flux ($m^3\ m^{-3}$)
θ_{FC}	=	Soil field capacity ($m^3\ m^{-3}$)
θ_r	=	Soil residual moisture ($m^3 m^{-3}$)
θ_s	=	Soil saturated moisture ($m^3 m^{-3}$)
θ_{steady}	=	Steady moisture assumed at G_{max} ($m^3\ m^{-3}$)
θ_{wp}	=	Soil wilting point ($m^3 m^{-3}$)
V	=	Soil volume (m^3)
Δz_i	=	Soil layer thickness (m)
z_{i-1}, z_i	=	Depths of the i^{th} layer boundaries from soil surface (m)
z_r	=	Rooting depth (m)
z_L	=	Total soil depth (m)

Abstract

The aim of the present work was to improve the predictive capabilities of current modelling methods used to assess the long-term biosphere impacts of underground repositories for radioactive wastes. A number of issues related to parameter and conceptual uncertainties associated with compartmental biosphere models that simulate transport and accumulation of radionuclides in soils were addressed.

The structure of compartmental models used for radiological risk assessments has not evolved noticeably over the past few decades and most of these models rely on simple assumptions. For example, compartmental models used to predict activity concentrations of radionuclides released into soils over very long timescales (typical of the lifetime of underground disposal repositories) assume arbitrary model specifications such as soil layer thickness (the vertical discretisation of the soil column) and length of the time step. Moreover, the majority of the available models assume invariant sorption characteristics of radionuclides with soil depth and hence employ constant solid-liquid distribution coefficient (K_d) values regardless of soil characteristics known to affect radionuclide sorption (e.g. pH, redox potential, moisture content and organic matter). The empirical K_d has a profound effect on long-term predictions of radionuclide behaviour in soil since it determines the degree of radionuclide retardation due to interaction with the soil. It is associated with considerable uncertainty due to differences in experimental conditions and methods used for its measurement and the variation in soil characteristics.

In this study, three soil types (arable, grassland and woodland) were incubated under anaerobic conditions and the behaviour of naturally occurring selenium, iodine, rhenium and uranium, expressed as K_d, was investigated.

The results indicate that variation in soil characteristics (e.g. moisture content, pH, mineral and organic carbon content) is a significant source of K_d variability. Soils relatively higher in organic matter content (e.g. top soils) have higher sorptive capacities for trace elements than mineral subsoils and hence higher K_ds. Dynamic, complex behaviour of K_d under flooded, anaerobic soil condtions was measured over a 3 week period in soil microcosms. This dynamic behaviour was driven by the shift in soil redox potential which was associated with solubilisation of soil organic and mineral (Fe oxide) phases. Overall, the maximum observed variation in K_d over the entire incubation period did not exceed 2 orders of magnitude.

Biosphere models were constructed which combined a physically-based water flow model and the compartmental approach and used to simulate the long-term vertical distribution of radionuclides in the soil as well as radionuclide dynamics under different environmental conditions. Investigating radionuclide dynamics on a short timescale could only be achieved using models with a daily time step since short-term variation was obscured by a longer (annual) time step. Simulation results give insights into some of the limitations of available biosphere modelling methods for radiological risk assessment that are often overlooked. For example, soil radionuclide activity concentrations calculated using compartmental models are sensitive to the vertical discretisation (i.e. thickness of soil layers into which the soil column is divided) and time step of the model, hence the structure of the model should not be set arbitrarily. The discretisation procedure proposed in the present study may provide a useful framework to select the appropriate structure of biosphere assessment models. With respect to the effect of uncertainy in K_d on model calculations, the results show that equilibrium timescales and radionuclide activity concentrations in the soil at equilibrium increase as the K_d increases. For example, the time to reach steady state radionuclide activity concentrations in the vegetated topsoil increased 14-fold and 7-fold, respectively, when K_d was increased 28-fold, which is a small variation compared to the uncertainty of K_d commonly reported in the literature (e.g. a few orders of magnitude). The K_d also affects short and long-term radionuclide dynamics in soils; the activity concentration of a radionuclide with low K_d (weakly sorbing) is more responsive to seasonal fluctuations in climatic and hydrological conditions than a radionuclide with a large K_d (strongly sorbing). Radionuclide uptake by plant roots, especially those which access highly contaminated soil layers adjacent to the contaminated aquifer, could

be an important mechanism that provides a direct pathway between shallow, contaminated aquifers and the soil surface where elavated contamination poses greater risks.

Chapter 1 Introduction

1.1. Radioactive waste legacy

The world has exploited nuclear power for a variety of civil and military applications; nuclear power plants generating electricity have been in operation over the last six decades. Although the production of electricity from nuclear fuel does not involve emission of greenhouse gases such as carbon dioxide to the environment, this "clean" electricity comes at a price. A legacy of hazardous long-lived radioactive waste of all forms (low, intermediate and high levels) has accumulated. According to the latest report of the Nuclear Decommissioning Authority on radioactive waste in the UK, the total volume of radioactive waste from all sources is 4,720,000 m^3. Of this volume, low level waste (LLW), intermediate level waste (ILW) and high level waste (HLW) make up 93.8%, 6.1% and less than 0.1%, respectively (NDA, 2011).

Some of this waste is already in storage. The decommissioning of old power stations, however, will generate more waste over several decades. A significant part of this waste will have decayed naturally within a few hundred years. Nevertheless, it is important to have a long-term approach to the management of long-lived fission products (e.g. ^{14}C, ^{79}Se, ^{99}Tc, and ^{129}I) given the number of human generations over which these materials can remain hazardous.

1.1.1. Geological disposal approach

Nuclear industries and regulatory bodies around the globe have been seeking solutions to the problem of long-term management of radioactive waste. The desired solution should provide long-term protection of both the environment and the public against the risks of any potential releases of radioactivity into the environment accessible by biota. Many options have been considered and assessed and deep geological disposal is generally considered the best available solution to this long-term management problem: many countries have initiated their national R&D programmes on deep geological disposal of radioactive wastes (SKB, 2010; Posiva, 2010).

Site selection is an important aspect of deep geological disposal whereby candidate sites are assessed to establish their suitability for hosting the repository. A successful site has to provide sufficient isolation of the waste against natural transport processes and also any major natural events (including earthquakes and glacial activity) as well as anthropogenic intrusion.

1.1.2. Long-term radiological risks

Given the long timescales over which deep geological disposal must remain effective there is potential for some release of fission products from the repository system. The waste continues to decay naturally and to produce thermal energy which, combined with the chemical environment of a repository, will induce degradation of waste canisters. Long-lived fission products are thus expected to escape the repository system. Escaping radionuclides will be transported by groundwater through the repository barriers into the surrounding geosphere. Ultimately, radionuclides may reach biosphere systems, including lakes, rivers,

forests and agricultural land. Low lying points on the landscape (e.g. riparian zones) are the probable discharge points for radionuclides migrating to the earth's surface (Marklund et al., 2006). Once these radionuclides reach the surface, they will become accessible to biota including crops, livestock and humans.

1.2. Overview of some safety-relevant radionuclides

It is therefore important to understand the biogeochemistry of long-lived radionuclides to identify key accumulation, immobilisation and remobilisation mechanisms. The sub-soil is a heterogeneous environment, with physical and biogeochemical characteristics that vary spatially as well as temporally. These characteristics determine to a large extent the behaviour of radionuclides in the sub-soil. The following three sub-sections provide a brief review of the geochemistry of three elements that have long-lived radionuclides and that, due to their chemical characteristics, will contribute significantly to long-term radiological doses from a geological repository.

1.2.1. Iodine

Iodine (I) is mainly found in nature as stable ^{127}I. Of its several radioactive isotopes, it is ^{129}I with a physical half-life of 15.6 million years (Santschi and Schwehr, 2004) that has received considerable attention as a long-lived radioactive hazard (Hou et al., 2009; Hu et al., 2008). Most ^{129}I comes from anthropogenic sources including nuclear weapons testing, ^{235}U fission in nuclear reactors (with a yield of 1%) and high level waste (spent nuclear fuel), responsible for the majority of the global inventory of ^{129}I. A small amount of ^{129}I is produced naturally in the

upper atmosphere by cosmic spallation of trace quantities of xenon (John et al., 2007).

Biogeochemical cycling of I in the subsurface environment is complicated by its chemical speciation; it can exist in multiple oxidation states (VII, V, I, 0 and -I) depending on the prevailing physicochemical conditions. Iodate (IO_3^-), methyl iodide (CH_3I), elemental iodine (I_2) and iodide (I^-) are the main chemical species of I in soils (Hou et al., 2009; Hou, 2004; Hou et al., 2001; Muramatsu and Yoshida, 1999). Important mechanisms pertinent to the immobilisation of I include sorption onto iron and aluminum oxides (Whitehead, 1984; Whitehead, 1974; Whitehead, 1973) and association with soil organic matter, which has been shown to be a major sink for soil I (Ashworth and Shaw, 2006b; Sheppard et al., 1995; Sheppard and Thibault, 1992). Yamaguchi et al (2010) found that I introduced into organic-rich, moist soils as inorganic IO_3^- and I^- species was transformed into organic I within 60 days. Mobilisation of I into soil solution is promoted by soil reduction, for example following soil waterlogging (Maillant et al., 2007; Ashworth and Shaw, 2006b; Ashworth and Shaw, 2006a; Muramatsu et al., 1996).

1.2.2. Selenium

Selenium (Se) is a non-metallic element that has several stable as well as radioactive isotopes. Of the radioactive Se isotopes, only ^{79}Se warrants concern from a radiological risk perspective due to its long physical half-life (3.77×10^5 years) (Shaw and Ashworth, 2006). ^{79}Se is produced from ^{235}U fission in nuclear reactors with a yield of about 0.04%, and it is also present in spent nuclear fuel.

Selenium is a multivalent element (VI, IV, 0 and -II) whose behaviour is strongly influenced by its redox state. In aerobic environments (~E_h = 400 mV) Se is present predominantly as soluble inorganic oxyanions (selenate SeO_4^{2-} and selenite SeO_3^{2-}) under a wide range of pH values. As soil conditions become more reducing ($E_h \leq 200$ mV), oxidised Se species are transformed into insoluble elemental Se and selenide Se^{-2} (Séby et al., 1998).

Selenium removal from soil pore water is strongly governed by its interactions with soil components. Sorption, which involves a group of mechanisms that controls solid-liquid distribution of Se in soils, depends largely on the chemical speciation of Se. Selenate has a low affinity for soil solids such as metal (Mn, Fe and Al) oxides compared to SeO_3^{2-} which can be retained by these minerals by forming inner-sphere complexes (Dhillon and Dhillon, 2000; Balistrieri and Chao, 1990; Bar-Yosef and Meek, 1987). Complexation with soil organic matter is another important retention mechanism for Se in soil (Wang and Gao, 2001; Gustafsson and Johnsson, 1994). Selenium oxyanions can be biologically reduced and incorporated into soil organic matter, especially into the low-molecular-weight fractions of the humic substances (Gustafsson and Johnsson, 1994). This mechanism, however, is not yet well understood.

1.2.3. Technetium

As an element with no stable isotopes, technetium (Tc) is considered to be extinct on earth but can be found in the environment primarily as a fission product originating in the nuclear fuel cycle. Technetium possesses several radioactive isotopes but, of these, only ^{97}Tc, ^{98}Tc and ^{99}Tc have sufficiently long half lives to represent a long-term radiological risk (their physical half-lives are: 2.6×10^6,

4.2×10^6 and 2.1×10^5, years, respectively). However, with a fission yield of 6% only ^{99}Tc is produced in sufficient quantities to be of concern (John et al., 2007).

Technetium has a range of valencies; VII, IV, III, II and 0, with VII and IV being the most important. Technetium behaviour in the environment is closely correlated with its redox behaviour. In aerated soils ($E_h > 200$ mV) speciation is dominated by Tc^{VII} in the form of TcO_4^- (pertechnetate anion), which has physicochemical similarities with the nitrate (NO^{3-}) anion. Like nitrate, pertechnetate does not bind strongly to soil surfaces, thus it has a high mobility (Brookins, 1988). In anaerobic (reduced) soils, Tc^{VII} is reduced to the sparingly soluble, tetravalent, Tc^{IV} which can be strongly sorbed to soil mineral surfaces or precipitated as hydrous TcO_2 depending on its concentration (Icenhower et al., 2010; Morris et al., 2008).

As there are no naturally occurring surrogates for all chemical species of Tc, rhenium (Re) has been proposed as a non-radioactive analogue (Kim et al., 2004; Kim and Boulègue, 2003). Technetium and Re are similar in many respects; they have similar oxidation states (e.g. VII and IV) and they both form oxyanions (TcO_4^- and ReO_4^-) in their VII oxidation state. However, whether or not Re is an appropriate non-radioactive surrogate of Tc remains a controversial question (Maset et al., 2006; Wharton et al., 2000).

1.2.4. Uranium

Uranium (U) exists in nature in the form of several isotopes with different abundance primarily ^{238}U (99.27%), ^{235}U (0.72%) and a very small amount (by mass) of ^{234}U (0.0055%). Other U isotopes are not present naturally (^{236}U, ^{233}U and ^{232}U) but can be produced by nuclear transformations. The most abundant U isotope,

^{238}U, has a very long physical half-life of 4.5 billion years (John et al., 2007). Uranium occurs in nature in various oxidation states, although hexa- and tetravalent U are the most environmentally significant species. Uranium mobility and sorption onto soils in the subsurface is very much dependent upon its speciation. In aerated ($E_h < 200$ mV), acidic (pH < 5) soils, $U^{(VI)}$ as uranyl ion (UO_2^{2+}), is the dominant species that can adsorb onto soil fractions such as clays (Pabalan and Turner, 1996) and oxides (Vandenhove et al., 2007; Um et al., 2007). At higher pH (≤ 7) U sorption decreases as UO_2^{2+} hydrolyses to form soluble hydroxide complexes. Under alkaline conditions U becomes more mobile as it can be complexed by a number of inorganic (e.g. $OH^-, CO_3^{2-}, PO_4^{3-}$) and organic (humic acids) ligands (Vandenhove et al., 2009a; Luo and Gu, 2009; Um et al., 2007; Bednar et al., 2007; Echevarria et al., 2001; Langmuir, 1978). Under reducing conditions $U^{(VI)}$ can be reduced into the less mobile $U^{(IV)}$ species that binds strongly to soil surfaces.

1.3. Modelling radionuclide migration in terrestrial ecosystems

1.3.1. Biosphere models

As part of performance assessment calculations, the safe operation of geological repositories has to be demonstrated over long timescales of several thousand years (Xu et al., 2008; Avila, 2006a). Scenarios of the potential release of radionuclides from the repository system have to be identified and associated environmental contamination and human exposures assessed (radiological risk assessments) to ensure risks are in compliance with national and/or international standards.

Conceptual and mathematical modelling are essential parts of the assessment approach that is used to assess migration and accumulation of radionuclides following their release into surface and subsurface environments. A staged conceptual biosphere modelling methodology was developed by the IAEA (2003) as a frame of reference for biosphere modelers addressing risks from radioactive waste disposal facilities. The primary objective of this methodology was to provide a formal and defensible procedure for the development of 'reference' or 'assessment biospheres' in general. The approach begins with a description of the biosphere to be modeled; i.e. provision of sufficient detail about the systems to be considered. This information enables justification of the conceptual models of the biosphere and its subsystems and includes the important features, events and processes relevant to the assessment. A conceptual model is then constructed on the basis of the information collected during the previous stages and dependent upon the media (compartments) of interest (e.g. soil, sediment, water, plants, etc.) in which radionuclides will migrate or accumulate. The conceptual model is then translated into a mathematical model. It should be noted that there may exist many alternative mathematical models for one conceptual model depending on availability of data to parameterise the model. Finally, concentrations of radionuclides in the environmental media are calculated and used to estimate radiological doses. This methodology has been applied extensively in long-term radiological assessments (Klos, 2010; Klos, 2008; Karlsson et al., 2001; Bergström et al., 1999).

Despite advances in methods used to formulate and solve biosphere models, there is still considerable uncertainty associated with their results. This partially originates from the incomplete understanding of the physical and biogeochemical processes that control the behaviour of many radionuclides in the environment.

Sorption is one particular example where research is still ongoing to improve biosphere assessment results and reduce uncertainty. Sorption has an important impact on the fate of radionuclides in the biosphere and, therefore, on assessment results. Elevated sorption resulting from a combination of radionuclide, speciation and soil type, can retard and accumulate radionuclides advancing with flowing groundwater. Sorption is, however, a complex process that depends not only on the mineralogy of the soil but also on a number of (often interacting) biogeochemical factors (e.g. moisture content, redox potential, speciation, microbial activity, etc.).

Soil properties and processes controlling sorption are expected to change over the long timescales associated with radiological risk assessments and, therefore, the scenarios which biosphere modelling must address. Spatial and temporal changes to soil moisture content, soil oxidation-reduction status and budgets of soil organic matter are among the processes that may lead to mobilisation or immobilisation of radionuclides in the biosphere. Although radionuclide sorption strongly correlates with soil physicochemical variables, it has, however, been represented in biosphere models in a rather simplistic way that often uses a equilibrium K_d (e.g. Klos, 2008; Agüero et al., 2008).

1.3.2. The K_d parameter

Radionuclide sorption is frequently quantified using an empirical solid-liquid distribution coefficient (K_d) which is often determined empirically. Physicochemical variables are usually strictly controlled during a laboratory experiment or, at most, one variable is adjusted at a time. This is impossible under normal environmental conditions in which interacting physical and biogeochemical factors collectively control radionuclide sorption behaviour. For example, empirical determination of K_d

(e.g. in batch experiments) involves equilibrating tracer-free solid and tracer-spiked liquid phases for a pre-determined period before calculating K_d as the ratio of radionuclide activity concentrations in the solid and liquid phases. Often, the ratio of mass of solid to volume of liquid (solid-liquid ratio, SLR) used in these experimental protocols is small (~0.1 w/w). This supersaturated soil slurry is not representative of the unsaturated conditions prevailing within the vadose zone (i.e. above the water table). The SLR has a known impact on K_d which Sheppard et al. (2007) demonstrated by incubating soil samples at different SLRs and found that K_ds of a number of trace elements decreased as SLR increased. These authors attributed this impact to the dilution resulting from using excess water and they recommended K_d measurements should be made at moisture contents close to the soil's field capacity since that is when leaching occurs. Chemical speciation of radionuclides is also affected by artificially low SLR: at low SLRs, soil E_h can be lowered which affects chemical speciation and consequently K_d values.

Differences in experimental conditions have resulted in a great deal of uncertainty in data bases of empirical K_d available for biosphere modelers (IAEA, 2009). Thus, an alternative statistical approach has been proposed to estimate K_d based on correlating K_d with soil physical and chemical characteristics (Sheppard, 2011; Vandenhove et al., 2007). Soil properties including texture, organic matter content and pH are proposed as predictors of K_d which can be easily measured. Such statistical models can be used to predict site-specific K_d values for biosphere assessment models and, by adjusting predictor variables over realistic ranges, the evolution of K_d can be explored under simulated future biosphere scenarios.

1.4. Project objectives and thesis outline

The overall purpose of this thesis was to develop a reliable modelling methodology to improve the prediction of long-term transport and accumulation of safety-relevant radionuclides in soils. Given the importance of K_d as a key parameter in almost all biosphere models, the thesis also explores the relationship between K_d and soil properties with the intention that the modelling methodology can be readily applied to different environmental settings using readily available site-specific soil properties.

The thesis is organised into six chapters. Experimental methods used, such as the set-up of the anaerobic incubation (microcosms) and the environmental analyses, are described in Chapter 2. Chapter 3 examines the effect of variation in experimental design, particularly the microcosm design and the soil solution extraction method, on *in-situ* K_d. Soil physicochemical factors that control *in-situ* K_d are also investigated and a set of Se, I, Re and U parametric K_d models are developed and validated using the experimental observations. The development of a modelling methodology for predicting the transport and accumulation of radionuclides in soils is presented in Chapter 4. This methodology is then applied to a set of hypothetical scenarios, the simulation results from which are presented in Chapter 5. The final chapter summarises the conclusions of the work and makes recommendations for future research.

Chapter 2 Experimental materials and methods

This chapter describes materials and experimental methods employed throughout this work. Standard laboratory procedures for soil and aqueous phase characterisation, in addition to experimental designs for soil anaerobic incubation, are presented.

2.1. Study area and soil sampling

Soil samples were collected from Sutton Bonington, Leicestershire, East Midlands (Fig. 2-1).

Fig. 2-1 Map of Sutton Bonington area (Grid Reference 52° 49′ 49″ N-1° 14′ 26″ W), Leicestershire showing soil sampling locations (•).

The site consists of arable land on sandy loam soil, surrounded by a strip of permanent grassland, adjacent to established woodland. The differing land uses influence the soil properties e.g. pH and organic matter content. Samples were taken at a range of depths using a 10 cm diameter auger at 10 cm increments (to minimise cross contamination between depth samples) and placed in suitably labeled plastic bags for return to the laboratory.

2.1.1. Particle size distribution

Soil texture (i.e. percentage of clay, silt and sand) was determined using a laser diffraction analyser (Beckman Coulter®). A sample (0.5 g) of < 2 mm sieved, air dried soil was added to a 50 ml polycarbonate centrifuge tube, then 25 ml of hydrogen peroxide (H_2O_2) was added and left to react overnight. To ensure all organic matter had been removed the centrifuge tube was heated at 60°C in a water bath for 1–1.5 hours and then at 90°C for an additional 1–1.5 hours. De-ionised water (25 mL) was added to each tube prior to centrifugation at 3500 rpm for 4 minutes. The solution was then decanted before an additional 35 mL of de-ionised water was added prior to shaking and centrifugation at 3500 rpm for a further four minutes. The solution was again decanted and 25 mL of 'Calgon' (35 g of sodium hexametaphosphate, 7 g sodium carbonate in 1 L of de-ionised water) was added prior to analysis. Samples were kept on a shaker until 30 minutes before analysis when they were placed in an ultrasonic bath to ensure all soil particles were fully disaggregated prior to measurement.

2.1.2. pH

Approx. 5 g of < 2 mm sieved soil was weighed into a 50 mL centrifuge tube to which 12.5 mL de-ionised water was added (1:2.5 soil/water ratio). Soil slurries were equilibrated for 30 minutes by shaking on an end-over-end shaker before pH was measured using a glass electrode and pH meter (Radiometer Copenhagen ABU 80 Autoburette) calibrated with pH 4.01 and 7.0 buffers.

2.1.3. Oxidation-reduction potential (E_h)

Soil redox potentials characterise the soil system with respect to prevailing oxidation-reduction conditions and provide ancillary information that assists in the interpretation of the geochemical behaviour of redox sensitive elements. A practical method for monitoring redox conditions involves using *in-situ* platinum electrodes which can be left in soil for the duration of experiments lasting from days to months. Platinum electrodes were constructed and calibrated in the laboratory. A 1 cm length of platinum wire (99.95%) was connected to a copper wire with a crimp connector and sealed with epoxy resin. In order to determine the standard potential of a reference Ag/AgCl electrode in combination with the Pt electrode, the system was calibrated using standard solutions of hydroquinone and pH buffers (4.01 and 7.0) with known standard potentials.

Soil redox measurements were made by inserting the Pt and reference electrodes into the soil and connecting them to a high impedance multimeter. After allowing time for equilibration (approx 10-15 mins), the voltage was recorded and corrected to give the redox potential relative to the standard hydrogen electrode (E_h) by adding the standard potential of the reference electrode (0.22 V).

An alternative, combination redox electrode was also used to measure soil redox potential during experiments. The combination electrode (Thermo Scientific ORP glass/platinum electrode) was connected to a standard pH/E_h meter and the electrode/meter system was calibrated following the same procedure described above.

Soil redox potential was measured by inserting the calibrated combination redox electrode half-way through the wet soil and leaving it to stabilise for few minutes before the meter reading was recorded and corrected.

2.2. Carbon analysis

2.2.1. Total and organic carbon determination

Soil total and organic carbon concentrations were determined using a CNS elemental analyser (FlashEA® 1112) following standard methods. A known mass (~15 mg) of finely ground, oven dried soil was added to a tin capsule to which ~5 mg of vanadium pentoxide (V_2O_5) was also added to catalyse combustion.

Total organic carbon was determined by weighing ~15 mg of oven dried soil into a silver capsule and adding a few drops of 50% v/v HCl to remove inorganic carbon. After heating for 2 hours at 80°C on a hotplate ~5 mg of vanadium pentoxide was added. All samples (for total carbon or total organic carbon) were combusted at 900°C in a pure oxygen environment. Calibration was undertaken using reference materials (peat soil with 0.4% total inorganic carbon and 15.5% total organic carbon; sandy soil: 0.1% total inorganic carbon and 0.8% total organic carbon). All analyses were undertaken in duplicate.

2.2.2. Humic and fulvic acid determination

Soil fulvic and humic acid concentrations were determined by adding 2 g of < 2 mm sieved, air dried soil to a polycarbonate centrifuge tube into which 30 mL of 0.1 M NaOH was added to release organic carbon from the solid phase. The resulting slurry was shaken on an end-over-end shaker for 24 hours before centrifugation (15 min at 2400 rpm) and recovery of the supernatant. Total organic acid concentrations (fulvic + humic) were measured in the supernatant using a combustion catalytic oxidation/NDIR total organic carbon analyser (Shimadzu TOC-V_{CPH} analyser) after dilution with MQ water.

A subsample of the supernatant was adjusted to pH 2 with 50% HNO_3 before being made up into 10 mL using MQ water and left to stand for 24 hours to allow humic acids, which are insoluble in acidic environments, to precipitate. The sample was then filtered (0.22 μm) to remove the precipitate and fulvic acid determined.

2.2.3. Total and organic dissolved carbon determination

Total and organic carbon concentrations of soil porewater were determined using a TOC analyser (Shimadzu TOC-V_{CPH}). A calibration curve in the range 0 – 50 mg L^{-1} was prepared from stock potassium hydrogen phthalate and sodium hydrogen carbonate + sodium carbonate standards. Samples with high carbon contents (e.g. woodland soils) were diluted with MQ water before analysis when necessary.

2.3. Soil digestion

Soil elemental composition was determined by measuring elemental concentrations on soil digests. Approximately 250 mg of finely ground soil was

weighed into PFA Teflon vessels; 4 mL of concentrated trace element grade trace element grade nitric acid (HNO_3) was added and samples were heated overnight on a block digester. The heating regime comprised 30 minutes at 30°C, 1 hour at 50°C, 14 hours at 80°C and then cooling to 30°C. Concentrated hydrofluoric acid (2.5 ml) plus 2 mL HNO_3 and 1 mL perchloric acid ($HClO_4$) were then added to the vessels followed by further heating at 80°C for 8 hours, 100°C for 2 hours, 120°C for 1 hour 140°C for 3 hours 160°C for 4 hours and 50°C afterwards. Vessel contents were carefully transferred into 50 mL volumetric flasks and topped up to 50 mL using MQ water before analysis using ICP-MS (see Section 2.6).

2.4. Total iodine extraction

Soil I was extracted using the method of Watts and Mitchell (2008). Approximately 250 mg of < 2 mm, air dried soil was weighed into a 50 mL centrifuge tube, and 5 mL of 10% tetramethyl ammonium hydroxide TMAH (Afla Aesar, 25 % w/w aqueous solution) added. The tube lid was replaced loosely and its contents heated for 3 hours at 70°C (with shaking after 1.5 h). After heating, 5 mL of MQ water were added to the slurry, before being shaken and centrifuged at 2500 rpm for 20 minutes. The supernatant was decanted into a 50 mL universal tube and topped up with MQ water to achieve a final matrix of 0.5% TMAH.

2.5. Extraction of amorphous oxides

Amorphous iron and manganese oxide pools were determined by ascorbate extraction (Anschutz et al., 1998). Approximately1 g of < 2 mm sieved soil was added to a 50 mL polyethylene centrifuge tube with 20 mL of extraction reagent.

The extraction reagent which consisted of 0.17 M trisodium citrate and 0.59 M sodium bicarbonate adjusted to a final pH of 8.0 using ascorbic acid. The resulting slurries were shaken for 24 hours on an end-over-end shaker before centrifugation and filtering with 0.22 μm Millipore syringe filters. The filtered supernatant was diluted (1:10) with 0.1 M HCl prior to analysis by ICP-MS for Mn and Fe.

2.6. ICP-MS analysis

Concentrations of major (Al, Ca, Fe, K, Mg, Mn, Na) and trace (As, Cd, Cr, Cu, I, Ni, Pb, Se, Re, Zn, U) elements were determined using Inductively Coupled Plasma Mass Spectrometry (Thermo-Fisher X Series II ICP-MS) to analyse soil digests or TMAH extracts (for I only). Most measurements were made in CCT^{ED} mode (collision cell technology incorporating kinetic energy discrimination) to reduce polyatomic spectral interferences. Iodine was measured in standard mode and Se in H_2 mode (Table 2-1).

Table 2-1 Operational modes and settings of the ICP-MS used to determine concentrations of major and trace elements in soil digests and solution samples.

ICP-MS parameters	**Multielements**	**Selenium & Rhenium**	**Iodine**
Operation mode	CCT^{ED}	CCT^{ED}	Standard
Cell gas	7% H_2 in He	H_2	None
Gas flow rate	3.5 mL min^{-1}	4 mL min^{-1}	None
Int. standard	^{45}Sc, ^{103}Rh, ^{193}Ir	^{69}Ga, ^{115}In, ^{193}Ir	^{115}In
Matrix	2% HNO_3	2% HNO_3 4% Methanol	1% TMAH
Calibration range	0-100 μg L^{-1}	0.01-10 μg L^{-1}	0-100 μg L^{-1}

Methanol was added to the internal standard for Se and Re determination to improve ionisation efficiency in the ICP-MS and hence stability and sensitivity. Working standards were prepared on the day of analysis from stock solutions (Spex Certiprep).

2.7. Microcosm designs

Soil samples were incubated under anaerobic conditions in microcosms designed to allow for single (sacrificial) and repreated (mini column) sampling of the soil solution.

2.7.1. Mini column approach

A 'mini column' design (Fig. 2-2) was used to determine K_d's *in-situ* (Ashworth et al., 2008; Ashworth and Shaw, 2006b). Using this method, small volumes of soil can be incubated at realistic water contents allowing for the *in-situ* determination of redox potential E_h and sampling of the soil solution with minimal physical disturbance of the soil.

Rhizon Soil Moisture Samplers (Rhizon SMS from Eijkelkamp B.V.) were used for extraction of *in-situ* porewater samples (Fig. 2-3). Rhizon samplers have been used extensively for extraction of porewater samples from soils (see e.g. Shotbolt, 2008 and references therein).

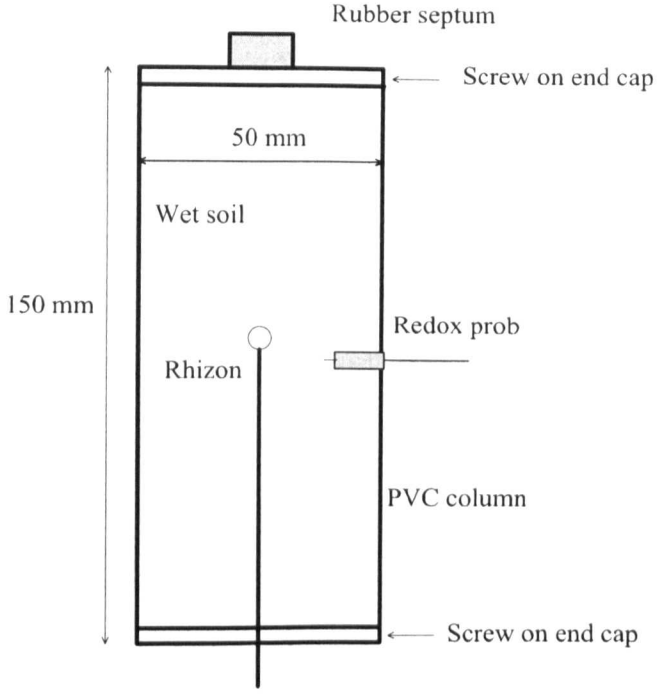

Fig. 2-2 A sketch of the design of mini column microcosm used for soil incubation under anaerobic conditions showing dimensions of the column, the permanently installed redox (E_h) Pt electrode and the Rhizon moisture sampler (Ashworth et al., 2008).

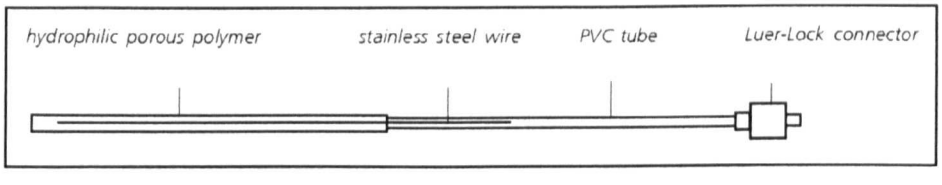

Fig. 2-3 A sketch of the Rhizon moisture sampler used to collect soil solution at different times during anaerobic incubation experiments.

Before sampling the columns were weighed to correct for any water losses due to leakage or evaporation. A syringe was then connected to the Rhizon sampler via the luer connector and the plunger was pulled out and held in place to apply a negative (suction) pressure. Once a sufficient volume of porewater was extracted (ca. 15 mL), aliquots of the porewater were preserved in HNO_3 (2% v/v) or TMAH (1% v/v) and refrigerated whilst awaiting analysis. The weights of the sample and the column were recorded after sampling before N_2-purged (deoxygenated) water was added to columns to replenish the extracted water.

The sampling time required to extract a sufficient volume of porewater varied depending on the soil type. Soils rich in organic matter (e.g. woodland topsoil) were more difficult to sample since it took more time to collect a sample from these soils than soils from less organic soils (e.g. arable subsoil).

2.7.2. Sacrificial approach

An alternative approach to measurement of native element K_d is that described by Sheppard et al. (2009; 2007). Columns are replaced by 60 mL plastic syringes and soil solution is separated by centrifugation. This approach allows for a greater flexibility regarding the operational definition of the dissolved phase. It does not, however, allow for repeat sampling of soil porewater over the course of an experiment time due to its sacrificial nature.

The contents of a microcosm (syringe) were first transferred into specially designed polyoxymethylene (Acetal) centrifuge tubes fitted with 20 μm stainless steel, mesh filters (Fig. 2-4).

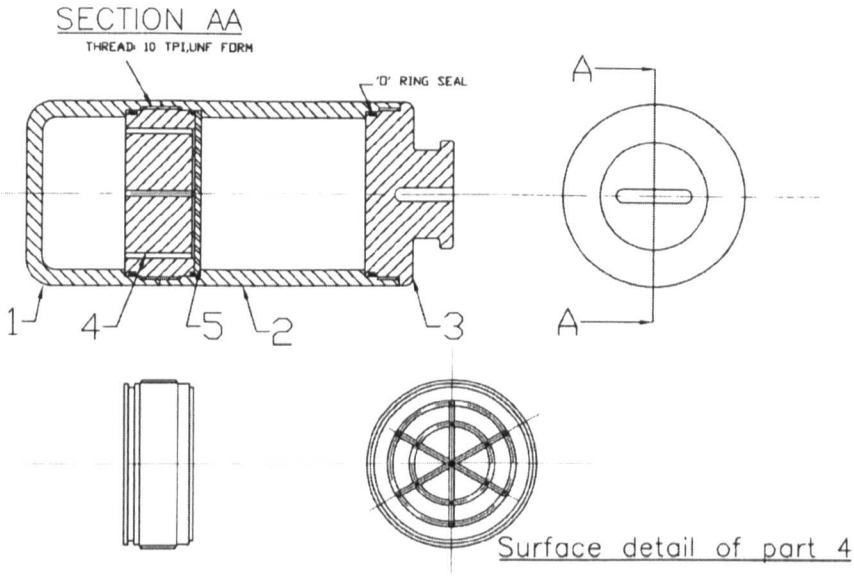

Fig. 2-4 A sketch of the design and different parts of the centrifuge tube used to separate soil solution from soil slurries incubated in sacrificial microcosms. 1 – pore water collector cup; 2 – upper soil container; 3 – screw-on acetal top; 4 – screw-on acetal filter and support; 5 – stainless steel filter (Di Bonito, 2005).

These tubes were specially manufactured to fit a Beckman J2-21 refrigerated-high speed centrifuge with AJ-10 rotor (rmax = 158 mm). The centrifuge buckets were spun at a relative centrifugal field (RCF×g) value of 600×g for 30 minutes at 4°C. Centrifugal force pushed the liquid through the stainless steel mesh down to the collection cup. Samples were then removed from the collection cups using a syringe and immediately filtered through 0.1 (Rhizon), 0.22 or 0.45 μm syringe filters. The choice of centrifuge speed and time were decided with reference to earlier work on porewater extraction methods (Di Bonito, 2005).

Chapter 3 Trace element mobility under flooded soil conditions

3.1. Introduction

The solid-liquid distribution coefficient (K_d), defined as the ratio of contaminant concentrations between soil and porewater phases, is an important parameter frequently encountered in risk assessment models (Xu et al., 2008; Klos, 2008; Avila, 2006a; Avila, 2006b; Karlsson et al., 2001) in which the K_d parameter is used to quantify contaminant mobility (Sheppard, 2011; Vandenhove et al., 2009b; Sheppard et al., 2009; Gil-García et al., 2009). Contaminants that are highly retarded by geological media have high K_d values whereas highly mobile ones have low K_ds. Variation in environmental conditions such as soil characteristics, water content and redox status affect the partitioning of contaminants, including radionuclides, between solid and liquid phases (Ashworth et al., 2008; Février et al., 2007; Ashworth and Shaw, 2006b; Ashworth and Shaw, 2005; Ashworth et al., 2003). Soil redox conditions are particularly important because they control the chemical speciation of many redox sensitive radionuclides (e.g. Se, I and U) which affects their mobility. Changes in soil redox conditions are stimulated by biogeochemical factors such as water content, organic carbon (OC) and biological activity. Changes in these biogeochemical factors due to climate

and/or land use change are very likely to occur over the long time periods considered by radiological assessments of geological repositories.

K_d is commonly quantified using simple protocols that involve equilibrating a background electrolyte spiked with a tracer with a geologic material, either a pure (mineral) or heterogeneous phase (such as soils), and determining partitioning of the tracer between the two phases (Rovira et al., 2008; Kamei-Ishikawa et al., 2008; Darcheville et al., 2008; Février et al., 2007; Nakamaru et al., 2005). A wide array of K_d determination approaches are available that vary in the complexity of the experimental design (e.g. microcosms and flow through columns) and the chemical form of the tracer used (e.g. iodate/iodide, selenate/selenite, etc.). Most laboratory procedures to determine K_d are implemented under controlled conditions for short equilibration periods (e.g. days). These conditions may not adequately represent real environmental conditions. Operational definition of the solid and liquid phases has a significant impact on empirical K_d values. Phase separation and filtration are critical experimental aspects that can be source of large variability in K_d measurements. Two widespread phase separation techniques that have been used in most K_d experiments for soil solution extraction are centrifugation (Sheppard, 2011; Sheppard et al., 2007) and Rhizon samplers (Ashworth et al., 2008; Ashworth and Shaw, 2006b). Gravitational forces applied to a sample during centrifugation provide efficient soil solution extraction from a wide range of pore sizes; however, solution from different pores is mixed and information on spatial variability is lost. This may not be a problem in e.g. batch tests where small sample volumes are used, but it can become a problem in experiments designed to obtain information about e.g. chemical zonation (spatial distribution) of radionuclides in column experiments. Samples taken using Rhizon samplers may not be representative of the spatial

distribution of the chemical species in the soil solution given their relatively large radii of influence (10 mm for coarse soils and 70 mm for those of smaller particle sizes). Samples can thus be considered to be of a qualitative nature (Di Bonito, 2005). Membrane filters used to filter soil solution would be expected to affect colloidal phase fractionation depending on the pore size of the filters. The existence of various sized colloids within the solution phase will therefore vary depending upon the membrane used. Consequently, the empirical value determined for a K_d will also be affected by the filtration method employed, especially for elements with a strong tendency to associate with colloids.

In this chapter, experiments that simulate physicochemical changes following soil flooding on a microcosm scale are described and discussed. The main objectives of these experiments were to:

1. investigate the effect of experimental methodology, in particular porewater separation and filtration methods, on K_ds.
2. investigate how K_d changed over time in a range of waterlogged soil types in response to physicochmeical changes.
3. identify key geochemical controls on K_d under dynamic soil conditions.
4. develop empirical models that predict K_d from basic soil properties.

3.2. Methods

3.2.1. Soil characterisation

Characteristics (texture, pH, OC and elemental composition) of the surface and subsurface soils used in these experiments were determined using standard methods (see Chapter 2).

3.2.2. Soil anaerobic incubation

Soils were incubated under anaerobic conditions in mini columns and sacrificial microcosms (Sheppard, 2011; Sheppard et al., 2007). Surface (0-20 cm) and subsurface (30-60 cm) arable soils and surface woodland soil were incubated under flooded conditions in mini columns for a maximum period of 4 weeks. Approximately 350 (±25) g of 2 mm sieved air-dried soil was packed into individual columns to a bulk density of ~1.4 g cm^{-3} (similar to the *in-situ* bulk density of Sutton Bonington soils). Soil moisture content was adjusted (50% v/v) gravimetrically using ultrapure water. A shallow (1 mm) standing layer of water persisted which indicated that the soils were fully saturated. This water content was maintained over the duration of the experiment by replenishing water sampled from the column with de-oxygenated ultrapure water through an opening on top of the column. Porewater was extracted *in-situ* through permanently fitted Rhizon samplers. The porewater sample was divided into 4 aliquots which were preserved for multi-element, ultra-trace level Se and Re, I and carbon analysis. Columns for each soil type were prepared in triplicate.

The sacrificial microcosm experiments used involved a greater number of soil types than the mini column experiments; in addition to the aforementioned soils, permanent grassland (surface and subsurface) and woodland (subsurface) soils were also incubated. Duplicate sacrificial microcosms were packed with 60 (±2) g of 2 mm sieved air-dried soil and their moisture content adjusted (50% v/v) with ultrapure water. The syringes were tightly sealed using Parafilm to minimise moisture loss. After incubating for one week, soil solution was extracted by ultracentrifugation and filtered using Rhizon samplers using the procedure described in Section 2.8.1. Aliquots of the filtrate were preserved for multi-element, ultra-trace level Se and Re, I and carbon analysis. Concentrations of Se, I, Re and U in 0.1 μm porewater filtrate was used to calculate K_d values for these elements.

In order to investigate effects of filter pore size on K_d, six sacrificial microcosms per soil type (36 microcosms in total) were prepared to allow duplicate samples to be sacrificed at each of three filter sizes. Aliquots of the resulting supernatant were filtered through 0.1, 0.22 and 0.45 μm membrane filters. These filtrates were used to calculate K_d values for Se, I, Re and U. All measured concentrations of trace elements in porewater samples are reported in Appendix 1.

3.2.3. *In-situ* soil redox potential (E_h)

The E_h of arable top and subsoils incubated in sacrificial microcosms was monitored over a month using permanently installed Pt and combined electrodes to check the consistency of readings using both methods (see Section 2.2.4). At the end of the experiment the Pt electrodes were removed from the soil and tested in buffer solutions (pH 4 and 7) of known potentials to identify any deterioration in their performance. In addition to empirically measured E_h values, estimates of E_h were

also calculated from thermodynamic principles. The Nernst model predicts redox potentials from the activities of certain redox species (a redox couple) present at equilibrium in soil solution. Within soils the most important redox couple is Fe^{2+}/Fe^{3+}. Electron exchange between ferric and ferrous iron species is more reversible than with other redox sensitive elements such as sulfur, hence the assumption of equilibrium is better justified if iron is considered to be the principal redox active element. Activity of Fe^{2+} in soil solution was estimated from geochemical modelling using the WHAM code (Tipping, 1998). Although this method has its own limitations (Stumm and Morgan, 1996) it provides a useful benchmark against which measured E_h can be compared. Reductive dissolution of iron hydroxide is an important redox reaction that has been extensively used to calculate equilibrium E_h values (e.g. Appelo and Postma, 2005):

$$Fe(OH)_3 + 3H^+ + e^- \rightleftarrows Fe^{2+} + 3H_2O$$

$$pe = \log K_{eq} - 3pH - \log\{Fe^{2+}\} \qquad (3\text{-}1)$$

$$E_h(V) = 2.303(RT/F)\,pe$$

where $\log K_{eq}$ = equilibrium constant for reductive dissolution of $Fe(OH)_3$, and equals 17.4 at 298.15 °K (Sposito, 2008), $\{Fe^{2+}\}$ for is the aqueous free ferrous ion activity, R = 8.314 J $°K^{-1}$ mol^{-1} (the gas constant), F = 96.483 kJ $volt^{-1}$ mol^{-1} (Faraday constant), T °K absolute temperature, E_h = redox potential in volts relative to a reference hydrogen electrode, and pe = electron activity.

Equation (3-1) assumes that iron solubility is controlled by the $Fe(OH)_3$ phase. Values of $\log K_{eq}$ are reported for standard temperature conditions (i.e. 298.15 °K)

and this value needs to be temperature-corrected to meet experimental conditions (i.e. 289.15 °K) by applying van't Hoff's equation:

$$\ln\left(\frac{K_{eq2}}{K_{eq1}}\right)=\frac{\Delta H_r^0}{R}\left(\frac{1}{298.15}-\frac{1}{T_2}\right) \qquad (3\text{-}2)$$

$$\Delta H_r^0 = 3\Delta H^0_{H_2O} + \Delta H^0_{Fe^{2+}} - \Delta H^0_{Fe(OH)_3}, \Delta H^0_{H_2O} = -285.8\ kJ\ mol^{-1},$$

$$\Delta H^0_{Fe^{2+}} = -89.1\ kJ\ mol^{-1}, \Delta H^0_{Fe(OH)_3} = -823\ kJ\ mol^{-1}$$

$$\Delta H^0_r = -123.5\ kJ\ mol^{-1}$$

where K_{eq1}, K_{eq1} [1] and ΔH_r^0 are equilibrium constants at T_2 and 298.15 °K and standard enthalpy change for reaction in (3-1), respectively. Substituting these values into the van't Hoff's equation (R = 0.008314 kJ $°K^{-1}$ mol^{-1}), gives log K_{eq} = 20.96 at 289.15 °K.

Concentrations of individual iron species present in the soil solution were calculated using the model WHAM-VI (Tipping, 1998). The composition of the solutions were specified in WHAM input files using experimental data, including total porewater concentrations for Na, Mg, K, Ca, Cr(III), Mn, Co, Ni, Cu, Zn, Sr, Cd, Ba, Pb, Cl, pH and temperature (16 °C). Since the volume of soil solution was limited, it was not possible to determine the anion concentrations. Dissolved inorganic carbon was measured and included in the input file as an indicative

[1] Values taken from University of Rhode Island website (accessed June 2010): http://bilbo.chm.uri.edu/CHM112/tables/thermtable.htm

estimate of the bicarbonate ion (HCO_3^-). $Fe^{(III)}$ activity was included as a variable and calculated from (Di Bonito, 2005):

$$\log Fe^{3+} = \log K_{SO} - 3pH$$

$$\log K_{SO} = \log K_{SO}^{0} + 0.219\,\Delta H_r^0 \left(\frac{1}{298.15} - \frac{1}{T_2}\right) \qquad (3\text{-}3)$$

$$\log K_{SO}^{0} = 2.7 \text{ and } \log K_{SO} = 3.21$$

where K_{SO}, K_{SO}^{0} are solubility products at T °K and 298.15 °K, respectively.

A limitation of the WHAM-VI code is that the number of binding sites available for dissolved metal in the aqueous phase is dictated by the concentration of active DOC, an unknown parameter. Thus, assumptions were made regarding this parameter: it was assumed that fulvic acids (FA) make up the colloidal phase and they were the only significant component that plays a role in binding dissolved iron by providing binding sites. Measured DOC concentrations in soil porewater samples were assumed to be equivalent to FA concentrations (S. Young, personal communication, 2010). The simulation was run for an open system (carbonate in equilibrium with atmospheric CO_2) and fixed pH.

3.2.4. K_d calculations[2]

Throughout this study, K_d refers to the ratio between the concentration of an element in the solid phase and its concentration in the aqueous phase. An adjustment

[2] Throughout this thesis, the term K_d will be used synonymously with the "linear isotherm" sorption model.

of the solid phase concentration is necessary, particularly for poorly sorbed contaminants, if the 'total' (effectively the solid plus solution phase) solid phase concentration is used, to represent the solid phase, to account for the soluble fraction retained within the solution phase (Sheppard et al., 2009; Ashworth and Shaw, 2006b). Although sampling of soil solution removes a portion of the dissolved elemental mass from the microcosms this will not induce trace element desorption from the solid phase because there is no change in the concentration of trace elements in solution. Even following addition of ultrapure water to the microcosms to compensate for the loss of solution the resulting desorption is difficult to predict. Desorption depends on element exchangeability and the size of the labile pool in the solid phase which control resupply of element mass removed from solution by sampling. For example, as a result of their investigation of desorption of indigenous trace metals (Cd, Cu, Ni and Zn) from riverine and esturine sediments, Millward and Liu (2003) found that quantity of metal desorbed was not proportional to the amount on the solid phase, and although estuarine sediments had high total metal concentrations, these metals were not exchangeable with solution and may have been irreversibly bound. K_d was calculated by dividing the adjusted soil solid phase concentration (mg kg^{-1} dry soil) by soil porewater concentration (mg L^{-1}) at the time of sampling:

$$K_d = \frac{(V \rho C_{solid}) - (V \theta C_{porewater})}{V \rho C_{porewater}} \qquad (3\text{-}4)$$

where V = volume of soil (L), ρ = soil bulk density (kg L^{-1}), C_{soil} = total soil concentration (solid + porewater) (mg kg^{-1} soil), $C_{porewater}$ = dissolved phase concentration (porewater) (mg L^{-1}), and θ = volumetric soil water content (L L^{-1}).

3.2.5. Statistical analysis

Correlation between empirical K_ds and soil physicochemical properties was evaluated using non-parametric Spearman's rank correlation testing. Time series of log K_d values, pH, porewater DOC and Fe concentrations were determined and tested for significant correlations. Since log-transformed K_ds are normally distributed (Sheppard, 2011; Sheppard et al., 2007), all statistical analyses were conducted on log transformed K_d values. pH, DOC and soluble Fe concentrations were used as predictor variables given their well established influence on K_d (Sheppard et al., 2007; Echevarria et al., 2001). Regression models were derived using a classical stepwise linear regression procedure using observations obtained during column microcosm experiments and SPSS software. The validation dataset, i.e. the data against which model predictions were compared, consisted of observations obtained during the sacrificial microcosm experiment. However, this validation dataset did not have time series of pH measurements; therefore the initial pH of the soil was used in K_d models that required pH data. This assumption is reasonable given the typical buffering capacity of a soil; the maximum change in soil pH over the three weeks incubation period did not exceed 1 unit for the three soil types. The overall performance of the K_d regression models was tested using the Nash - Sutcliffe model efficiency criterion (Nash and Sutcliffe, 1970).

3.3. Results

3.3.1. Soil characteristics

Physical and chemical soil properties known to affect K_d were determined following standard laboratory procedures (see Chapter 2). The properties of soil samples collected from the Sutton Bonington area are shown in Table 3-1. Sutton Bonington soils had the same texture regardless of the land use; according to the NRCS soil texture scheme[3] these soils belong to the sandy loam category. All but the acidic woodland soils had near neutral pH, typical of arable land. Contents of OC and trace elements decreased with depth; the most rapid decrease was observed in the woodland. The enrichment of this organic-rich soil with trace and major elements is due to their affinity for the soil organic phase.

Elemental concentrations in Sutton Bonington soils fall within reported worldwide ranges: 0.5-20 mg $(kg\ soil)^{-1}$ for I (Whitehead, 1984), 0.01-2 mg $(kg\ soil)^{-1}$ for Se (Fernández-Martínez and Charlet, 2009) and 0.7-9 mg $(kg\ soil)^{-1}$ for U (Hooda, 2010). Rhenium concentrations were higher than the continental average of 0.4 μg $(kg\ soil)^{-1}$, but within the range of 0.018-4.77 μg $(kg\ soil)^{-1}$ measured in 55 Japanese agricultural soils (Tagami and Uchida, 2008). Rhenium and carbonate were below detection limits in some soils.

[3] http://soils.usda.gov/technical/aids/investigations/texture/

Table 3-1 Summary of SB soil properties: sampling depth, particle size distribution (texture), pH, inorganic (IC) and organic carbon (OC) and concentrations of major (manganese and iron) and trace elements (Se, I, Re and U). Standard errors are shown in brackets after the reported mean values of each soil property.

Soil type	ID	Depth	pH	Texture			Org. C		Elemental composition					
				Clay	Silt	Sand	IC	OC	Mn	Fe	Se	I	Re	U
		(cm)		(%)	(%)	(%)	(%)	(%)	(mg kg^{-1})	(mg kg^{-1})	(mg kg^{-1})	(mg kg^{-1})	(µg kg^{-1})	(mg kg^{-1})
Arable top	SB-AT	0-20	7.3	6	45	49	2.5	2.2	225 (4)	13444 (151)	0.25 (0.01)	3. 98 (0.15)	2.03 (0.15)	1.23 (0.07)
Arable sub	SB-AS	40-50	6.8	6	48	46	0.0	0.8	365 (6)	19918 (268)	0.23 (0.01)	2.29 (0.02)	2.27 (0.003)	1.31 (0.02)
Grass top	SB-GT	0-20	6.4	6	46	48	0.0	2.4	213 (2)	12345 (169)	0.25 (0.01)	4.15 (0.85)	2.3 (0.05)	1.27 (0.01)
Grass sub	SB-GS	40-50	6.5	6	45	49	0.0	-	315 (4)	16762 (257)	0.175 (0.01)	4.15 (0.10)	undetectable	1.22 (0.04)
Wood top	SB-WT	0-20	4.3	6	50	44	0.0	10.5	152 (2)	12350 (43)	0.61 (0.01)	4.32 (0.13)	3.36 (0.20)	1.17 (0.04)
Wood sub	SB-WS	40-50	3.8	6	47	47	0.0	1.7	264 (2)	15300 (132)	0.10 (0.03)	2.07 (0.25)	undetectable	1.19 (0.03)

3.3.2. Mobility of major and trace elements under anaerobic conditions

Soil flooding resulted in changes in pH, E_h and porewater concentrations of major (Fe and org C) and trace (Se, I, Re and U) elements. For arable soils pH fluctuated around pH 7 with a transient increase at day 7 of the incubation (Fig. 3-1). The pH of the woodland topsoil increased by one unit over the 3-week incubation period but remained acidic.

All soils exhibited decreasing E_h following soil flooding (Fig. 3-1). The E_h trends for the two arable soils were similar but distinct from that for the woodland topsoil. The E_h values of the two arable soils, on average, were lower than those of the woodland topsoil.

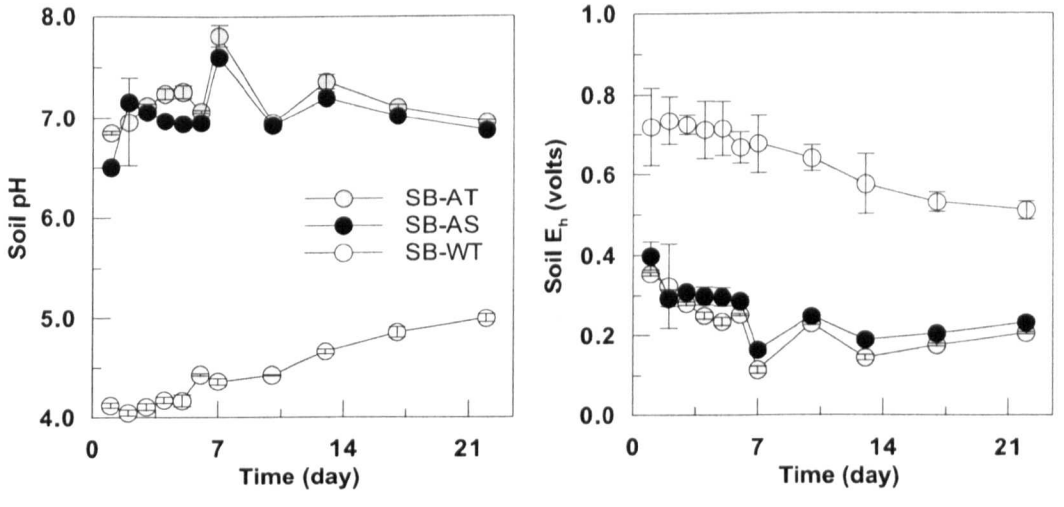

Fig. 3-1 Changes in pH and E_h (Nernst estimates) of SB soils incubated in mini columns under anaerobic conditions as a function of time. Error bars represent standard errors of the means of single measurements from triplicate columns.

Time series of DOC and dissolved Fe concentrations for the arable and woodland over the incubation period are shown in Fig. 3-2. The figure shows a decrease in DOC concentrations over the initial 7 days for all soils. Afterwards, DOC concentrations for all soils increased and reached steady-states at day 22. DOC concentrations in the woodland topsoil at steady state were substantially higher than those of the arable topsoil and subsoil.

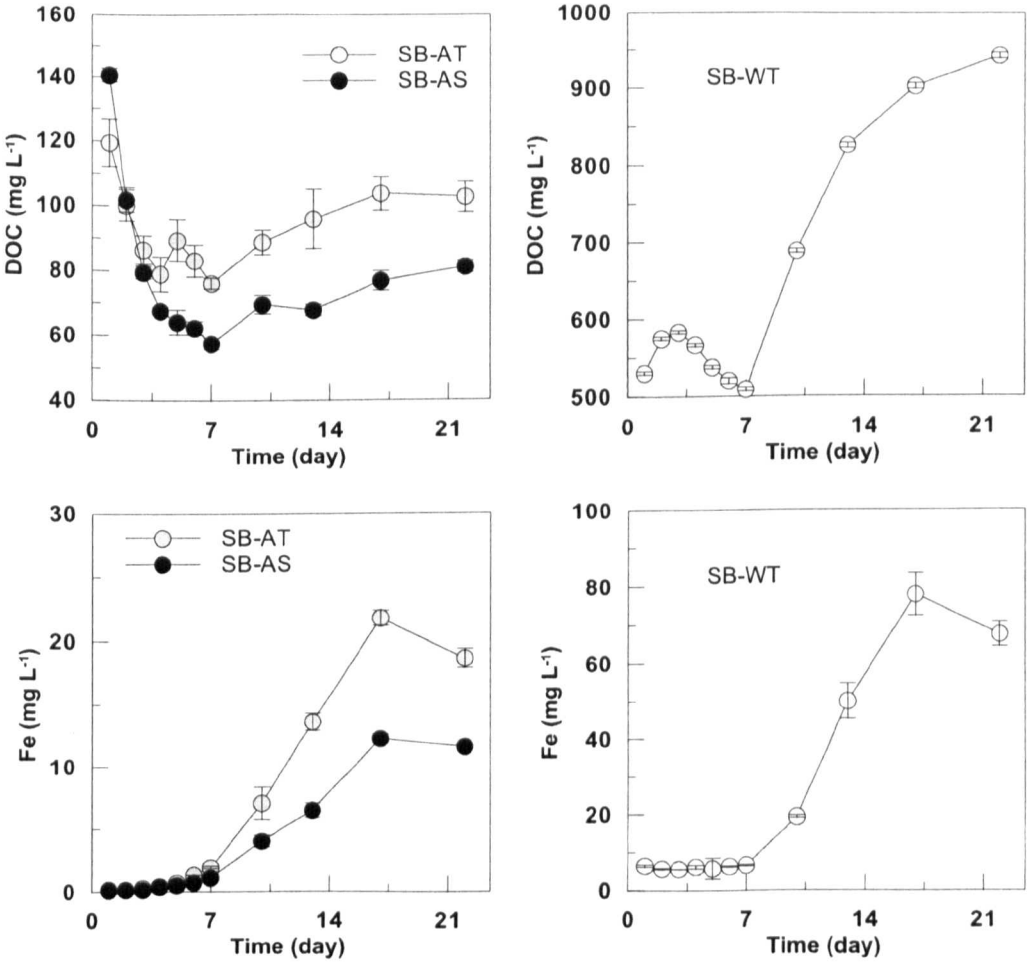

Fig. 3-2 Changes in DOC and Fe concentrations in solution of SB soils incubated in mini columns under anaerobic conditions as a function of time. Error bars represent standard errors of the means of single measurements from triplicate columns.

A rapid increase in porewater Fe concentrations for arable top and subsoils was observed over the first week of incubation (Fig. 3-2). In contrast, woodland porewater Fe concentration remained unchanged during the same period. Thereafter, porewater Fe concentration increased with time and reached a steady state by the third week of the incubation. By the end of the incubation period, Fe concentration in arable (top and sub) and woodland porewater had increased by 2 and 1 order of magnitude from their initial values, respectively.

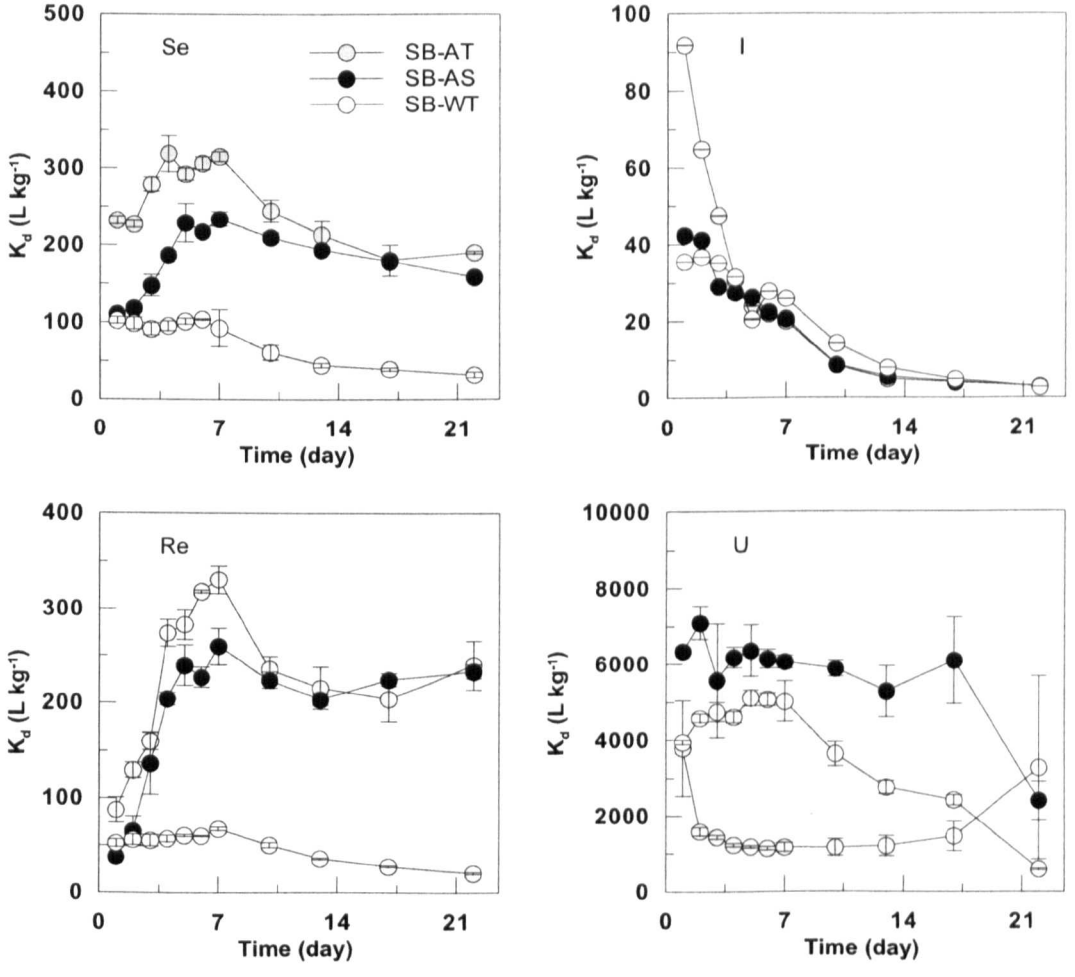

Fig. 3-3 Changes in Se, I, Re and U K_d determined for SB soils incubated in mini columns under anaerobic conditions as a function of time. Error bars represent standard errors of the means of single measurements from triplicate columns.

K_d values of Se, I, Re and U determined from soil and porewater concentrations over the course of the experiment are shown in Fig. 3-3. During the first incubation week, K_d values increased with time reaching a maximum at day 7. Mean K_d values for the woodland soil were lowest among soil types except for U. Afterwards, K_d values decreased with time for all soils, and this decrease was greatest for the woodland soil. By the end of the incubation period, Se and Re K_ds for the arable soils had increased to, and stabilised at 190 and 240 L kg^{-1}, respectively. For the woodland soil, the final Se and Re K_ds determined at day 22 were considerably lower (31 and 20 L kg^{-1}, respectively). Iodine K_d values for all soil types decreased with time, and by the end of the incubation period, I K_d values had decreased to 3 L kg^{-1} indicating high mobility.

Uranium had the highest K_ds amongst all the elements and for all soil types investigated. Initially, U K_d values for all soils were above 3500 L kg^{-1} indicating high affinity for the soil solid phase. Whilst U K_d values for the arable topsoil decreased to 1000 L kg^{-1} rapidly after flooding, K_d values for the arable subsoil remained relatively unchanged for longer. By the end of the incubation period, U K_d values for the arable subsoil had decreased to 2400 L kg^{-1}. A greater decrease in U K_d (to 590 L kg^{-1}) was observed for the woodland soil.

3.3.3. Effect of measurement method on soil E_h

Changes in measured and calculated E_h values of the flooded soils incubated in sacrificial and column microcosms over time are shown in Fig. 3-4. Initially, E_h of all soils (measured immediately after soil wetting) was c. 0.55 ± 0.10 V (value not shown).

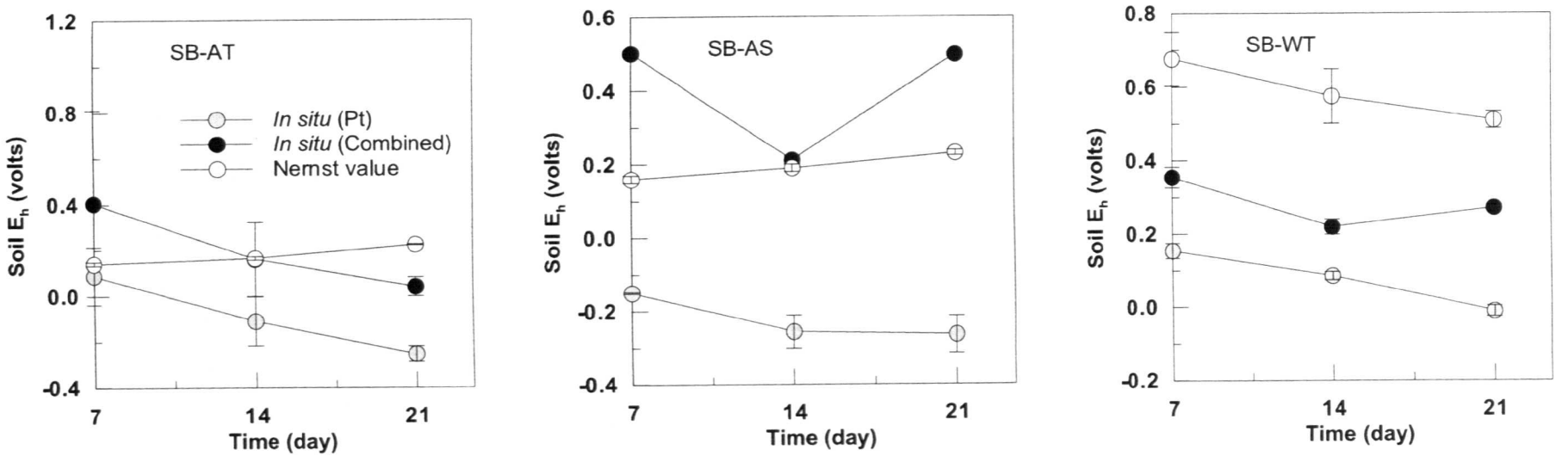

Fig. 3-4 Changes in E_h of SB soils determined using *in situ* Pt electrode and soluble Fe concentration (Nernst equation) in mini columns and a combined electrode in sacrificial microcosms as a function of time. Error bars represent standard error of the mean of single readings from duplicate (sacrificial) and triplicate (column) microcosms.

By the third week of the experiment, E_h value differed substantially depending on the measurement method as well as the soil type. E_h readings obtained using Pt electrodes for the arable top and subsoils were as low as c. -0.3 V; E_h readings for the woodland topsoil were higher (c. -0.01 V). In contrast, E_h readings obtained using the combined electrode for the same soils incubated in sacrificial microcosms were significantly higher ($p < 0.01$). Considerable divergence between the Pt and the combined electrodes' readings was observed for the arable subsoil (0.8 V). E_h values calculated using the Nernst approach fell between the Pt and the combined electrodes' values. E_h of arable soils incubated in sacrificial microcosms obtained using the combined and Pt electrodes are shown in Fig. 3-5. The results show that the combined electrode E_h readings were substantially higher than their Pt counterparts for arable top and subsoils at all times. The Pt readings were also characterised by large error bars indicating substantial variability between individual electrodes.

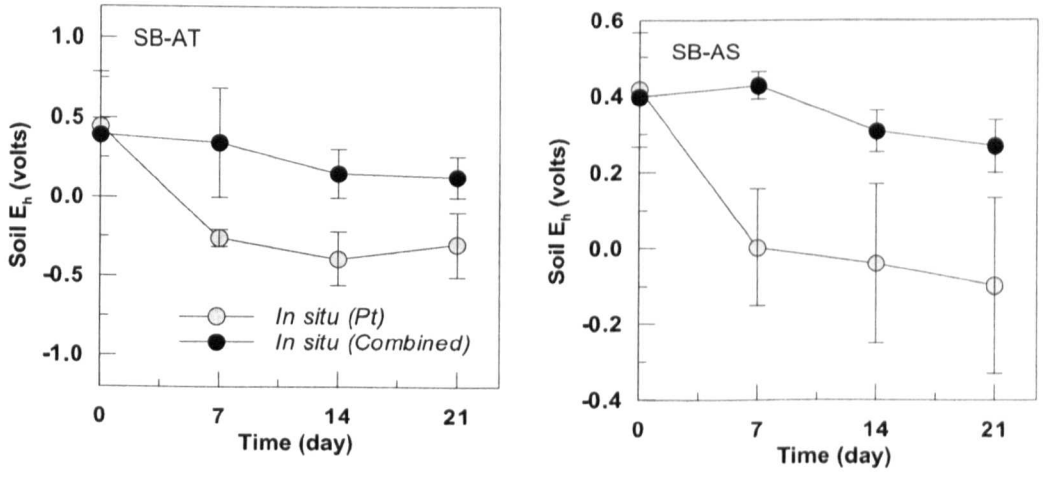

Fig. 3-5 Changes in E_h of SB arable top and subsoils determined using permanently installed Pt and combined electrodes in sacrificial microcosms as a function of time. Error bars represent standard errors of the means of single measurements from duplicate microcosms

The functionality of three Pt electrodes that had been used for one month to record E_h values of soil slurries in microcosms was tested by measuring the potentials of two standard solutions (Fig. 3-6). The measurements indicated substantial electrode-dependent variation between initial and final E_h values of the standard solutions.

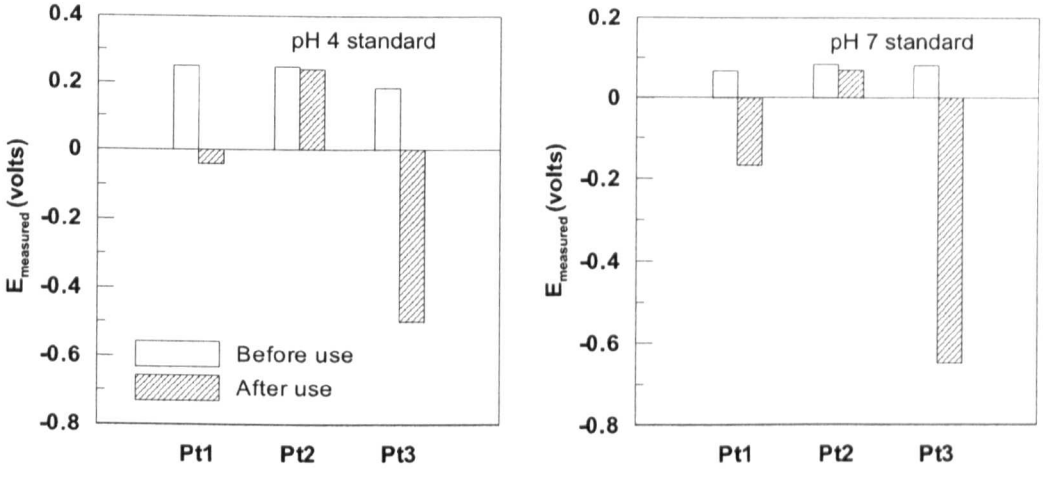

Fig. 3-6 Change in the performance of the Pt electrodes after a month of incubation. The electrodes were tested using standard solutions with known E_h values at pH 4 (0.463 V) and 7 (0.286 V). 'Before use' bars represent potential values measured using new Pt electrodes while 'After use' bars represent values measured using the same electrodes after one month of use in a soil suspension.

Change in porewater Fe concentrations in microcosms over time is shown in Fig. 3-7. The concentration of Fe in porewater varied depending on the incubation method. Porewater Fe concentrations increased with time and higher dissolved Fe concentrations were observed in the columns compared with the sacrificial microcosms.

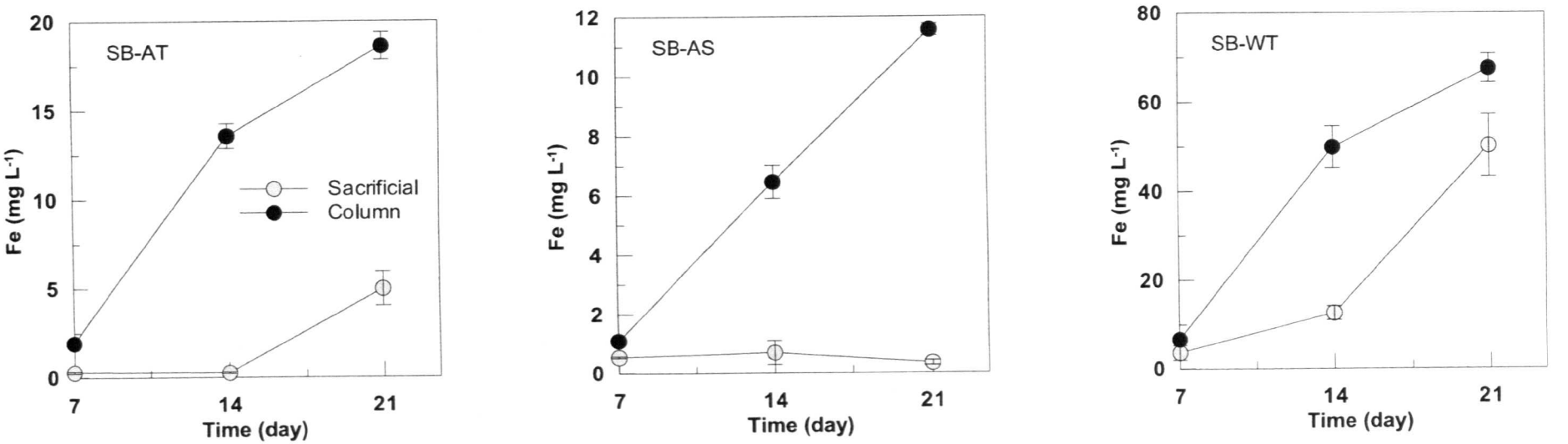

Fig. 3-7 Changes in soluble Fe concentration in SB soils incubated in sacrificial and column microcosms under anaerobic conditions as a function of time. Error bars represent standard error of the mean of single readings from duplicate (sacrificial) and triplicate (column) microcosms.

The increase of porewater Fe concentrations was rapid in the columns relative to the sacrificial microcosms. Also, changes in porewater Fe concentrations over time were soil-type specific. The highest porewater concentrations of Fe were measured in the woodland topsoil (note the difference in the range of the y-axes).

3.3.4. Effect of experimental design on K_d

Fig. 3-8 shows values of Se, I, Re and U K_ds for all soils computed from 0.1 μm filtrates after 7 days' incubation in sacrificial and column microcosms. Selenium and I K_ds determined using the sacrificial design were significantly different (ANOVA test, $p < 0.05$) from those determined using the columns for the arable topsoil. However, the incubation method did not seem to have a significant effect ($p > 0.05$) on Se, I and U K_ds for the arable subsoil and the woodland topsoil. In contrast, Re K_d was significantly affected ($p < 0.05$) by the incubation method regardless of soil type, with values determined using the sacrificial method being substantially lower than their column counterparts. Overall, the difference in K_d between the two experimental designs was less than an order of magnitude for all elements and soil types. The effect of the pore size of the membrane filters on K_d values was assessed by comparing K_ds computed from trace element concentrations in different porewater filtrates.

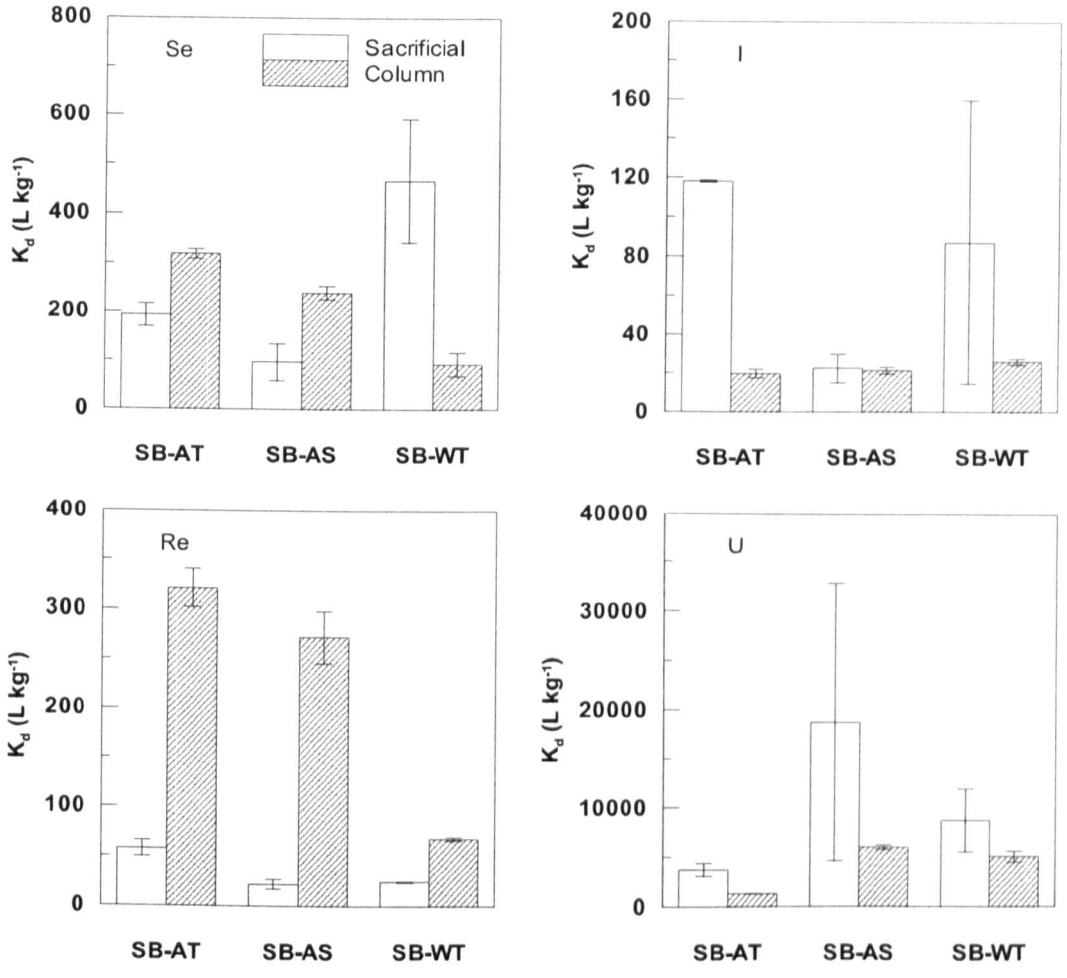

Fig. 3-8 Differences between sacrificial and column K_d values computed from porewater 0.1 μm filtrates 7 days after soil wetting. Error bars represent standard errors of the means of single measurements from duplicate microcosms.

Concentrations of Fe and DOC in porewater filtrates, in addition to K_d values of Se, I, Re and U computed from 0.1, 0.22 and 0.45 μm filtrates of porewater sampled from the sacrificial microcosms are presented in Fig. 3-9 and Fig. 3-10.

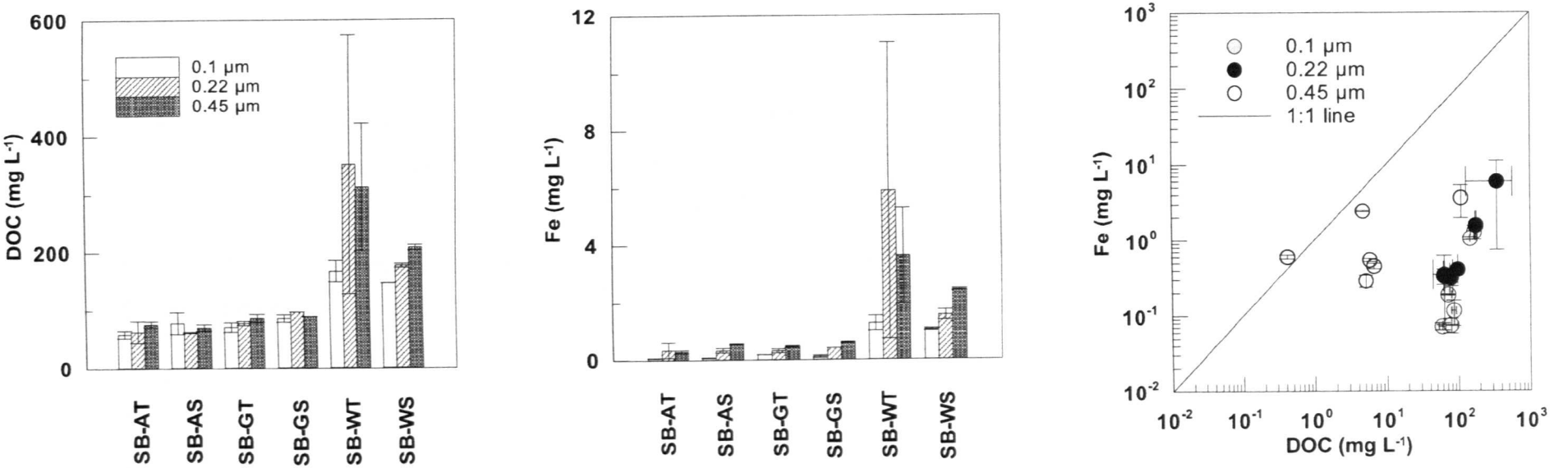

Fig. 3-9 DOC and Fe concentrations in three porewater filtrates measured after 7 days of incubation as a function of soil type. Concentrations of DOC are larger than soluble Fe concentrations for all soil types and filtrates as distribution of (Fe, DOC) pairs around the 1:1 line show. Samples collected from the sacrificial microcosms. Error bars represent standard errors of the means of single measurements from duplicate microcosms.

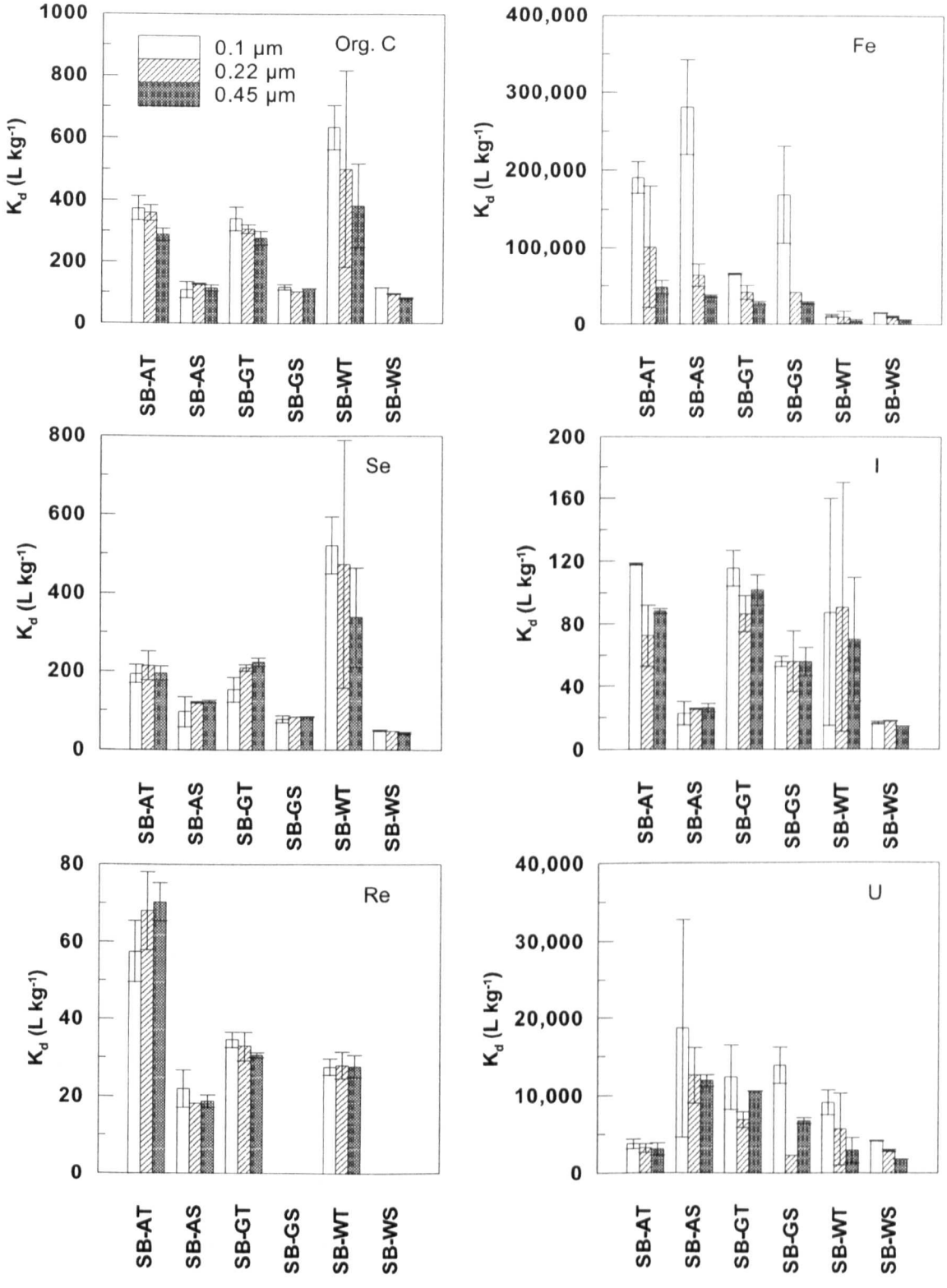

Fig. 3-10 Differences between sacrificial K_d values computed from porewater 0.1, 0.22 and 0.45 µm filtrates 7 days after soil wetting as a function of soil type. Error bars represent standard errors of the means of single measurements from duplicate microcosms.

For all soils the porewater Fe concentration increased with membrane pore size. Consequently, Fe K_d was sensitive to the pore size of the membrane filter used to filter porewater samples. DOC concentration was not, within experimental error, affected by the membrane pore size. For most soil-trace element combinations, the variation in K_d due to membrane pore size was less than one order of magnitude. The effect of soil type on K_ds, however, was highly significant ($p < 0.05$) for all elements.

3.3.5. Correlations between K_d and soil parameters

Changes in K_d values of Se, I, Re and U as a function of pH, DOC and Fe are shown in Fig. 3-11 to Fig. 3-13. There seems to be no simple relationship between soil pH and K_d, particularly for the arable soils. In contrast, the association between these two variables is relatively strong for the woodland soil as the Spearman's correlation tests show (Table 3-2). Over the first week of incubation K_d of Se, Re and U increased as the woodland soil pH increases, afterwards, it decreased as pH continued to decrease over time. In contrast, I K_d decreased as woodland soil pH decreased over the incubation period.

Changes in K_d as a function of soil DOC are presented in Fig. 3-12. Strength and significance of the association between DOC and K_d are summarised in Table 3-2. Strong and significant inverse correlations between DOC and K_d of Se, I, Re and U were observed for the woodland topsoil. For the arable soils, however, this correlation was only significant for Se and Re. For I, two distinct K_d trends with respect to DOC concentration were observed depending on sampling time. During the first incubation week, I K_d and DOC concentration decreased simultaneously; then, I K_d decreased as DOC concentration decreased.

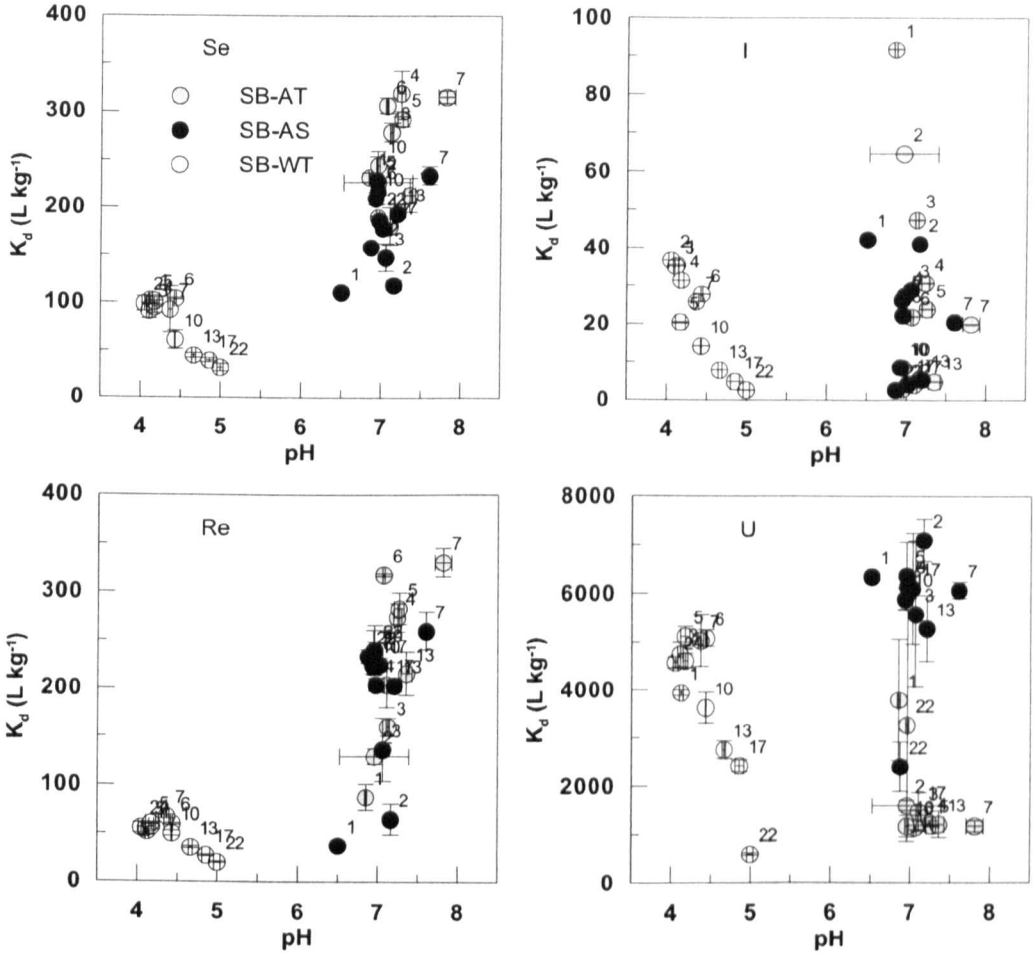

Fig. 3-11 Changes in K_d as a function of soil pH for three SB soils. Labels refer to sampling day. Error bars represent standard errors of the means of single measurements from triplicate columns.

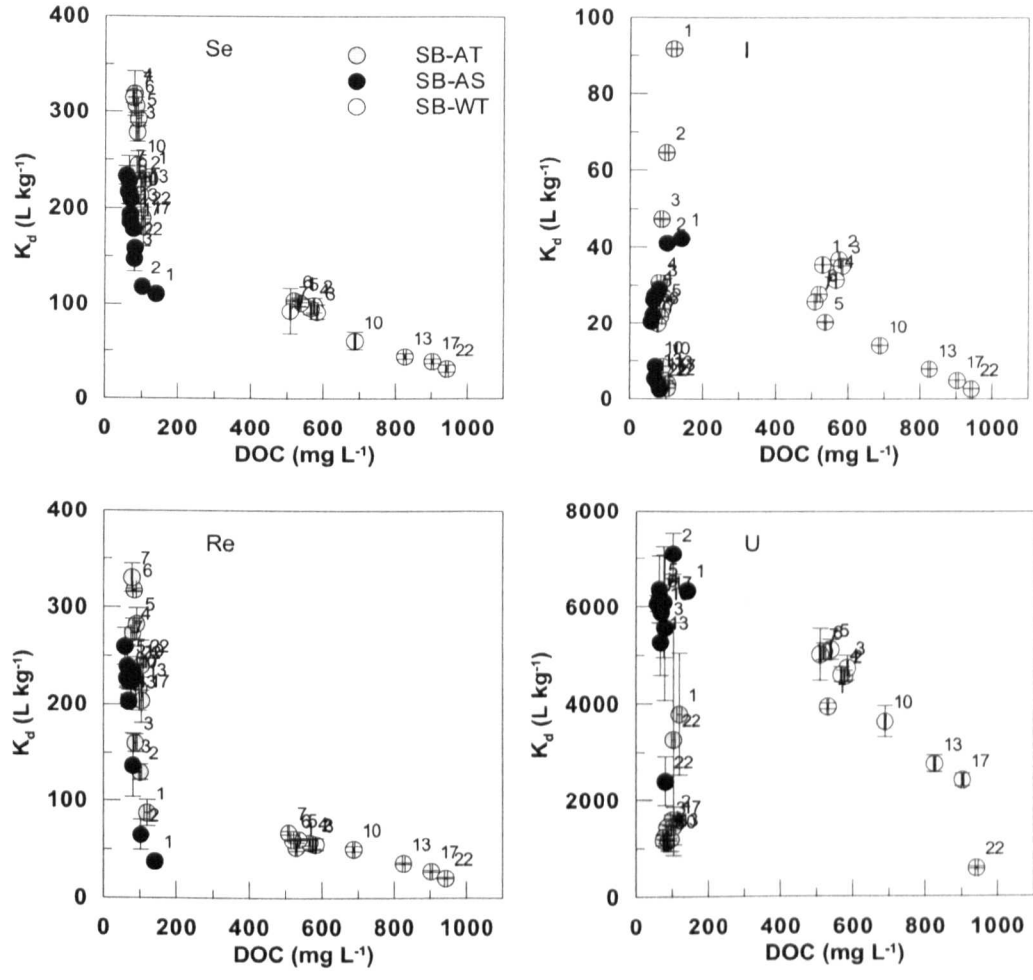

Fig. 3-12 Changes in K_d as a function of DOC concentration in soil solution for three SB soils. Labels refer to sampling day. Error bars represent standard errors of the means of single measurements from triplicate columns.

Changes in K_d as a function of dissolved Fe concentration for all elements and soil types are presented in Fig. 3-13. The strength and significance of associations between Fe concentrations and K_ds are summarised in Table 3-2. A strong and significant inverse association between dissolved Fe concentration and K_d was observed for the organic woodland topsoil. However, except for I, this relationship was insignificant for the arable soils. The relationship between dissolved Fe concentration and K_d was complex and appeared to be time dependent, particularly for Se and Re in the arable soils. For instance, Se and Re K_ds

increased with dissolved Fe concentrations over the first week of incubation thereafter, they decreased as dissolved Fe concentrations decreased.

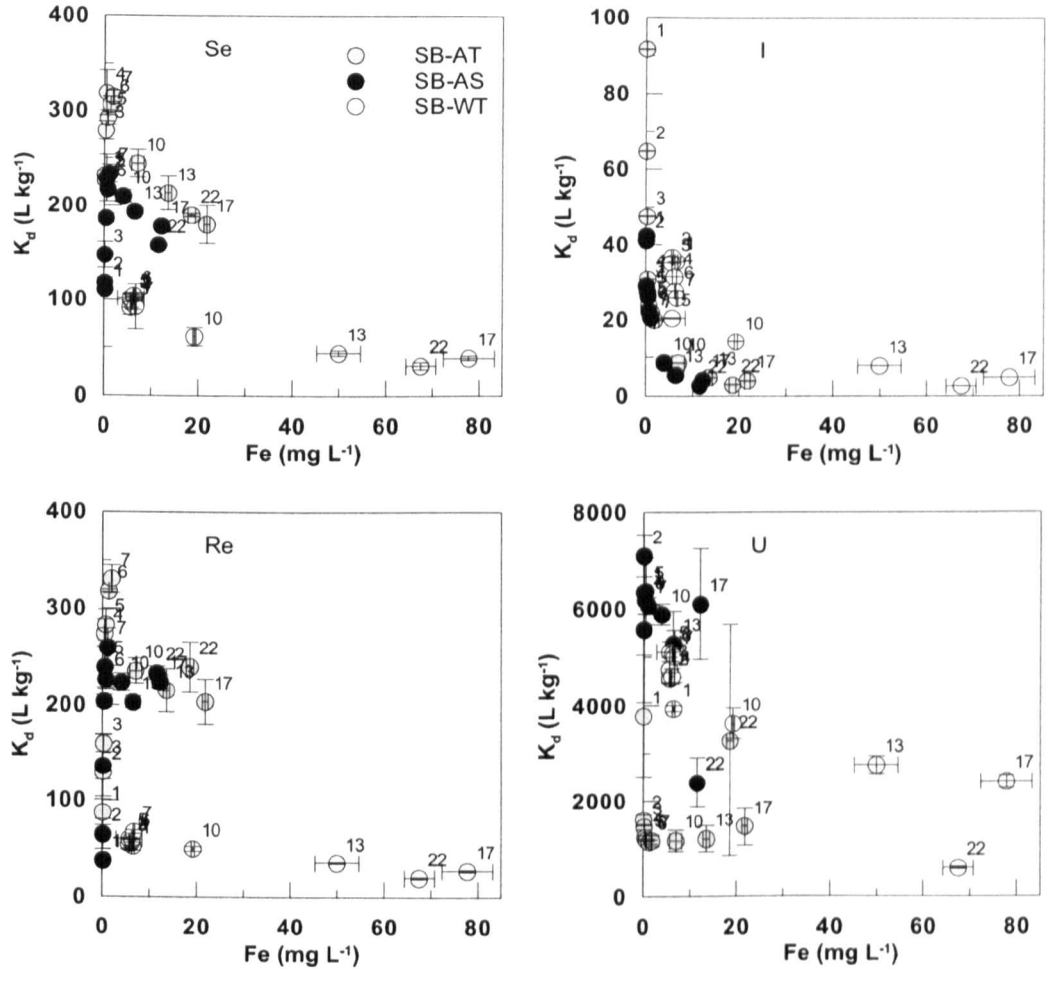

Fig. 3-13 Changes in K_d as a function of soluble Fe in solution for three SB soils. Labels refer to sampling day. Error bars represent standard errors of the means of single measurements from triplicate columns.

Table 3-2 Spearman's correlation coefficients between column K_d (L kg^{-1}) pH, DOC and dissolved Fe concentrations in SB porewaters. (*) denotes statistically significant ($p \leq 0.05$) and (**) denotes highly significant ($p \leq 0.01$) correlations.

Soil type	**Se**			**I**			**Re**			**U**		
	pH	**DOC**	**Fe**	**pH**	**DOC**	**Fe**	**pH**	**DOC**	**Fe**	**pH**	**DOC**	**Fe**
SB-AT	0.41 (0.20)	-0.86 (**)	-0.44 (0.2)	-0.21 (0.53)	-0.07 (0.83)	-0.99 (**)	0.56 (0.07)	-0.71 (*)	0.36 (0.3)	-0.49 (0.13)	0.75 (*)	-0.24 (0.5)
SB-AS	0.24 (0.48)	-0.95 (**)	0.38 (0.3)	-0.04 (0.92)	0.25 (0.43)	-0.96 (**)	0.03 (0.94)	-0.71 (*)	0.56 (0.07)	-0.10 (0.80)	-0.03 (0.94)	-0.61 (*)
SB-WT	-0.61 (*)	-0.86 (**)	-0.66 (*)	-0.90 (**)	-0.61 (*)	-0.82 (**)	-0.53 (0.10)	-0.89 (**)	-0.65 (*)	-0.55 (0.08)	-0.83 (**)	-0.74 (**)

3.3.6. Predicting K_d from soil properties

Parametric (empirical) K_d models were derived by stepwise regression between log K_d as the dependent variable and pH, DOC and dissolved Fe concentrations as independent variables. The regression analyses were conducted on the column dataset (DOC, Fe and K_ds determined in 0.1 μm filtrates). The empirical K_d models for Se, I, Re and U are summarised in Table 3-3. The most significant K_d predictor variables were element specific. DOC concentration was of significance except for I; inclusion of soil pH and dissolved Fe concentration did not improve the fit of Se and Re models. For all elements but U, more than 70% of the variability in log K_d data was accounted for by the regression model. For the stepping criteria used, none of the soil parameters tested could account for the variability in U log K_d.

The performance of the parametric K_d models was assessed by comparing their predictions against sacrificial K_d values for all soil-element combinations. Values of the intercept, slope and coefficient of determination (R^2) of the regression lines presented in Fig. 3-14 are reported in Table 3-4. Also reported are values of Nash-Sutcliffe indices (NS). Ideally, a perfect model in terms of performance would have an intercept of zero, a slope and NS index of one.

Table 3-3 Parametric K_d models: log K_d (L kg^{-1}) = intercept ± S_1 × pH (-) ± S_2 × log DOC (mg L^{-1}) ± S_3 × log Fe (mg L^{-1}). Total number of observations = 99. Numbers in brackets represent standard errors of the number to the left of the bracket. Parameters that did not improve model fit were excluded (insignificant). Stepping criteria: entry and removal F probabilities: 0.05 and 0.1, respectively. (*) denotes statistically significant ($p \leq 0.05$) and (**) denotes highly significant ($p \leq 0.01$) correlations.

Element	Intercept	Slope (S_i)			Coefficient of determination
		pH	Log DOC	Log Fe	R^2
Se	3.38 (0.07)	excluded	-0.55 (*)	excluded	0.77
I	2.7 (**)	-0.2 (**)	excluded	-0.55 (*)	0.87
Re	3.70 (0.09)	excluded	-0.73 (*)	excluded	0.78

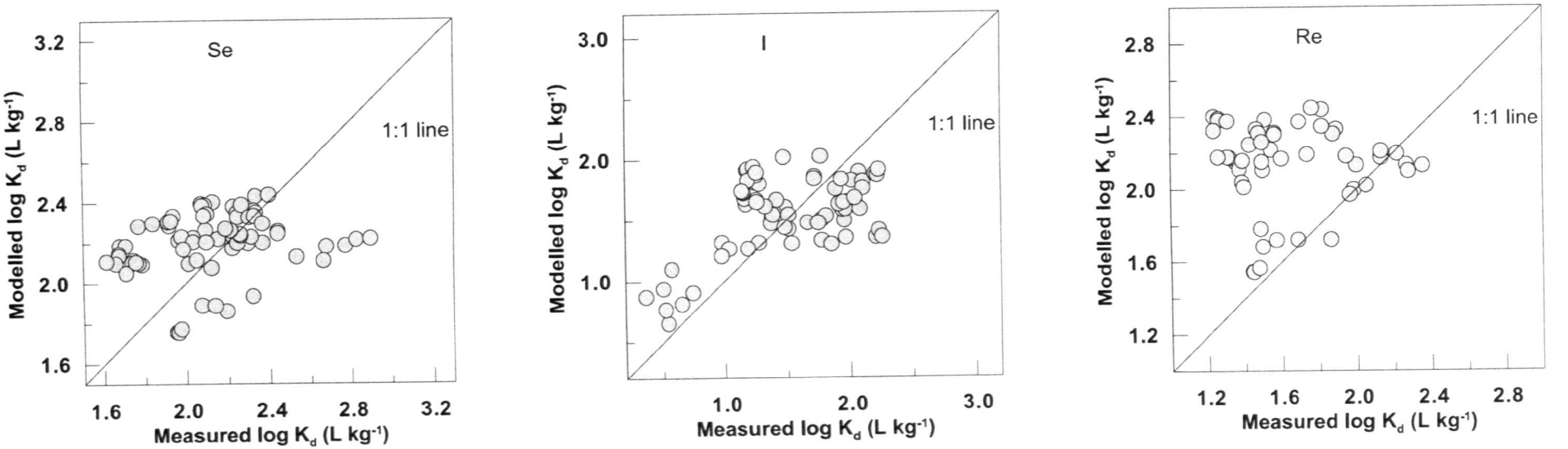

Fig. 3-14 Goodness of fit of the parametric models that predict K_d from soil characteristics (details in Table 3-3). Models were derived from column K_d values and validated using sacrificial K_d values for Se, I, Re and U. Total number of observations = 73.

Table 3-4 Performance descriptors for the parametric K_d models (n = 73 observations except for Re where n = 50 observations). (*) denotes statistically significant ($p \leq 0.05$) and (**) denotes highly significant ($p \leq 0.01$) correlations.

Element	**Intercept**		**Slope**		**Coefficient of determination**	**Nash-Sutcliffe index**
	Value	***p* value**	**Value**	***p* value**	**R^2**	**NS**
Se	1.94 (0.14)	(**)	0.12 (0.06)	(**)	0.05	-0.12
I	1.06 (0.10)	(**)	0.33 (0.06)	(**)	0.27	-3.15
Re	2.17 (0.18)	(**)	-0.02 (0.11)	(**)	0.001	0.25

3.4. Discussion

Observed changes in soil pH are typical of flooded soils which have a tendency towards neutral pH (Kögel-Knabner et al., 2010). The decrease in E_h with time suggests the development of anaerobic conditions in the flooded Sutton Bonington soils. Such anaerobic conditions result from microbial respiration during which readily available OC is metabolised and soil oxygen is exhausted. Flooding drastically limits exchange of gases between soil and the atmosphere and an oxygen-deprived environment is established. The gradual increase in porewater Fe concentrations for all soils also confirms the development of anoxic conditions in these soils. The increase in dissolved Fe concentration results from reductive dissolution of Fe oxy(hydr)oxides, and subsequent release of reduced Fe^{2+} into soil solution (Kögel-Knabner et al., 2010; Ponnamperuma, 1972). The critical E_h (at pH 7) at which this occurs falls between 0.1 V (Sparks, 2003) and -0.1 V (Sposito, 2008). The higher Fe concentrations observed in the woodland soil solution may not indicate stronger anoxia in this soil compared to the arable soils given its acidic nature. High acidity enhances dissolution of Fe solid phases. Decreasing E_h and low pH, particularly for the woodland soil, also induce solubilisation of soil OC. An initial release of OC was observed for all soils immediately after flooding; initial DOC concentration in the woodland soil was 4 times higher than that of the arable soils due to its higher OC content. The decrease in DOC concentrations over the first week of incubation is probably due to utilisation of DOC by soil microorganisms for respiration. The increase in DOC concentrations observed after day 7 coincides with an increase in Fe concentrations, which is probably partially attributable to the release of OC bound to Fe phases upon the reductive dissolution of these phases. In

fact, complexation with Fe oxy(hydr)oxides and subsequent precipitation from soil solution have been shown to be important OC stabilisation mechanisms in soils (Heckman et al., 2009; Nierop et al., 2002; Kaiser and Guggenberger, 2000). In addition, the rise in the woodland soil pH during the experiment may have induced further solubilisation of OC (Kalbitz et al., 2000).

K_d varied during the incubation period; the maximum variation was observed for I (c. 2 orders of magnitude, Fig. 3-3). This temporal variation in K_d is probably due to physicochemical changes within the columns (e.g. pH, E_h). Because these changes are controlled by soil characteristics such as mineralogy, organic matter content and biological activity, K_d variation was also soil-specific. For example, Se and Re K_ds determined for the arable top and subsoils were very similar, whereas those determined for the woodland topsoil were an order of magnitude lower. Uranium K_d determined for the arable topsoil was on average 3 times lower than that for the arable subsoil due, perhaps, to the higher carbonate content of this soil which enhances U mobility.

Overall, Se, I, Re and U K_ds determined for Sutton Bonington soils using the column approach were not dissimilar from those reported in the literature despite methodological differences. The range of Se K_ds for Sutton Bonington soils falls within the K_d range reported by the IAEA (2009) for a wide range of soil types. The K_d range for Sutton Bonington soils is also within the range reported by Sheppard et al. (2007) for 51 Canadian agricultural soils and by Sheppard et al. (2009) for 7 Swedish soils. The GM of Se K_d for Sutton Bonington soils is lower than the generic IAEA (2009) K_d value and that of Sheppard et al. (2007) for the Canadian soils but higher than the value reported for the Swedish soils (Sheppard et al., 2009).

The range of I K_d determined for Sutton Bonington soils falls within the range of values reported by IAEA (2009) and overlaps with the range for the Swedish soils (Sheppard et al., 2009). The geometric mean (GM) value for Sutton Bonington soils is higher than the generic IAEA (2009) K_d value but substantially lower than that for the Swedish soils.

K_d data for Re in the literature is scarce. Nevertheless, the range of Re K_d for Sutton Bonington soils falls within the range of values reported for 81 Canadian agricultural soils (Sheppard et al., 2007), and overlaps with the range reported for 3 Swedish soils (Sheppard et al., 2009). The GM of Sutton Bonington K_d is higher than those for the Canadian and Swedish soils. The range of U K_d for Sutton Bonington soils falls within the IAEA (2009) range and overlaps with the range for the Canadian (Sheppard et al., 2007) and the Swedish (Sheppard et al., 2009) soils.

The U GM K_d for Sutton Bonington soils is higher than the IAEA (2009) and the Canadian soils (Sheppard et al., 2007) values but lower than that reported for the Swedish soils (Sheppard et al., 2009).

Table 3-5 Site-specific K_d (L kg^{-1}) determined empirically and calculated from Sheppard's parametric equations for a suite of trace elements and averaged for six SB soils and published (non-site specific) data. GM = geometric mean and GSD = geometric standard deviation.

Element	Minimum – maximum					GM (GSD)				
	SB Measured	IAEA (2009)	Sheppard (2007)	Sheppard (2009)	SB Calculated[4]	SB Measured	IAEA (2009)	Sheppard (2007)	Sheppard (2009)	SB Calculated
Se	41 – 789	0.7 – 200	20 – 9100	10 – 140	180 – 490	142 (1.8)	200 (3)	290 (4.3)	35 (–)	325 (1.5)
I	2 – 180	0.01 – 580	–	60 – 3900	150 – 165	20 (2.7)	7 (5)	–	720 (–)	160 (1.0)
Re	17 – 349	–	6 – 600	12 – 39	–	97 (2.5)	–	54 (3.4)	24 (–)	97 (2.5)
U	110 – 32750	0.7 – 67000	8.8 – 22000	610 – 44000	90 – 680	3234 (2.7)	200 (120)	960 (6.4)	4000 (–)	240 (2.2)

[4] Values calculated using Sheppard's regression models. No models for rhenium (Re) were available in the original publication.

The observations show greater Se and Re mobility in the flooded woodland soil compared to the arable soils, and greater Se and Re desorption was observed from the woodland soil compared with the arable soils. This indicates that organic soils serve not only as a sink for these trace elements but also as a source. Changes in the environmental conditions, such as those induced by flooding and drying cycles, would bring about changes in soil physicochemical properties that stimulate desorption of organically-bound elements into soil porewater.

The observed trends of Se, I, Re and U K_ds and their correlations with other soil parameters imply that partitioning of these elements is a complex, time - dependent process. The decrease in soil Se mobility upon flooding might be due to its chemical speciation and the interactions of its chemical species with the solid phase. Aqueous Se consists of inorganic (selenate SeO_4^{2-} and selenite SeO_3^{2-}) as well as organic species (Tolu et al., 2011; Gerla et al., 2011; Zhang et al., 1999). Selenite has a greater affinity than selenate to soil minerals (e.g. oxy-hydroxides) (Duc et al., 2003; Balistrieri and Chao, 1990) and Se immobilisation may be attributed to selenite sorption onto soil surfaces. As soil E_h continues to fall within the microcosms the aqueous speciation of Se will have shifted towards selenite, and perhaps insoluble elemental Se (Séby et al., 2001; Masscheleyn et al., 1991). The decrease in Se mobility observed for the woodland soil was much smaller, probably due to its higher E_h and its acidic nature. More Se was solubilised from the woodland soil over time compared with the arable soils, perhaps due to its acidic nature as acidic extractants (e.g. nitric acid) have been found to be effective in leaching Se from soils (Tolu et al., 2011). Soluble selenate might have been the most stable Se species under the relatively higher redox conditions of the woodland soil. The subsequent increase in Se mobility with time for all soils coincided with solublisation of soil Fe

and OC. This implies that chemical speciation itself may have less effect on Se mobility than Fe and OC solubilisation. Selenium is solublilised as part of the OC solubilisation.

Rhenium behaviour with respect to its mobility trends was similar to that of Se. The initial decrease in Re mobility following flooding, however, is somewhat inexplicable. It is unlikely that Re immobilisation was related to its chemical speciation since insoluble Re species are only stable under very strong reducing conditions. Dolor et al. (2009) concluded that neither direct nor short-term indirect microbial processes involving iron and sulfate-reducing bacteria were likely to explain Re fixation in their sediments. Subsequent Re mobilisation may be attributed to the release of Fe- and OC-bound Re into soil porewater upon solubilisation of these phases since the increase in dissolved Re concentrations coincided with the increase in dissolved Fe and OC concentrations.

In contrast to Se and Re, mobility of I increased with incubation time for all soils. The continuous I mobilisation observed in the experiments may have been driven by development of anoxic conditions in microcosms. Such anaerobic conditions would be expected to result in iodide and organic I desorption from the soil (Schwehr et al., 2009; Yoshida et al., 2007; Yamaguchi et al., 2006; Sheppard and Thibault, 1992). In addition to I desorption, solubilisation of Fe and organically bound I is another important mechanism for I mobilisation from Sutton Bonington soils.

The rapid increase in U mobility observed for the arable topsoil upon flooding may be attributed to its carbonate content. The presence of dissolved carbonate in porewater has been found to increase the efficiency of soil U extraction (Zhou and Gu, 2005; Kohler et al., 2003). Zhou and Gu (2005) reported that leaching their U-

contaminated soils with varying concentrations (0 - 1 M) of $NaHCO_3$ extracted most of the U within the first 20 hours of the extraction, and extraction became very slow thereafter. The initial, rapid increase in U mobility in the arable topsoil conforms to the findings of Kohler et al. (2003) and Zhou and Gu (2005). The effect of redox status of the arable topsoil on U mobility appears to have been outweighed by the effect of complexation with carbonate. Uranium would be expected to form insoluble species (e.g. uraninite) as E_h fell in microcosms (Takeno, 2005) resulting in decrease in U mobility. However, presence of carbonate ions may have inhibited U immobilisation by complexing dissolved U, perhaps as uranyl, and forming soluble complexes such as $UO_2(CO_3)_2^{2-}$ (Barnett et al., 2000; Duff and Amrhein, 1996). In contrast, desorption of U from the arable subsoil and the woodland topsoil was limited, perhaps, due to the very low (undetectable) carbonate content of these soils. The increase in U mobility observed for the woodland soil after day 7 of the incubation was probably due to solubilisation of soil organic matter and Fe phases.

Overall, soil pH did not seem to have a strong effect on the mobility of the trace elements investigated in this work, probably due to soil buffering capacity. Only Se and I K_ds were strongly correlated with woodland soil pH. Soil pH may have affected the mobility of these elements indirectly by solubilising soil organic matter. The rise in soil pH drives solubilisation of soil organic matter (Grybos et al., 2009; Kalbitz et al., 2000) and the subsequent release of organically-bound trace and major elements into soil porewater. In fact, this can also be inferred from the significant, negative correlation between K_ds of most elements and the concentration of DOC in the porewater, which is an indicator of soil organic matter solubilisation. Organic matter is an important binding phase (i.e. a sink) for Se (Weng et al., 2011; Gerla et al., 2011), I (Shimamoto et al., 2011; Schwehr et al., 2009; Whitehead, 1974) and U

(Vandenhove et al., 2007) in soils. On the other hand DOC, in particular humic acids, may enhance the mobility of Se (Weng et al., 2011), hinder sorption of U (Bednar et al., 2007), complex reduced U (Gu et al., 2005) or promote its dissolution (Luo and Gu, 2009). In contrast, I K_d decreased over time irrespective of the change in DOC concentrations (Fig. 3-12), particularly over the first week of the incubation. Rather, I K_d was strongly correlated with porewater Fe concentrations, implying that soil Fe, rather than OC, phases such as hydrous ferric oxides are major binding phases for I in these soils, particularly in the arable soils which had near neutral pH. This is consistent with previous findings reported on I sorption by soils (Whitehead, 1984; Whitehead, 1973) and by Fe oxides (Nagata and Fukushi, 2010; Nagata et al., 2009).

E_h is a notoriously difficult parameter to measure empirically and it varies spatially and temporally in natural environments such as soils. Throughout the incubation experiments reported here, the value of soil E_h varied according to the method of measurement. Values obtained using Pt electrodes permanently installed in the soil were substantially different from those obtained using the combined electrode or estimated using Nernst model and porewater Fe concentrations in column microcosms. There was strong evidence that Pt electrode measurements made in this study were unreliable. This was supported by the divergence of Pt E_h readings for the arable top and subsoils from those of the combined electrode (Fig. 3-15). Although E_h readings of both methods were initially identical, Pt E_h readings fell rapidly over time. On average (over three incubation weeks), Pt E_h readings were c. 0.3, 0.6 and 0.2 V lower than the combined electrode readings for arable topsoil, arable subsoil and woodland topsoil, respectively.

Testing some of the working Pt electrodes after removal from the microcosms indicated that they were malfunctioning. This deterioration may have been due to ingress of solution past the epoxy resin seal resulting in loss of insulation. Water ingress into the platinum-aluminum-copper joint would allow corrosion, resulting in erratic readings of electrical potentials. Fiedler et al. (2007 and references therein) reported this problem with permanently installed Pt electrodes during field studies. In fact, removal of epoxy resin seal from my Pt electrodes in the present study resulted in a substantial decrease in the measured potential ($E_{measured}$) of the standard solutions (Fig. 3-15). Nernst E_h estimates should be used with caution since many of the underlying assumptions rarely hold true in nature. In particular, redox reactions are often at disequilibrium and irreversible, and electron shuttling may be hindered by some activation energy barriers (Stumm and Morgan, 1996). Another conceptual uncertainty is connected with the Fe solubility. Calculations assume that the solubility of Fe is governed by $Fe(OH)_3$, with phases such as goethite (FeOOH), magnetite (Fe_3O_4), siderite ($FeCO_3$) and pyrite (FeS_2) not considered. Added to the conceptual uncertainty is uncertainty associated with the thermodynamic database of the WHAM geochemical code which was used to estimate dissolved Fe activities in the aqueous phase.

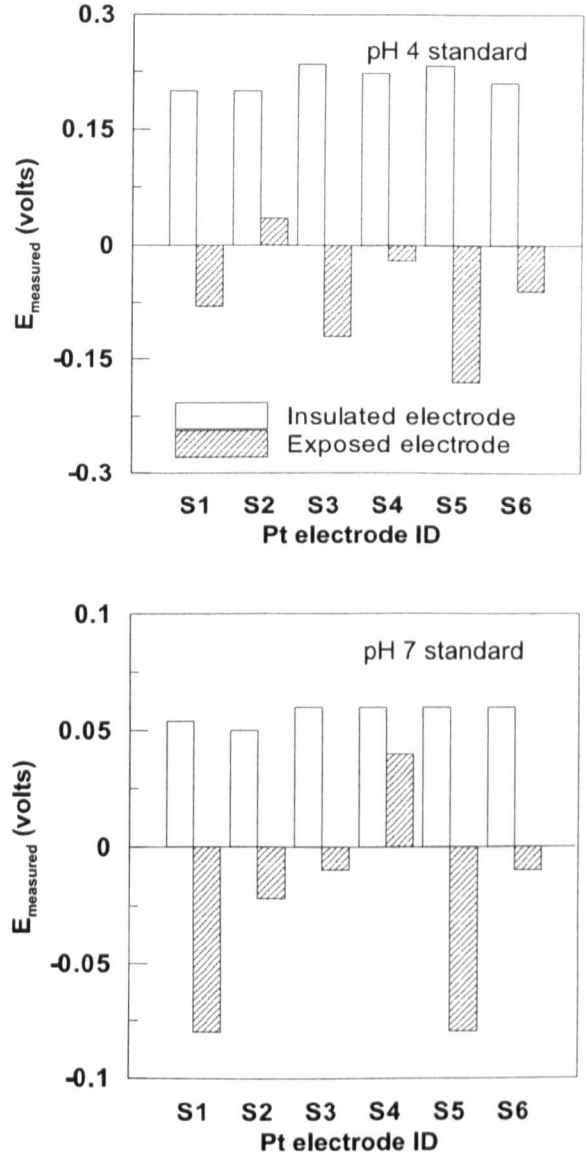

Fig. 3-15 Change in the performance of Pt electrodes after removal of electrode sealant. 'insulated electrode' bars represent potential values measured using intact Pt electrodes while 'exposed electrode' bars represent values measured using the same electrodes after removing the sealant.

The range of E_h values obtained by the Nernst model and the combined electrode is consistent with the range of redox potentials (0.7 to -0.3 V) in natural soils (Sparks, 2003). High E_h in the acidic woodland soil after 7, 14 and 21 days exemplify situations where estimated (Nernst estimates) and measured (the combined electrode) data differ. One possible explanation for this divergence is the fact that Nernst E_h values were calculated from Fe concentration in 0.1 µm (Rhizon) porewater filtrates. As the results of the filtration experiment showed (Fig. 3-7), porewater Fe concentrations decreased as the pore size of the membrane filter decreased. This would underestimate the calculated E_h values. It should be mentioned that none of the E_h (both Nernst-derived and measured) values was pH adjusted. Although such an adjustment could be implemented using a conversion factor of -59 mV per unit pH (e.g. Bohn et al., 2001) to convert E_h to a common pH, this conversion is, however, invalid for oxidation/reduction reactions where the electron to proton stoichiometric ratio is different from unity. For the redox reaction (reductive dissolution of iron hydroxide) assumed to control iron solubility in soil solution for Nernst-derived E_h this ratio is 1:3.

Despite the limitations of measured and estimated E_h values, the increase of porewater Fe concentrations over time qualitatively confirmed the progression of anoxia in the sacrificial and column microcosms. The E_h range 0.1 to 0 V defines Fe reduction in the redox cascade (Sparks, 2003). It can be inferred from porewater Fe concentrations that the geochemical conditions within the columns shifted towards anoxia at a faster rate than they did within sacrificial microcosms. The use of permeable Parafilm as a sealant and the relatively small size of the sacrificial microcosms compared to the columns will have allowed diffusion of atmospheric

oxygen into the soil. As a result, geochemical conditions within the sacrificial microcosms were less anoxic than in the closed columns.

Overall, the choice of experimental setup (i.e. microcosm design, porewater separation and filtration methods) did not seem to have a significant effect on K_ds of Se, I, Re and U. However, the fact that column and sacrificial designs differed not only in porewater separation techniques but also in many other respects (geochemical conditions within the microcosms, porewater sampling scheme and filtration methods) rendered the direct comparison between their K_ds difficult. For example, sacrificial microcosms were sacrificed, i.e. sampled once, in order to extract porewater whereas porewater was frequently sampled from the columns (daily over the first week). Therefore it was necessary to replenish the solution removed in order to maintain their moisture content. This procedure might have diluted the concentrations of the trace elements in solutions in columns. The apparent increase in K_d over time during the first week of the experiment may have been a consequence of depletion of the limited labile (exchangeable) pool due to successive sampling of soil solution from the columns and addition of ultrapure water to maintain the moisture content of the columns and the slow resupply from the non-labile pool in the solid phase.

To assess the significance of this dilution effect on K_ds, changes in the porewater concentrations of trace elements over the first incubation week were predicted by applying mass balance principles. It was assumed that the porewater concentrations were controlled solely by sampling losses. The initial porewater concentrations were calculated from concentrations measured in the first porewater samples collected 24 hours after soil wetting. Time series of these calculated concentrations were constructed and compared against time series of measured values. Comparison

between measured and predicted porewater concentrations shows discrepancies between the two quantities (Fig. 3-16 to Fig. 3-19) suggesting a dilution effect cannot entirely explain the higher K_d values for columns compared to those determined using the sacrificial method. There are clearly other biogeochemical factors involved, perhaps chemical speciation and sorption onto solid phases. Results also suggest that desorption of the soil water-soluble Se and Re was relatively rapid. In contrast, I desorption extended over several days. Steady-state porewater U concentrations in the carbonate-free soils (arable subsoil and woodland topsoil) were achieved within few days. These observations are consistent with the findings of previous research on Se (Tolu et al., 2011; Zhang and Moore, 1996), Re (Tagami and Uchida, 2008) I (Ishikawa et al., 2010; Hou et al., 2003; Sheppard and Thibault, 1992) and U (Zhou and Gu, 2005). Another respect in which the sacrificial and column designs differed is the redox conditions which might explain the difference in their K_ds, especially those of the redox sensitive elements (Se and I). Selenium speciation in the oxic soil porewater was probably dominated by the soluble selenate and organic Se species especially in the organic woodland soil (Zhang et al., 1999; Zhang and Moore, 1997a; Zhang and Moore, 1997b). As the E_h in the columns dropped to values at which selenate is unstable (0.285 to 0.25 V), selenate might have been reduced to selenite (Zhang et al., 2004) which has a high K_d due to its affinity to soil solid phases (Ashworth et al., 2008; Ashworth and Shaw, 2006c). Further soil reduction (-0.01 to -0.04 V) would reduce selenite into colloidal (0.2 to 0.4 μm) $Se^{(0)}$ (Zhang et al., 2004). These processes would result in high columns K_ds. Given their higher E_h, such Se speciation may have been limited in the sacrificial microcosms, and selenate, which has a low K_d, may have been the dominant species. Selenium behaviour in the woodland topsoil with respect to its

mobility did not conform to that in the arable soils. One possible explanation may be the continuous Se desorption stimulated by Se removal (sampling) from soil porewater. Also, Se (as selenite) adsorption onto soil phases might have been limited by the increase in the pH (Rovira et al., 2008).

Measured porewater I concentrations in the columns increased during the course of the experiment and it is probable that, in addition to desorption from the solid phase, porewater organic I transformed into iodide under the redox conditions encountered in the columns. This process may have been limited in the less anoxic sacrificial microcosms. Organic I and iodide are the dominant species in the porewater (Shimamoto et al., 2011; Yamaguchi et al., 2010; Sheppard et al., 1995). Organic I has a much higher K_d than iodide (Shimamoto et al., 2011; Ashworth and Shaw, 2006b; Ashworth et al., 2003); however, dissociation of porewater organic I can release iodide under anoxic conditions. This mechanism has been recently reported by Shimamoto et al. (2011) who also calculated iodide and organic I K_ds for flooded Japanese topsoils and found that organic I K_d was 2 times higher than that of iodide.

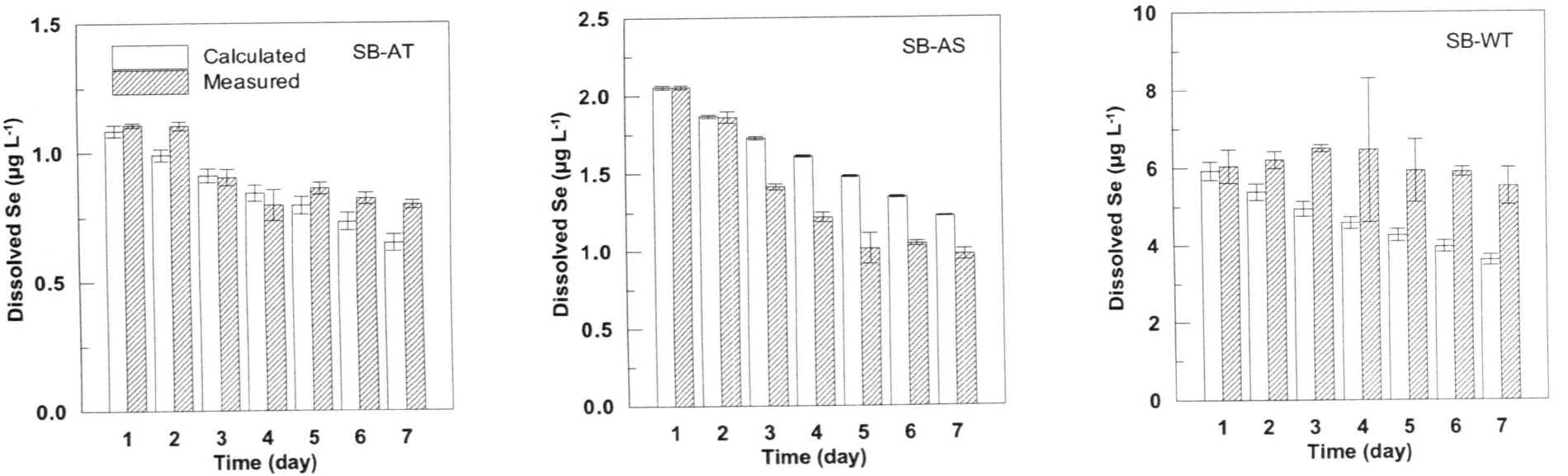

Fig. 3-16 Measured and calculated Se concentration in solution of SB (a) arable topsoil, (b) arable subsoil and (c) woodland topsoil incubated in mini columns as a function of time. Error bars represent standard errors of the means of single measurements from triplicate columns.

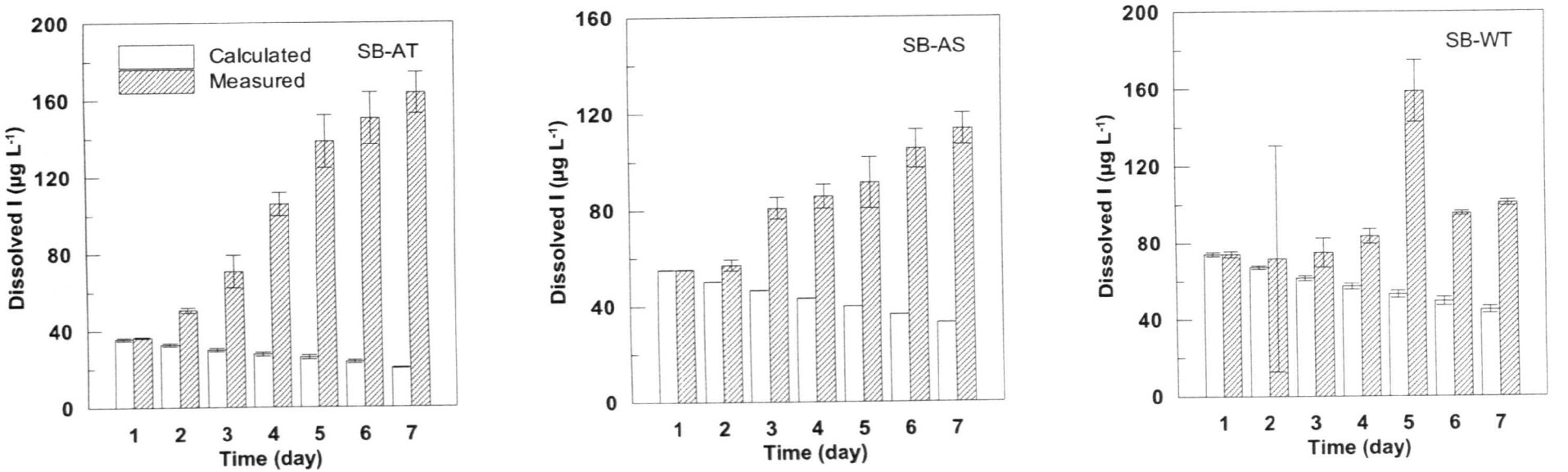

Fig. 3-17 Measured and calculated I concentration in solution of SB (a) arable topsoil, (b) arable subsoil and (c) woodland topsoil incubated in mini columns as a function of time. Error bars represent standard errors of the means of single measurements from triplicate columns.

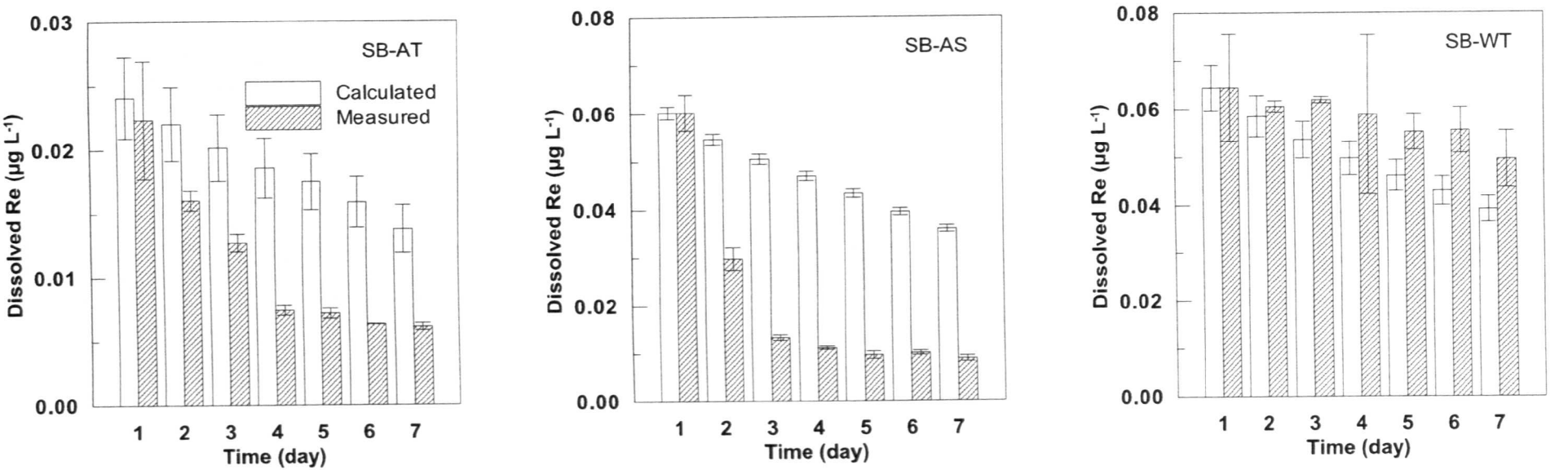

Fig. 3-18 Measured and calculated Re concentration in solution of SB (a) arable topsoil, (b) arable subsoil and (c) woodland topsoil incubated in mini columns as a function of time. Error bars represent standard errors of the means of single measurements from triplicate columns.

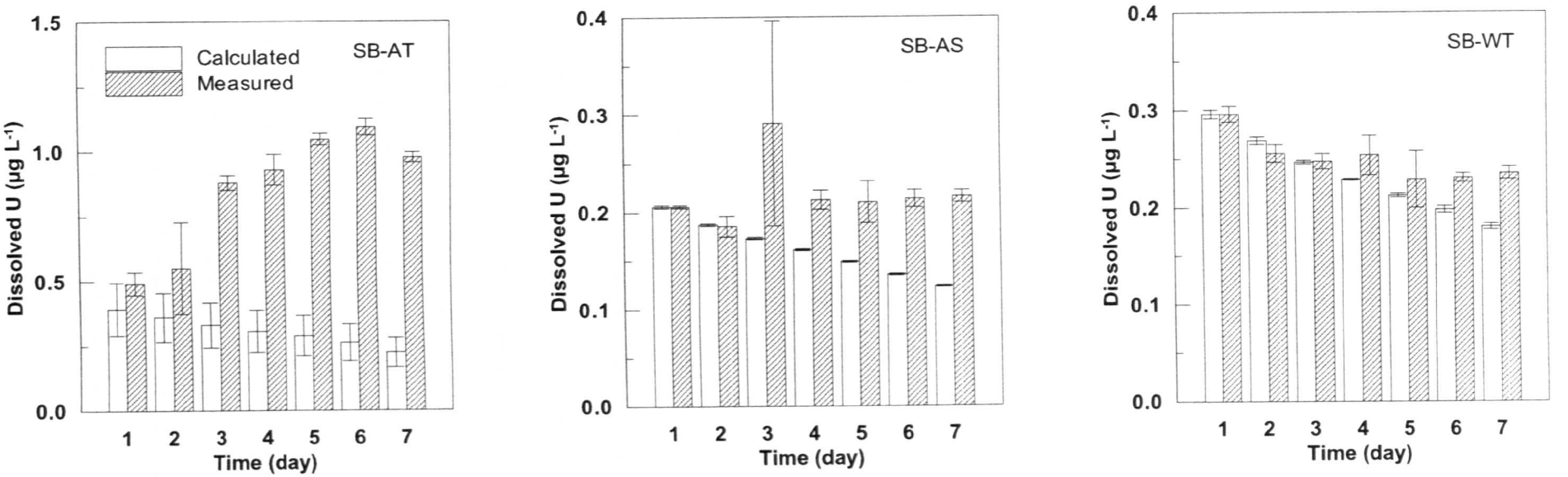

Fig. 3-19 Measured and calculated U concentration in solution of SB (a) arable topsoil, (b) arable subsoil and (c) woodland topsoil incubated in mini columns as a function of time. Error bars represent standard errors of the means of single measurements from triplicate columns.

The systematically higher sacrificial Re K_ds compared with the columns K_ds cannot be explained by differences in redox conditions between the two designs. Porewater Re, as ReO_4^- (Yamashita et al., 2007), can be immobilised by reduction to insoluble Re species such as ReO_2 (Yamashita et al., 2007) and ReS_2 (Chappaz et al., 2008). However, ReO_4^- is recalcitrant to chemical reduction even under Fe-reducing conditions (Maset et al., 2006). Although Re removal from the aqueous phase mediated by microbes is a possible pathway, Dolor et al. (2009) found that neither direct nor short-term indirect microbial processes involving sulfate and Fe-reducing bacteria were likely to explain Re fixation in sediments in their experiments.

The only significant difference between the sacrificial and column K_ds of U was observed for the limed arable topsoil. For this particular soil, redox conditions may have had a secondary role to that of carbonate equilibria in controlling U mobility. It is well known that dissolved U can form soluble complexes with carbonate/bicarbonate anions such as $UO_2(CO_3)_2^{-2}$ (Um et al., 2007; Zhou and Gu, 2005). In contrast to the sacrificial microcosms, which may have allowed for CO_2 exchange with the atmosphere through the permeable Parafilm, diffusion of CO_2, which is produced during microbial respiration, out of the columns might have been limited. As a result, the rise in CO_2 pressure within the columns would result in carbonate dissolution and production of bicarbonate. These conditions within the columns may give rise to lower U K_ds compared with the sacrificial values.

The experimental data indicated a strong correlation between porewater Fe and DOC (Fig. 3-9), which is probably attributed to Fe-humic substances (HS) complexes (Pédrot et al., 2011). The pore size of the membrane filters used to filter the porewater had a significant effect on dissolved Fe concentrations as well as Fe

K_d. The effect, however, was insignificant for DOC concentrations and OC K_d. These observations are consistent with the observations of Pokrovsky et al. (2006) who found a strong decrease in permafrost porewater Fe concentrations during ultrafiltration (5 μm, 0.22 μm, 0.025 μm, 10 kDa and 1 kDa) but no change in DOC concentrations. They concluded that Fe colloidal size was in the large 0.22 μm to 10 kDa while DOC was concentrated in the < 10 kDa fraction.

Overall, no significant variation in K_ds with membrane pore size (0.1, 0.22 or 0.45 μm) was observed for the trace elements and soils investigated in this study. This indicates that colloidal size < 0.1 μm contributed most to porewater trace element concentrations. This may be attributed to the low content (~6% v/v) of clay (< 2 μm) in Sutton Bonington soils and/or abundance of small-sized organic species in porewater. Research has shown that aquatic humic substances ranging from 0.1 to 1000 kDa, particularly low molecular weight humics, are effective in binding dissolved species of Se (Weng et al., 2011; Yamada et al., 1998), I (Shimamoto et al., 2011; Rädlinger and Heumann, 2000) and U (Graham et al., 2008; Singhal et al., 2005). The fact that OC, Se, I, and U K_ds, unlike Fe, were not affected by the pore size of the membrane filter suggests that the dissolved species of these trace elements were probably associated with low molecular weight DOC.

The experimental data suggested a strong and a highly significant ($p < 0.01$) effect of soil type on K_d (Fig. 3-10), this effect seemed to be more influential in determining K_ds than the choice of experimental design. For example, K_ds of Se, I, Re and OC determined for arable, grassland and woodland topsoils were higher than those determined for the subsoils by less an order of magnitude. This may be attributed to the higher organic matter content of these soils. Therefore, much of the K_d uncertainty can be attributed to variation in soil characteristics and mineralogy.

The slopes of the modelled versus measured K_d regression lines (Table 3-4) are smaller than 1 indicating that the parametric K_d models (Table 3-3) under-predicted K_d relative to the empirical values. Nash-Sutcliffe indices were considerably lower than one indicating poor predictive power of the models. This modest predictive power of the parametric K_d models may have been partially due to that fact that the set of predictor variables considered were far from comprehensive. The environmental variables used as predictor variables characterise the soil aqueous phase with no reference to the solid phase (due to the limited types of soil investigated in this work). The empirical models, for instance, did not consider soil organic matter and mineralogy (e.g. texture, iron and aluminum content) which have been found to be significant soil parameters that improve the quality of the parametric K_d models (Gil-García et al., 2009; Sheppard et al., 2007). Therefore, the models derived from the empirical data and described here are perhaps more valuable when the K_d temporal variability, resulting from time dependent processes that affect soil solution characteristics, is of special interest. In contrast, most available parametric K_d models (e.g. Sheppard, 2011; Vandenhove et al., 2009b; Vandenhove et al., 2009a; Sheppard et al., 2009; Vandenhove et al., 2007; Sheppard et al., 2007) relate radionuclide K_d to environmental variables that characterise the soil solid phase, and hence they are valuable tools, if robust enough, for predicting radionuclides K_ds for different soils. The limited predictive capability of the parametric K_d models reported here also underlines the fact that K_d variability cannot be explained by simple relationships since trace element mobility in soils is influenced by many inter-correlated biogeochemical factors.

Nevertheless, DOC seemed to be a key K_d predictor variable for most of the trace elements investigated in this work highlighting the importance of soil organic

carbon as a binding phase. Solubilisation of the soil particulate OC in response to changes in soil saturation and redox status resulted in an increase in the mobility of OC-bound trace elements (negative coefficients for log DOC in the models). The significance of soil organic matter content as a key environmental variable for K_d prediction has also been reported by Sheppard et al. (2009) and Gil-García et al. (2009) for I and Vandenhove et al. (2007) for U parametric K_d models.

Dissolved Fe concentration became more significant than DOC as a predictor variable in the case of I suggesting, perhaps, a higher affinity of this element to Fe minerals of Sutton Bonington soils. The increase in porewater Fe concentration resulted from reductive dissolution of Fe minerals such as (oxy)hydroxides which release their trace element contents into the porewater leading to a decrease in K_d (negative coefficients for log Fe in I model). Correlation between I K_d and the content of solid phase Fe in soils has also been reported in the literature (Gil-García et al., 2009). The reported correlation, however, was positive indicating that soils with higher Fe contents had higher sorption capacities for I whereas the negative correlation observed for Sutton Bonington soils indicates the concomitant solubilisation of soil Fe and I which enhanced I mobility.

Soil pH was identified as a significant environmental variable that partially explained the variability in the empirical I K_d dataset. This contrasts with the parametric models of Gil-García et al. (2009) who found no significant effect of soil pH on I. The negative coefficient for soil pH in the model also contradicts the positive correlation reported by Sheppard (2003) and the model of Sheppard et al. (2009) which positively correlated log K_d of I to the product of soil pH and clay content. The linear decrease in U log K_d with soil solution pH reported here is

consistent with previous studies (Sheppard et al., 2009; Sheppard et al., 2007; Echevarria et al., 2001)

3.5. Conclusions

Response of soil physicochemical attributes to an inundation event (e.g. rise of a water table) was simulated in the laboratory using two designs: (a) sacrificial and (b) column microcosms. With respect to the practical aspects of the two designs, the sacrificial microcosms were easy to prepare and handle compared with the columns. This design was more flexible regarding porewater filtration although porewater extraction by ultracentrifugation was laborious. The sacrificial design circumvented the problem of porewater dilution encountered in the columns. Unlike the columns, the sacrificial design may not be appropriate for kinetic studies designed to obtain information by repeated sampling at different times during the experiment as this would require high levels of replication.

Following soil wetting, redox potential (E_h) dropped indicating progression to anaerobic conditions. Three different methods were used to characterise soil redox conditions: (a) permanently installed platinum (Pt) electrodes, (b) a combined Pt electrode, and (c) estimation of E_h using porewater Fe concentrations (Nernst model). The E_h could not be precisely quantified and its value was very sensitive to the method used. Prolonged exposure of Pt electrodes to soil affected their performance such that their readings were systematically lower than those obtained using the other two methods. Estimates of E_h based on the Nernst model were higher than the E_h measured with Pt electrodes; however, there are many considerations that can limit the interpretation of Nernst estimates. For instance, measured porewater Fe concentration decreased as the pore size of membrane used to filter porewater samples decreased. As a result, E_h estimated using Fe concentration in solution samples obtained using the Rhizon samplers may have underestimated its values in the column microcosms. Whilst the combined Pt electrode circumvented

the limitations of the *in-situ* Pt electrodes and the thermodynamically estimated (Nernst) values, their invasive nature (it had to be inserted half-way into the soil) may be undesirable. Nevertheless, redox conditions in sacrificial and column microcosms were characterised qualitatively by monitoring the change in the concentrations of the redox marker, Fe, in porewater. The data indicated a difference in redox potential between the two microcosm designs; the sacrificial microcosms were less anaerobic than the columns and their progression to anaerobic conditions was slower.

K_d varied depending on experimental design (methodological variability). This variation may be attributed to geochemical factors; particularly the influence of redox conditions within the microcosms on trace element speciation and dissolution of binding Fe and OC phases. For instance, under anaerobic conditions Se became less mobile while I mobility increased. Differences between sacrificial and column K_d of these elements conformed to their redox chemistry. The maximum observed variation between sacrificial and column K_ds was less than one order of magnitude. K_d was insensitive to the pore size (0.1, 0.22 and 0.45 μm) of the membrane filter used to filter porewater. As a result, use of Rhizon samplers (0.1 μm) in this work may have had little or no effect on K_d. However, only dissolved Fe concentrations decreased as the filtration membrane filter pore size decreased indicating a strong size distribution of Fe in the range 0.1 - 0.45 μm. The fact that DOC, Se, I, Re and U was not affected by the size of membrane pores suggests a potential role of low molecular weight DOC in mobilising these trace elements in subsurface environments.

Soil characteristics were identified as another source of variation in K_d (spatial variability). Variation in K_d due to variation in Sutton Bonington soil characteristics,

however, did not exceed one order of magnitude. In fact, the effect of soil type on K_d was more significant than that of the methodological variability although a strong interaction between the experimental design and the soil type was observed. For example, the highest Se and I sacrificial K_ds were measured for the organic arable, grassland and woodland topsoils, whereas the lowest column K_ds were those measured for the woodland topsoil. Again, this effect of experimental design could be due to differences in geochemical conditions within both microcosm designs and their effect on processes such as chemical speciation, sorption and reductive solubilisation of soil minerals (e.g. Fe oxy-hydroxides) and organic phases. These processes control K_d temporal changes (temporal variability). Solubilisation of soil OC was associated with mobilisation of Se, I, Re and U particularly in the organic woodland soil. This underscores the importance of soil organic matter as a source for trace elements, including radionuclides, in organic soils under flooded conditions.

Despite the fact that predicting K_d from basic soil properties is desirable for many practical reasons, the application of such a concept remains fairly challenging. Development of K_d predictive models from soil pH, DOC and Fe was attempted for a limited soil set. The predictive power of these models, however, was modest and highlighted the need for a larger population of soil samples with a range of characteristics in order for the model to be adequately comprehensive and predictive. Therefore, in order to investigate the effect of spatial variation of soil properties on K_d and model predictions, the parametric K_d models developed by Sheppard et al. (2009) were used in the present work to estimate K_d values at different soil depths. This is addressed in detail in the next chapter.

Chapter 4 Development of the RIGEMA modelling approach

4.1. Introduction

Compartmental biosphere models have become an essential tool for assessing the long-term radiological risks associated with potential releases from geological repositories of radioactive waste. The conception and structure of these models are straightforward. A compartmental biosphere model is a representation of the biosphere whose components (e.g. soil, lake, vegetation, humans, etc.) may be represented by single and/or multiple compartments. Radionuclides are released into this biosphere system from a source and migrate within and between these compartments driven by a number of mechanisms which can include water, gas and biologically-driven material fluxes. Retardation of radionuclide migration and its accumulation within the soil is primarily controlled by sorption.

The structure of compartmental biosphere models for radiological assessments has not evolved much over recent years. Furthermore, although a model's structure has a profound effect on its predictions, the choice of its number of compartments and the resolution of these compartments are rarely justified. For example, the review of a number of available models for modelling vertical transport of radionuclides in soils and sediments shows that a clear and transparent criterion for the discretisation of a soil column (i.e. thickness of the soil layer)

is lacking. It is a common practice to discretise biosphere compartmental models on a rather arbitrary basis with little or no justification (Klos, 2010; Klos, 2008; Karlsson et al., 2001; Bergström et al., 1999).

Soil layer thickness adopted by such models influences the residence time and dispersion of radioactivity within the soil column (Smith and Elder, 1999; Kirchner, 1998; Boone et al., 1985). The residence time of a radionuclide within the system is proportional to the thickness of the soil layer; i.e. a radionuclide resides longer in a thicker layer. Consequently, the numerical dispersion effect, which is an artefact of the modelling process, increases in proportion to layer thickness (Smith and Elder, 1999). It follows that the number of model layers cannot be arbitrarily chosen (Kirchner et al., 2009; Smith and Elder, 1999; Kirchner, 1998).

Another source of concern regarding available compartmental biosphere modelling approaches relates to the characterisation of soil hydrology. Hydrological fluxes (measured and/or estimated) are a prerequisite for modelling radionuclide dynamics within the system. Nevertheless, characterisation of soil hydrology as part of the biosphere modelling has usually been simplistic. Often, biosphere models for radiological impact assessments (Klos, 2010; Klos, 2008; Avila et al., 2006; Avila, 2006b; Avila, 2006a; Karlsson et al., 2001; Bergström et al., 1999) have employed the principles of mass balance to calculate the direction and magnitude of soil water fluxes and the degree of soil saturation. Whilst this is convenient given the long timescales associated with radiological risk assessments; the mass balance approach has limitations. For example, Dripps and Bradbury (2007 and references therein) recommend a daily time step to avoid budget calculation errors in water balance models; they suggested monthly time steps may lead to as much as 25% errors in recharge calculations. Furthermore, an annual mass balance approach can cause

seasonal hydrological variability to be overlooked; one consequence of this is it may underestimate upward water flow in wet environments where annual precipitation exceeds evapotranspiration.

This chapter describes the process of developing a physically calibrated compartmental modelling approach to simulate the vertical migration and accumulation of radionuclides in soils. The methodology combines the physically-based flow model of Richards (1931) and the generalised ecological modelling (GEMA) approach of Klos (2010; 2008). This combined approach is hereafter referred to as RIGEMA.

4.2. Alternative hydrological model formulations

Two candidate hydrological models were implemented. The first was an empirical model that could be readily integrated and run simultaneously with the radiological model. The performance of this hydrological model was then measured against a second model, the physically-based flow model of (Richards, 1931). Despite its rigorous foundations, Richards model was not the first choice because integrating the model into the compartmental radiological model was considered likely to be cumbersome.

4.2.1. A revised empirical water budget model

Water budget models have been widely used in groundwater recharge modelling and planning irrigation schedules for arable lands (Dripps and Bradbury, 2007; Liu et al., 2006; Kendy et al., 2003; Doorenbos and Pruitt, 1977). These models have also been suggested as practical alternatives to the more complex, physically-based

Richards model (Richards, 1931). However, one shortcoming of this approach has been the inadequate quantitative representation of the upward capillary flux term of the mass balance equation (Liu et al., 2006). Most recharge and irrigation models are concerned with gravity-driven water movement, and they pay less attention to capillary-induced flow. The migration of the radionuclides from the saturated zone upwards towards the soil surface is primarily driven by capillary rise, probably assisted by plant root uptake and translocation of both water (i.e. evapotranspiration) and radionuclides. Therefore, simulation of upward movement of soil water is important in the context of risk assessment of geological disposal repositories. A modelling approach was developed to simulate the upward capillary flow in response to transient changes in soil water conditions. The model operates on a daily time step, and includes various hydrological processes.

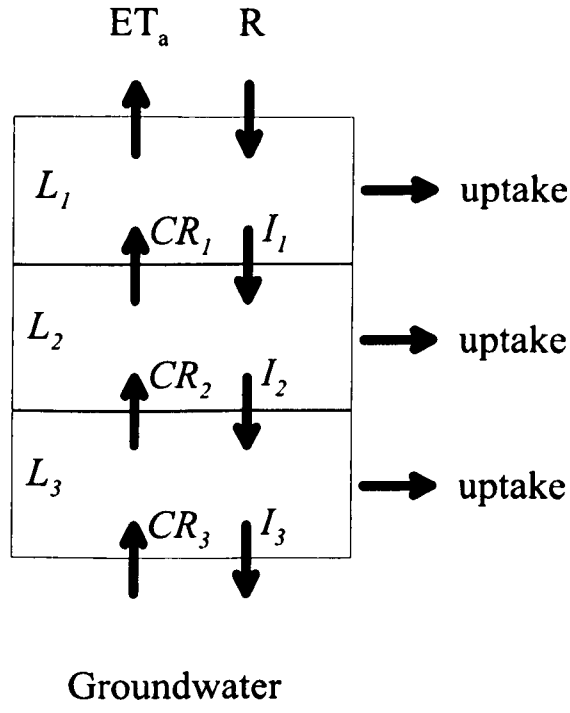

Fig. 4-1 A conceptual (compartmental) model of the soil column showing various water fluxes into and out of individual soil layers (L): rainfall R (m day^{-1}), evapotranspiration ET_a (m day^{-1}), capillary rise CR (m day^{-1}), infiltration I (m day^{-1}) and plant uptake (m day^{-1}).

During each daily time-step, surface water inputs (precipitation and/or irrigation) were added to the uppermost layer. The water in excess of the layer's maximum capacity (saturated level) was then distributed downward in a simple 'tipping bucket' fashion (Kendy et al., 2003) until all individual layers were filled to their maximum or all water had been distributed. Any extra water was then added to the groundwater (aquifer) as a recharge. The rate of change in water storage in the individual layers is the net difference between all inputs and outputs of water for that layer. The generic form of the soil water mass balance equation is given by:

$$\frac{\Delta\theta_i}{\Delta t} = \left(\sum_{\text{all inputs}} \text{inputs}_i - \sum_{\text{all outputs}} \text{outputs}_i \right) \Delta z_i \qquad (4\text{-}1)$$

where:

$\frac{\Delta\theta_i}{\Delta t}$	($m^3\ m^{-3}\ day^{-1}$)	rate of change in water content in the i^{th} soil layer
$\sum_{\text{all outputs}}$	($m\ day^{-1}$)	precipitation, irrigation, percolation, capillary rise
Δz_i	(m)	soil layer thickness

4.2.1.1. Percolation flow module

Water in excess of a soil layer's field capacity (i.e. water that cannot be held in place against gravity) percolates downward as a function of hydraulic conductivity and water content within a soil layer. The description of soil hydraulic conductivity was problematic because there are a variety of water release models of $K_{(\theta)}$ (e.g. van Genuchten, 1980; Brooks and Corey, 1964) which require a detailed description

of the soil hydraulic properties which was not available. An alternative was the approach of Kendy et al. (2003) and Wegehenkel (2005). This combines the principle of mass conservation and an exponential decay function:

$$\frac{d\theta_i}{dt} = \frac{K_{(\theta_i)}}{\Delta z_i} \qquad (4\text{-}2)$$

$$K_{(\theta_i)} = K_s \exp\left(\beta \frac{\theta_{s,i} - \theta_i}{\theta_{s,i} - \theta_{wp,i}}\right) \qquad (4\text{-}3)$$

where

K and K_s	($m\ day^{-1}$)	hydraulic and saturated hydraulic conductivities, respectively
$\theta_{s,i}$, $\theta_{wp,i}$	($m^3\ m^{-3}$)	soil water content at saturation (soil porosity) and at wilting point
β	(-)	dimensionless, adjustable parameter with a value between 13 and 16.

By substituting (4-3) into the mass conservation equation, separating variables and integrating, the volumetric moisture content $\theta_{t,i}$ of the i^{th} layer after infiltration is obtained:

$$\theta_{t,i} = \theta_{s,i} - \frac{(\theta_{s,i} - \theta_{WP,i})}{\beta} \ln\left(\beta \frac{K_{s,i}}{\Delta z_i (\theta_{s,i} - \theta_{WP,i})} + \exp\left(\beta \frac{\theta_{s,i} - \theta_{t-\Delta t,i}}{\theta_{s,i} - \theta_{WP,i}}\right)\right) \qquad (4\text{-}4)$$

Percolation Pr_i (m day^{-1}) from the i^{th} to i^{th}+1 layer was calculated as follows:

$$Pr_i = (\theta_{t-\Delta t,i} - \theta_{t,i})\,\Delta z_i \qquad (4\text{-}5)$$

4.2.1.2. Evapotranspiration module

Having distributed precipitation and/or irrigation water inputs through the flow domain, soil water storage was adjusted by subtracting evapotranspiration losses (ET_a). Potential evapotranspiration ET_P (m day^{-1}) was used directly if available, otherwise it was calculated using the Penman-Monteith formula (Allen et al., 1998).

Our model treated evaporation (atmospheric demand) and transpiration (vegetation demand) separately. The ET_P was divided into two components representing soil evaporation and plant transpiration following Beer's law and (Kendy et al., 2003):

$$E_p = ET_P \times \exp(-\kappa_b \times LAI) \qquad (4\text{-}6)$$

$$T_p = ET_P \times (1 - \exp(-\kappa_b \times LAI)) \qquad (4\text{-}7)$$

where E_p and T_p (m day^{-1}) are total potential evaporation and transpiration rates, respectively, κ_b is an extinction coefficient of radiation by the canopy (typically 0.39-0.63) (Feddes et al., 1978) and LAI is the leaf area index.

Distribution of evaporation and transpiration over the soil profile was assumed to follow an exponential pattern. Evaporation potentially removed water from depth

below the surface layer (Kendy et al., 2003) whereas transpiration removed water from all root-accessible layers. Total T_p and E_p were distributed between all layers according to Kendy et al. (2003):

$$u_{f,i}^{E} = \left(\frac{1}{1-\exp(-\delta)}\right)\left(\exp\left[-\delta\left(\frac{z_i}{z_L}\right)\right]\right)\left[1-\exp\left(-\delta\frac{z_i - z_{i-1}}{z_L}\right)\right] \quad (4\text{-}8)$$

$$u_{f,i}^{T} = \left(\frac{1}{1-\exp(-\delta)}\right)\left(\exp\left[-\delta\left(\frac{z_i}{z_r}\right)\right]\right)\left[1-\exp\left(-\delta\frac{z_i - z_{i-1}}{z_r}\right)\right] \quad (4\text{-}9)$$

where $u_{f,i}^{E}, u_{f,i}^{T}$ are evaporation and transpiration fractions, respectively, from the i^{th} layer defined by Z_{i-1}, Z_i (m) depths from the surface. δ is the water use distribution parameter, an empirical constant, which determines the curvature of the exponential function. Values of δ for most crops range from about 0.5 to 5.0 (Kendy et al., 2003). Because evaporation is usually more localised at the soil surface than transpiration, δ was assigned a value of 10 by Kendy et al. (2003), Z_L and Z_r (m) are total soil and rooting depths.

Potential evaporation and transpiration losses from the i^{th} layer during each time step were calculated from:

$$E_{P,i} = u_{f,i}^{E} \times E_P \quad (4\text{-}10)$$

$$T_{P,i} = u_{f,i}^{T} \times T_P \quad (4\text{-}11)$$

In each layer, the potential losses were restricted by water availability:

$$E_{a,i} = E_{P,i}\left(1-\frac{\theta_i}{\theta_{wp,i}}\right)^{-B_i} \quad (4\text{-}12)$$

$$T_{a,i} = T_{P,i}\left(1-\frac{\theta_i}{\theta_{wp,i}}\right)^{-B_i} \quad (4\text{-}13)$$

where B_i (m^{-1}) is the soil pore size distribution index.

4.2.1.3. Capillary flow module

A refined version of Doorenbos and Pruitt (1977) model was employed to simulate capillary flux within the flow domain (Liu et al., 2006). The empirical relationships of the model are applicable to a shallow groundwater table (<1.5 m) and low ET_a rates (≤4 mm day^{-1}). The magnitude of capillary flux G (m day^{-1}) is a function of soil hydrological properties, moisture content, ET_a, crop development stage and depth to water table:

$$\theta_{critical} = \frac{\theta_{FC}}{D_w^{b1}} \quad (4\text{-}14)$$

$$\theta_{steady} = \left(\frac{0.55\left(\theta_{FC}+\theta_{wp}\right)}{D_w^{b2}}\right) \quad (4\text{-}15)$$

$$G_{max} = \left(1-\exp(-0.6\times LAI)\right)ET_a \quad (4\text{-}16)$$

$$
\begin{aligned}
G_i &= 0 && \theta_i > \theta_{critical} \\
G_i &= G_{max}\left(\frac{\theta_{critical} - \theta_i}{\theta_{critical} - \theta_{steady}}\right) && \theta_{critical} \le \theta_i \le \theta_{steady} \\
G_i &= G_{max} && \theta_i < \theta_{steady}
\end{aligned}
\qquad (4\text{-}17)
$$

The magnitude of the capillary flux into a specific soil layer is controlled by the moisture content of the layer. Capillary flux is initiated when soil water content falls below a certain threshold. This threshold is a function of θ_{FC} (soil field capacity), D_w (m) (distance from the water table towards surface) and the empirical parameter b_1 which takes a value of -0.17 (Liu et al., 2006). The magnitude of the flux is assumed to be proportional to ET_a, (m day^{-1}); greater demand for water at the surface induces a higher flux. The flux, however, would reach a maximum, steady value G_{max} almost independent of ET_a but highly dependent on groundwater depth. When G_{max} is reached, soil moisture content assumes a steady value θ_{steady} which is a function of θ_{FC}, θ_{wp}, D_w and an empirical parameter b_2 which is assigned a value of -0.27 as recommended by Liu et al. (2006).

4.2.2. A physically-based water flow model (Richards equation)

Richards equation simulates variably saturated flow in porous media such as soils. It has a clear and sound physical basis, and has been used for a wide range of applications (van Dam and Feddes, 2000; van Dam et al., 1997; Vanclooster et al., 1996). Richards equation is:

$$\frac{\partial\theta}{\partial t}=\frac{\partial}{\partial z}\left(K_{(\theta)}\left(\frac{\partial h_{(\theta)}}{\partial z}+1\right)\right)-S_{(t,z)} \qquad (4\text{-}18)$$

where $K_{(\theta)}$ (m day^{-1}) is the soil hydraulic conductivity, $h_{(\theta)}$ (m) is the soil matric potential and $S_{(t,z)}$ (day^{-1}) is a sink term to account for soil water removal by plant roots (volume of water removed per volume of soil per unit time).

Soil heterogeneity, non linearity of soil hydraulic constitutive relationships (e.g. water release and retention curves) and changing boundary conditions are examples of complicating factors that make it imperative to solve Richards model numerically. HYDRUS 1D (Šimůnek et al., 2009; Šimůnek et al., 2008) is a freely available code designed for this purpose. It provides multiple choices of release and retention curves for users in the software library. For simulations in the present study, the frequently used and popular models of van Genuchten (1980) were used:

$$S_e=\frac{\theta-\theta_r}{\theta_s-\theta_r}=\begin{cases}1 & ;\ h\geq 0\\ \dfrac{1}{\left[1+|\alpha h|^n\right]^m} & ;\ h<0\end{cases} \qquad (4\text{-}19)$$

$$K_{(h)}=K_s S_{e(h)}^{\ell}\left[1-\left(1-S_{e(h)}^{1/m}\right)^m\right]^2 \qquad (4\text{-}20)$$

$$m=1-\frac{1}{n},\ n>1$$

where S_e is soil effective saturation, α, m and n are van Genuchten's model parameters and ℓ is a pore connectivity parameter, commonly given a value of 0.5 (Wheater et al., 2007; Mualem, 1976).

The sink term $S_{(t,z)}$ is calculated from potential evapotranspiration (ET_P). Roots are assumed to be exponentially distributed throughout the root zone and response of root uptake to water stress is simulated following the approach of Feddes et al. (1978).

4.3. Comparison of the hydrological models

Both the empirical (Liu et al., 2006; Kendy et al., 2003) and physically-based (Richards) models were used to simulate temporal changes in soil moisture content and water fluxes of bare land in North China Plain, 150 km south of Beijing, over a 300 days period. This site was selected for intercomparison of hydrological models because the empirical relationships of the capillary flux module described by Liu et al. (2006) were derived and validated using data obtained for the same site. In order to validate the empirical hydrological model used in their study, Liu et al. (2006) used observations from field experiments with winter wheat and summer maize cropped on silty soils in North China Plain. The site is characterised by a monsoon climate with a cold, dry winter and a hot, wet summer. Rainfall is scarce in winter but intense in summer. Potential evapotranspiration (ET_P) is low during winter (mid January ~5 mm day^{-1}) and high during summer (~60 mm day^{-1} in mid June). The experiments covered a range of climatic conditions and irrigation schedules. Liu et al. (2006) used observations of temporal changes (at 5 days interval) in groundwater table and soil moisture content at different soil depths over the growing season of winter wheat (9th October 1996 – 14th June 1997) and summer maize (20th June –

30th September 1997) used to assess the performance of their revised empirical water balance model. Specifically, 3 months observations (20th March – 15th June 1997) of weather conditions (rainfall and meteorological data for reference evapotranspiration calculations), soil moisture content and water storage in the root zone (0-1 m) were used as a basis for model validation.

Validating the hydrological models described in Section 4.2 using data reported in Liu et al. (2006) was not possible because many of the required parameters (e.g. meteorological data for calculating ET_0 and crop data such root depth and leaf area index) were not available from the original publication. Besides, it was decided to test the model's assumptions (its applicability to bare soil conditions) rather than evaluating its goodness of fit.

The time series of ET_p reported in Liu et al. (2006) was used as estimates of soil potential evaporation (E_p) to calculate actual daily evaporation (E_a) fluxes. Soil classification and hydrological properties needed to run the models are given in Table 4-1.

Table 4-1 Soil hydraulic properties reported in Liu et al. (2006) required by the empirical and physical hydrological models. Data was used as inputs to the models to predict changes in soil moisture content, water storage and water fluxes during the model-model comparison exercise.

Depth (m)	**Soil type**	**θ_s ($m^3\ m^{-3}$)**	**θ_{FC} ($m^3\ m^{-3}$)**	**θ_{wp} ($m^3\ m^{-3}$)**	**K_s (m day^{-1})**
0-0.7	Silt loam	0.48	0.37	0.17	0.13
0.7-1	Clay	0.51	0.43	0.28	0.18
1-2	Sand loam	0.46	0.32	0.09	0.24

The groundwater table is at a depth of c. 100 cm below the surface during April, dropping to 400 cm below the surface during July (Liu et al., 2006). For the model comparison exercise, an average groundwater table depth of 180 cm below the

surface was assumed. The variably saturated zone bounded by the groundwater table and the soil surface was modelled using 18 layers, each of which had a thickness (Δz) of 10 cm. Since the main objective of this exercise was to compare the two modelling methodologies, this thickness was judged to be sufficient for this purpose in order to keep the computational demand manageable. The empirical model was coded in the MATLAB programming language (MATLAB® 7.10, The MathWorks™). Richards flow model was solved using the HYDRUS-1D code. The hydrological parameters of both models were obtained from site specific data.

As simulation results showed, both modelling approaches could be used to simulate E_a, soil moisture content and water flux the dynamics. In general, E_a trends predicted by the two models were in reasonable agreement: both models showed a decrease in E_a in response to precipitation events and an increase in E_a after precipitation ceased (Fig. 4-2). Both models predicted increases and decreases in soil total water storage at similar points in time during the simulation. However, the empirical model under-estimated E_a relative to Richards model. Daily E_a, averaged over the entire simulation period (300 days) using the empirical model was 45% less than the Richards model predictions. Consequently, the empirical model over-estimated the cumulative water storage (summed over the 300-day period) in the soil column domain by 12% compared to Richards model (Fig. 4-3).

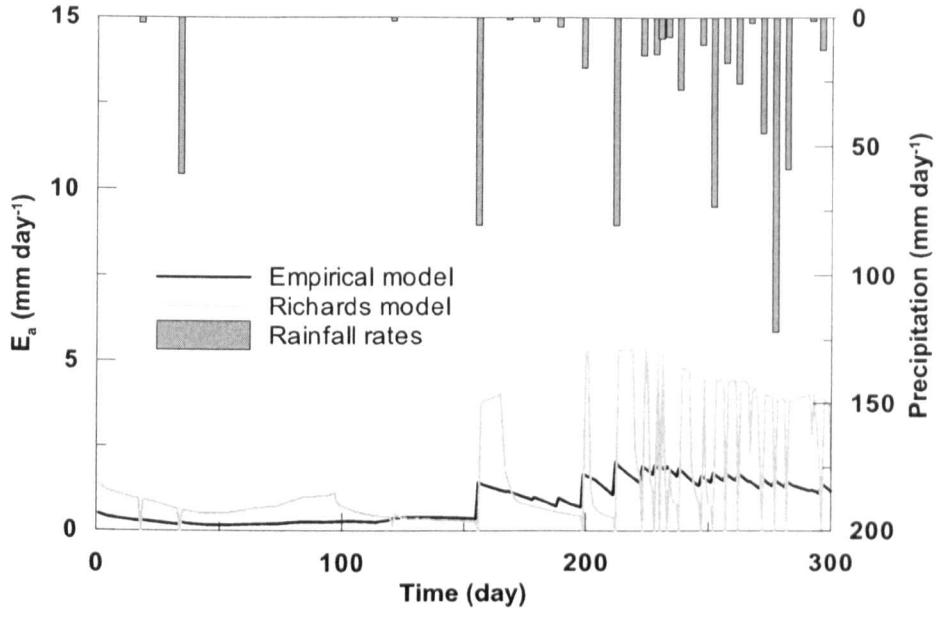

Fig. 4-2 Actual evaporation (E_a) from bare soil surface as a function of time in response to atmospheric conditions at Xiongxian, China calculated using the empirical and physical (Richards) hydrological models.

The most important difference between the two hydrological models was their ability to predict reliably the dynamics of soil water fluxes. Unlike the physical model of Richards, the empirical model, which assumes that capillary flux is assisted by plant root uptake and translocation of water (i.e. evapotranspiration), could not predict any capillary flux through the soil profile when no vegetation was present. Within the constraints of the empirical approach, the capillary flux is mainly driven by evapotranspiration; therefore, under bare soil conditions, i.e. LAI = 0, the empirical model failed to predict any capillary flux within the soil (Fig. 4-4). Obviously, this is a serious shortcoming of the empirical approach because it limited its applicability to soil with vegetative cover (i.e. LAI > 0).

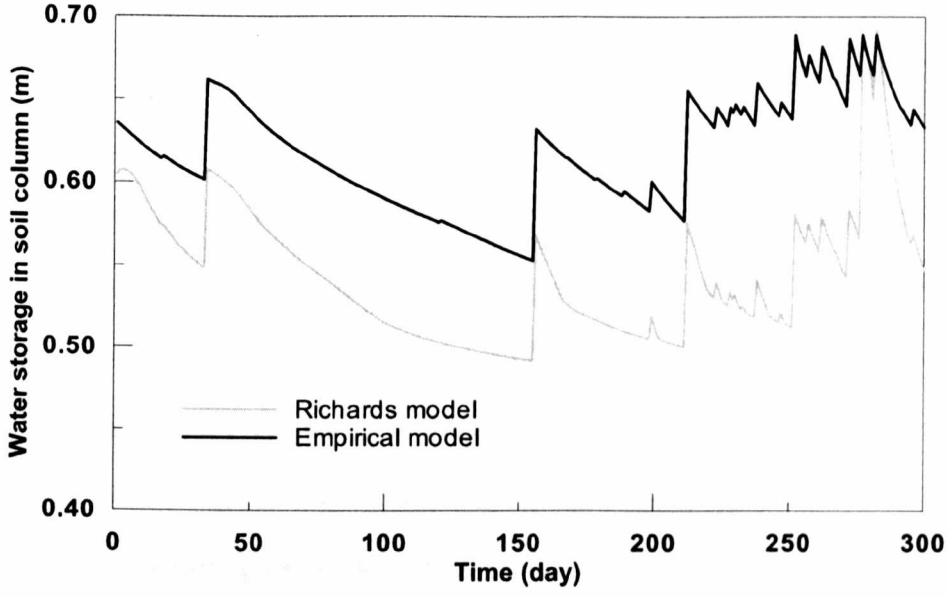

Fig. 4-3 Water storage in the bare soil column as a function of time in response to changes in atmospheric conditions at Xiongxian, China calculated using the empirical and physical (Richards) hydrological models.

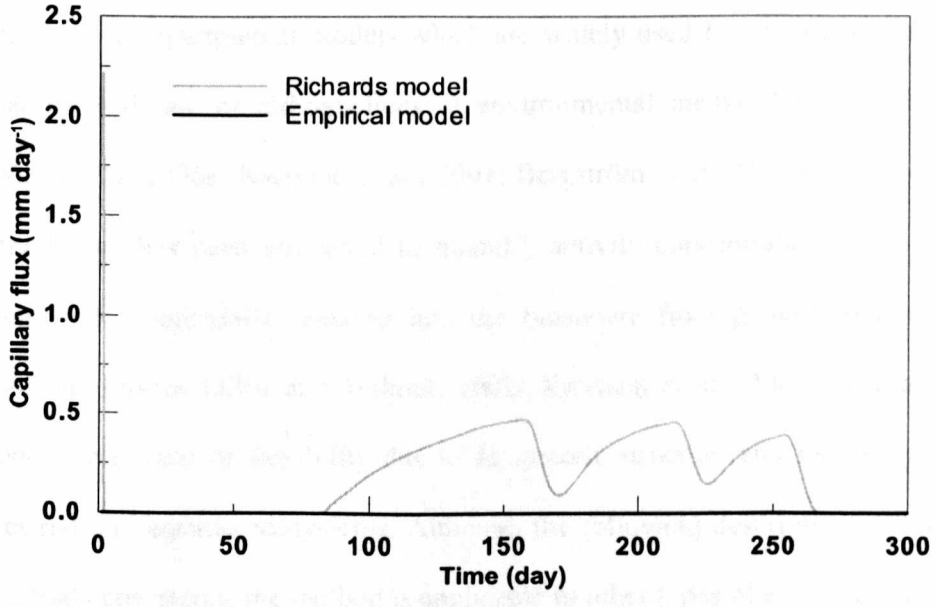

Fig. 4-4 Capillary flux through the lower boundary of the bare soil column as a function of time in response to changes in atmospheric conditions at Xiongxian, China calculated using the empirical and physical (Richards) hydrological models.

In real situations, capillary flux within soils still occurs even under bare soil conditions, and this is demonstrated by the results of the physical model. Richards model proved to be applicable even to bare soil conditions (Fig. 4-4). The integration of Richards flow model into the RIGEMA approach was expected to be cumbersome and computationally demanding, hence it was not considered as a first choice. However, the availability of the HYDRUS-1D code provided the necessary databases and the solver enabled its use in the modelling in this study. As a result, it was decided to adopt Richards model given its sound physical basis and proven reliability for hydrological modelling.

4.4. The Generalised Ecological Modelling Approach

The generalised ecological modelling approach, GEMA, (Klos, 2008) belongs to a family of compartmental models which are widely used for simulating long-term dynamics and fate of radionuclides in environmental media (Klos, 2008; Avila, 2006b; Avila, 2006a; Karlsson et al., 2001; Bergström et al., 1999). This modelling methodology has been employed to quantify activity concentrations of long-lived radionuclides potentially released into the biosphere from geological radioactive waste repositories (Kłos and Wilmot, 2002; Karlsson et al., 2001). The approach offers a great deal of flexibility due to its generic structure and its ability to link terrestrial and aquatic ecosystems. Although the following description is limited to terrestrial ecosystems, the method is applicable to other types of ecosystems.

In this version of GEMA, the soil column (biosphere) extended from the groundwater table up to the soil surface and was divided into a number of layers of equal thickness (Fig. 4-5), although the soil layers could have had different

thicknesses (the issue of model vertical resolution will be discussed in Section 4.5.2).

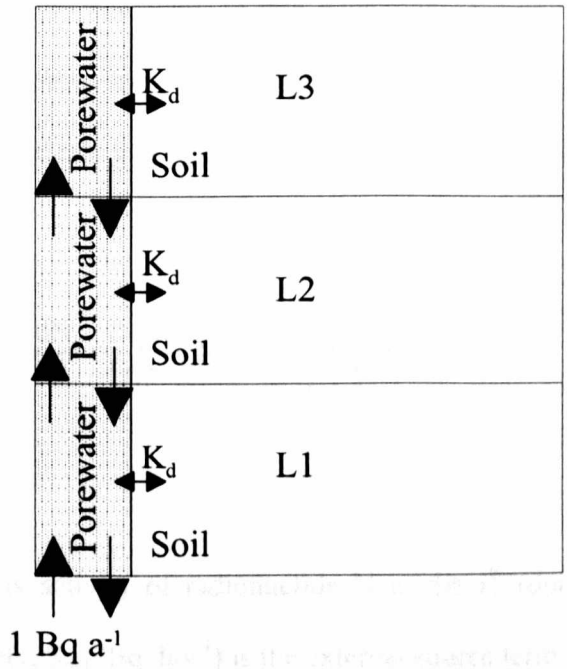

Fig. 4-5 A simple GEMA (radiological) model with 2 (solid and liquid) compartments and 3 soil layers (L1, L2 and L3). Vertical and horizontal arrows indicate water and radionuclide fluxes between soil layers and partitioning of radionuclides between solid and liquid phase, respectively.

A constant annual flux of radioactivity, 1 Bq a^{-1}, entered the system through the soil lower boundary. The use of constant inputs per year is a common practice that facilitates model-model comparisons and allows calculation of normalised input-dose conversion factors (Xu et al., 2008). The radioactivity introduced into the base of soil columns is transported within the soil profile via a number of processes that transfer both liquid and solid matter between the system layers. The relevance of these processes depends on the assessment context and endpoints, but any process which can be expressed in terms of a transfer rate constant can be represented.

Each model layer was represented by one state variable: total radionuclide concentration expressed in terms of liquid phase concentration. The state variables, which vary with time according to rate equations describing transport processes, represent total radioactivity in the respective layers. The system of inter-connected layers was translated into a system of ordinary differential equations (ODEs):

$$\frac{dN_i}{dt} = \left(\sum_{j,i} \lambda_{ji} N_j + S_{i(t)} \right) - \left(\sum_{j,i} \lambda_{ij} N_i + \lambda_N N_i \right) \qquad (4\text{-}21)$$

where $N_{i,j}$ (Bq) is activity of radionuclide N in the i^{th} (donor) and j^{th} (receptor) layers, respectively, $S_{i(t)}$ (Bq day^{-1}) is the external source term of radionuclide N into the i^{th} layer (this is applicable to the bottom layer only), λ_N (day^{-1}) is the decay constant of radionuclide N, $\lambda_{i,j}$ (day^{-1}) is the transfer rate constant between the i^{th} and j^{th} layers (Klos, 2008):

$$\lambda_{i,j} = \frac{1}{\Delta z_i} \left(\frac{F_{i,j} + K_{d,i} M_{i,j}}{\theta_i + (1 - \varepsilon_i) \rho_i K_{d,i}} \right) = \frac{F_{i,j} \left(1 + a \times K_{d,i} \right)}{\Delta z_i \theta_i R_i} \qquad (4\text{-}22)$$

$$\lambda_{i,j} = \sum_{k=process} \lambda_{i,j}^k \qquad (4\text{-}23)$$

where:

Δz_i (m) thickness of the i^{th} layer.

$F_{i,j}$ (m day^{-1}) water flux (liquid phase transport) from the i^{th} layer to j^{th} layer

$M_{i,j}$	(kg m^{-3})	soil flux from the i^{th} layer to j^{th} layer
K_{di}	(m^3 kg^{-1})	soil/porewater distribution coefficient in the i^{th} layer
ε_i	(-)	soil water content and porosity of the i^{th} layer
$\theta_{i,}$	(m^3 m^{-3})	soil water content of the i^{th} layer
ρ_i	(kg m^{-3})	material density of the i^{th} layer
a	(kg m^{-3})	suspended solid load in water
R_i	(-)	retardation factor in the i^{th} layer
$\lambda_{i,j}^{k}$	(day^{-1})	transfer rate between i^{th} and j^{th} over k processes

Water and solid material fluxes are the driving forces for transport of radioactivity within the soil (4-23). Dissolved radionuclides are carried with flowing water while radionuclides attached to very small soil particles can also be transported in the form of suspended solids in water.

$K_{d,i}$ is a key parameter that quantifies radionuclide attachment to the solid phase and accounts for retardation of radionuclide transport through the soil. GEMA implicitly assumes instantaneous partitioning of radionuclides between solid and liquid phases, the magnitude of which is a function of numerous interacting factors (e.g. soil moisture, organic matter content and redox conditions). These aspects of K_d have been addressed in the experimental section of this study, described in Chapter 3.

4.5. The integrated RIGEMA modelling approach

Richards (hydrological) and GEMA (radiological) models were integrated into one modelling framework referred to as RIGEMA. This approach was applied to

simulate long-term distribution of some groundwater-borne long-lived radionuclides hypothetically released into the soil column of the Sutton Bonington site. Details of the site (climatic and soil data) are given in the site description section in Chapter 5. As an illustration of this methodology, a simple scenario was simulated with two different discretisation schemes. The purpose of this simulation exercise was to illustrate the application of the discretisation protocol and the effect of time step size and soil layer thickness on radionuclide distribution patterns in the soil column.

First, the discretisation procedure was implemented to identify the optimum number of soil layers in the model. Having optimised its structure, the RIGEMA model was used to simulate the dynamics and distribution of ^{79}Se and ^{129}I in the soil column. A constant, continuous release of 1 Bq a^{-1} of ^{79}Se and ^{129}I into the base of the column was assumed. ^{129}I and ^{79}Se were selected due to their relevance to long-term risk assessment of geological disposal, and their distinct sorption properties. According to a recent IAEA report (IAEA, 2009), Se has a K_d (200 L kg^{-1}) that is 25 times higher than that of I (7 L kg^{-1}).

Transfer rate constants within the RIGEMA model were parameterised using soil water contents and fluxes, calculated using HYDRUS-1D code, and other physical and chemical input values (e.g. soil porosity, K_d, diffusion coefficient, etc.). For simplicity, the transport processes involved were limited to advection and dispersion. Dispersive transport was parameterised following the method of Xu et al (2008; 2007):

$$\lambda_{i,j} = \frac{1}{\Delta z_i^2}\left(\frac{\theta_i\left(\alpha_L \frac{F_{i,j}}{\theta_i} + D_m\right)}{\theta_i + (1-\varepsilon_i)\rho_i K_{d,i}}\right) \qquad (4\text{-}24)$$

α_L (m) and D_m (m^2 day^{-1}) are longitudinal dispersivity of the soil and molecular diffusion, respectively. All symbols retain their definitions described earlier.

RIGEMA was solved numerically using a 4th order Runge Kutta routine coded using the MATLAB language. The solution was verified using Ecolego software (Ecolego v.5.0.269, Facilia AB), a piece of software that is designed to perform similar simulations.

4.5.1. Temporal resolution and seasonal variability

RIGEMA operates on a daily time step, and its inputs are provided as daily values (monthly and annual inputs are also possible if outputs on these timescales are required). The sensitivity of model predictions to the resolution of input data and time step was tested. Daily as well as annual time series of moisture contents and water fluxes were used to quantify the model transfer rate coefficients, and the model was run with daily and annual time steps. Values of the hydrological variables were estimated using HYDRUS 1D.

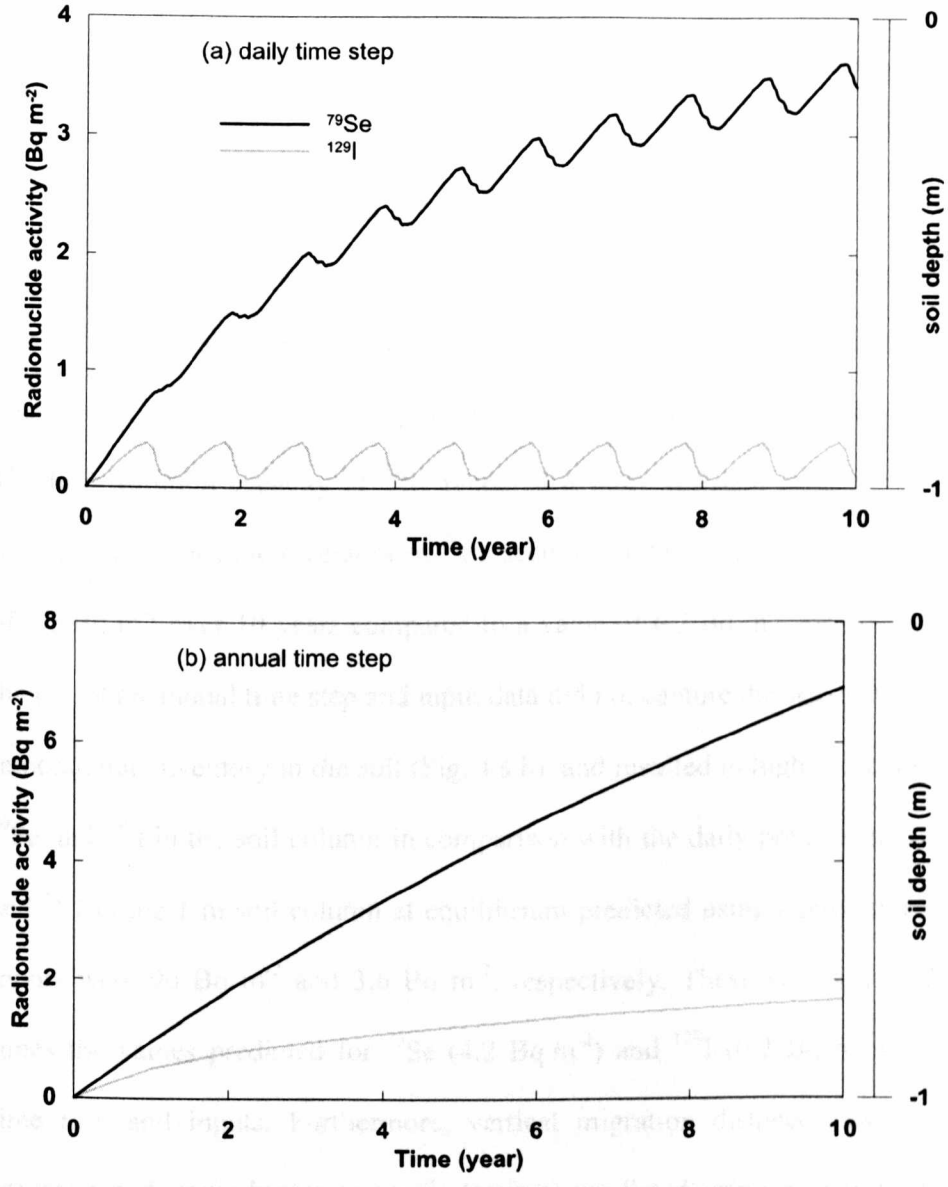

Fig. 4-6 Predictions of ^{79}Se and ^{129}I accumulation (total activity) within a 1 m bare soil column over a 10 years period using (a) daily and (b) annual time steps. Soil layer thickness was fixed at 1 cm.

Simulation results showed strong interactions between the dynamics of both hydrology and radioactivity. Fig. 4-6 show changes in total (sorbed and dissolved) inventories of ^{79}Se and ^{129}I within the soil column of bare land over 10 years.

Radionuclide inventory varied during the year in response to temporal changes in local hydrology and climatic conditions (Fig. 4-6 a). During wet seasons, when

gravity-driven water movement dominated, the poorly sorbing ^{129}I leached from the soil leading to a decrease in its inventory within the soil. In contrast, during dry seasons, soil content of ^{129}I increased in response to the higher evaporation and capillary flux. At equilibrium, the ^{129}I inventory during dry seasons of the year peaked at 0.4 Bq m^{-2} and dropped to 0.07 Bq m^{-2} (c. 440% decrease) during wet seasons. In contrast, the seasonal variability of the ^{79}Se inventory was less due to its higher K_d; ^{79}Se peaked at 4.4 Bq m^{-2} and dropped to 4.0 Bq m^{-2} (c. 10% decrease). The high sorption capacity of ^{79}Se rendered it more resistant to leaching from the soil column, hence the inventory of ^{79}Se accumulated to an approximate mean value of 3.5 Bq m^{-2} over 10 years compared to a value of 0.2 Bq m^{-2} for ^{129}I. In contrast, the use of an annual time step and input data did not capture the seasonal variation in radionuclide inventory in the soil (Fig. 4-6 b), and resulted in higher accumulation of ^{79}Se and ^{129}I in the soil column in comparison with the daily predictions. Total ^{79}Se and ^{129}I in the 1 m soil column at equilibrium predicted using annual time step and inputs were 96 Bq m^{-2} and 3.6 Bq m^{-2}, respectively. These values are 22 and 18 times the values predicted for ^{79}Se (4.2 Bq m^{-2}) and ^{129}I (0.2 Bq m^{-2}) using daily time step and inputs. Furthermore, vertical migration distances away from the contaminated groundwater reservoir (source) predicted using an annual time step were greater than those predicted on a daily basis; concentration - depth profiles of ^{79}Se and ^{129}I at equilibrium are presented in Fig. 4-7.

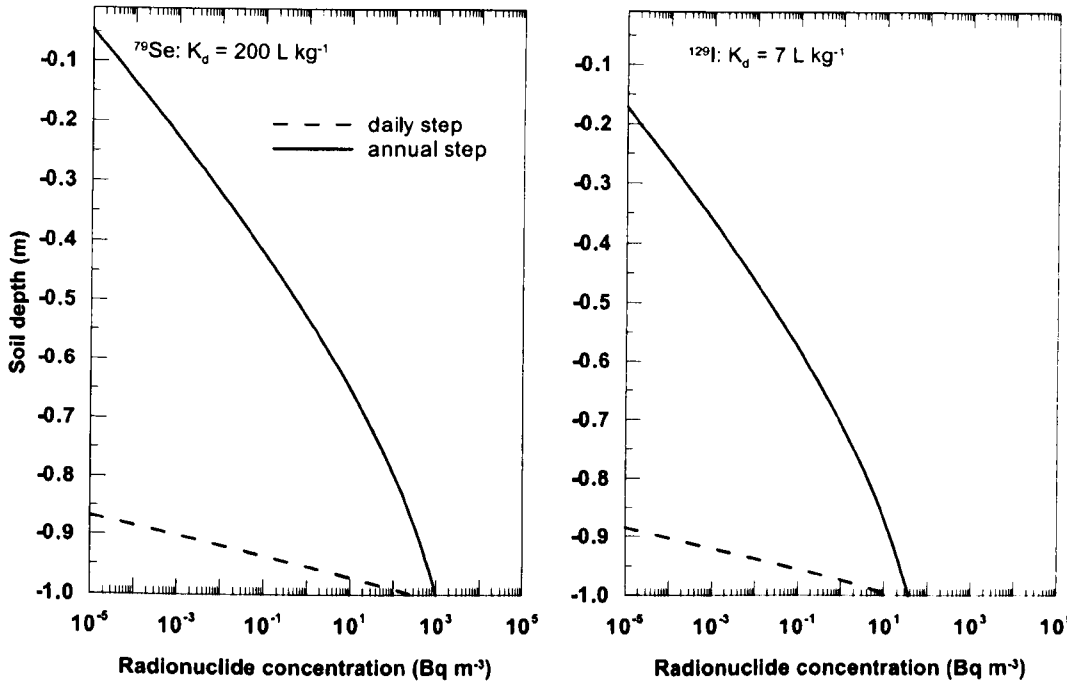

Fig. 4-7 Predictions of ^{79}Se and ^{129}I activity concentration - depth profiles at equilibrium (annual average) under bare soil conditions using daily and annual time steps. Soil layer thickness was fixed at 1 cm for all calculations (note the semi-log scale).

These differences between the daily and annual predictions reflect the pronounced effects of short-term variation in atmospheric and hydrological conditions on radionuclide transport in soils. Since total annual precipitation at Sutton Bonington exceeds total annual evapotranspiration, simulations of soil hydrology predicted net downwards infiltration and nil capillary rise throughout the soil column. Moreover, predictions on an annual basis showed ~ 100% decrease in annual percolation in comparison with simulations on a daily basis. This smaller percolation reduced leaching of radionuclides from the soil and resulted in slow accumulation and significant vertical diffusion-driven migration through the soil profile.

4.5.2. Effect of vertical discretisation on numerical dispersion

Soil hydrological conditions were simulated using HYDRUS 1D. Climatic conditions (4-year average of daily weather data collected between 2006 and 2010) and a static water table (pressure head h=0) at a depth of -100 cm were imposed as top and bottom boundary conditions, respectively. For the initial conditions, the matric potential profile was equilibrated in a preliminary simulation run for a period of one year with the soil column under hydrostatic (no-flow) conditions. The matric potential profile at equilibrium was then used for subsequent runs. Richards equation was solved repeatedly using three discretisation schemes (10, 1 and 0.5 cm).

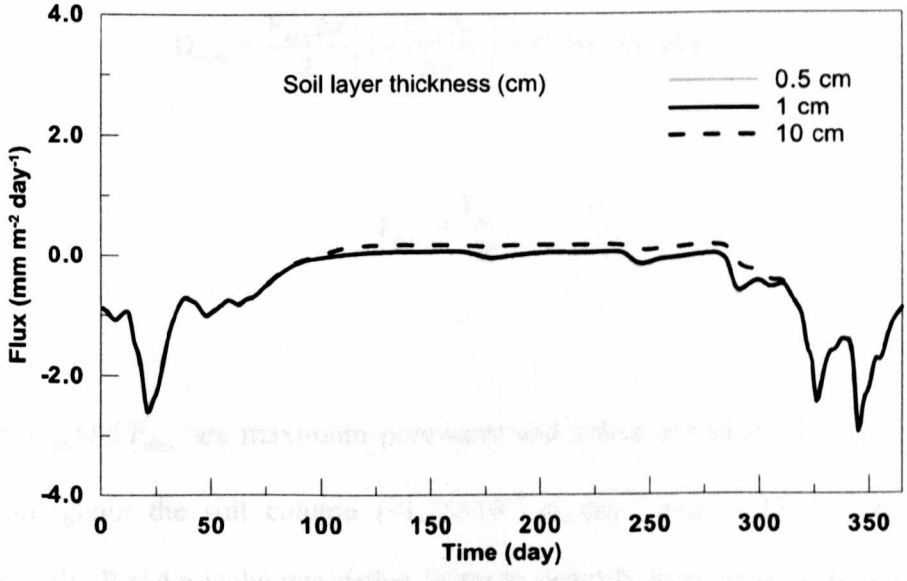

Fig. 4-8 Temporal changes in water flux through the bottom boundary of a 1 m bare soil column obtained by solving Richards hydrological equation for three soil layer thicknesses (see legend). Solutions using 1 and 0.5 cm thick soil layers are almost identical. Positive values represent capillary flux and negative values represent percolation through the bottom boundary of the 1 m soil column.

Fig. 4-8 shows soil water flux through the bottom boundary of the soil column over the one-year simulation period. No difference in the direction and magnitude of soil water flux was observed between the Δz = 0.5 cm and Δz = 1 cm schemes. Thus, it was decided that a soil layer thickness of 1 cm was sufficiently small (corresponding to a 100 layer model). This soil layer thickness is consistent with previously reported studies (Mathias et al., 2008; Butler et al., 1999; Kirchner, 1998).

The numerical dispersion coefficient D_{num} of the current model was calculated according to Smith and Elder (1999):

$$D_{num} = \frac{F'_{max}\Delta z}{2}\left(1 - \frac{F'_{max}\Delta t}{\Delta z}\right) = 7\times10^{-6}\ m^2\ day^{-1} \qquad (4\text{-}25)$$

$$F'_{max} = \frac{F_{max}}{R} \qquad (4\text{-}26)$$

where F_{max} and F'_{max} are maximum porewater and solute velocities during the year and throughout the soil column (~1.75×10^{-3} m day^{-1} and ~0.38×10^{-3} m day^{-1}) respectively; R = 4.6 is the retardation factor to quantify sorption of activity to solid phases calculated using a K_d value of 1 L kg^{-1} (this value represents a highly mobile radionuclide such as ^{36}Cl); Δz = 0.01 m is the thickness of the soil layers and Δt = 1 day is the time step. For the model numerical dispersion to be comparable to a representative estimate of the physical dispersion, the model numerical dispersion had to fulfil the following condition (which ensures that the numerical dispersion compares to a reasonable estimate of the effective dispersion):

$$D_{num} \approx \frac{\alpha_L \frac{F}{\varepsilon} + D_m}{R} \qquad (4\text{-}27)$$

where α_L (m) is the longitudinal dispersivity of the soil and ε (-) is soil porosity. The effective disperion coefficient ($\sim 10^{-5}$ m^2 day^{-1}) was computed using a value of 0.38×10^{-3} m day^{-1} for F' and parameters presented in Table 4-2.

Table 4-2 Parameters used to estimate the effective dispersion coefficient described by Smith and Elder (1999) which sets an upper limit on the numerical dispersion effect of the compartmental model.

Parameter	**Units**	**Value**	**Reference**
Molecular diffusion (D_m)	$m^2 day^{-1}$	$\sim 10^{-5}$	Assumed
Longitudinal dispersivity (α_L)	m	0.01	(Rausch et al., 2005)

The previous calculations assumed maximum porewater and advection velocities and a small retardation factor (due to the small K_d value). Consequently, the calculations represent a conservative assumption since the numerical and hydrodynamical dispersion coefficients are proportional to the retarded advective velocity. Therefore, criterion (4-27) is satisfied even for smaller retarded advective velocities. As a result, it was decided that the model with Δz = 1 cm was the optimum version that delivered a satisfactory solution of Richards model and maintained the numerical dispersion effect in line with effective dispersion.

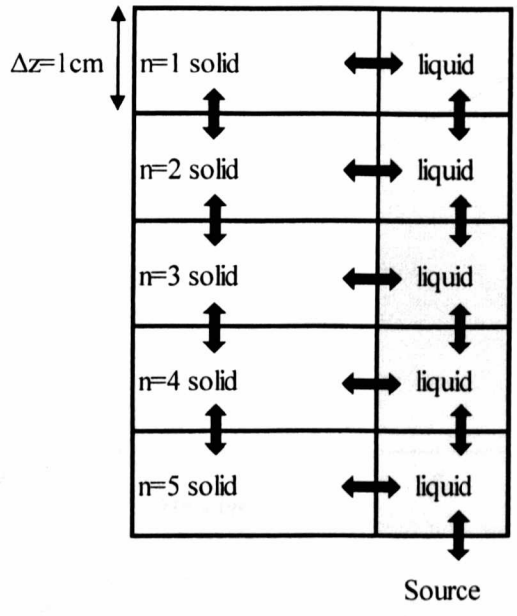

Fig. 4-9 A conceptual RIGEMA (integrated hydrological and radiological) model showing water and radionuclide transfers and phase partitioning between soil layers and solid and liquid compartments.

The importance of choosing appropriate discretisation to allow for the effect of numerical dispersion is illustrated in Fig. 4-10 and Fig. 4-11. Increasing the soil layer thickness used in the model by tenfold resulted in an increase in the time required to achieve steady state conditions in the soil with respect to radionuclide inventory due to the decrease in transfer rates which are inversely proportional to the soil layer thicknes (4-22) and (4-24). Increasing the thickness also resulted in higher inventories and greater vertical migration distances of ^{79}Se and ^{129}I in the soil column. The steady-state inventories of ^{79}Se and ^{129}I predicted using a layer thickness of 10 cm were 18 and 26 times, respectively, those predicted using a thickness of 1 cm. This can be attributed to the complete, instantaneous mixing assumed by compartmental models and the numerical dispersion effect which increases as soil layer thickness is increased.

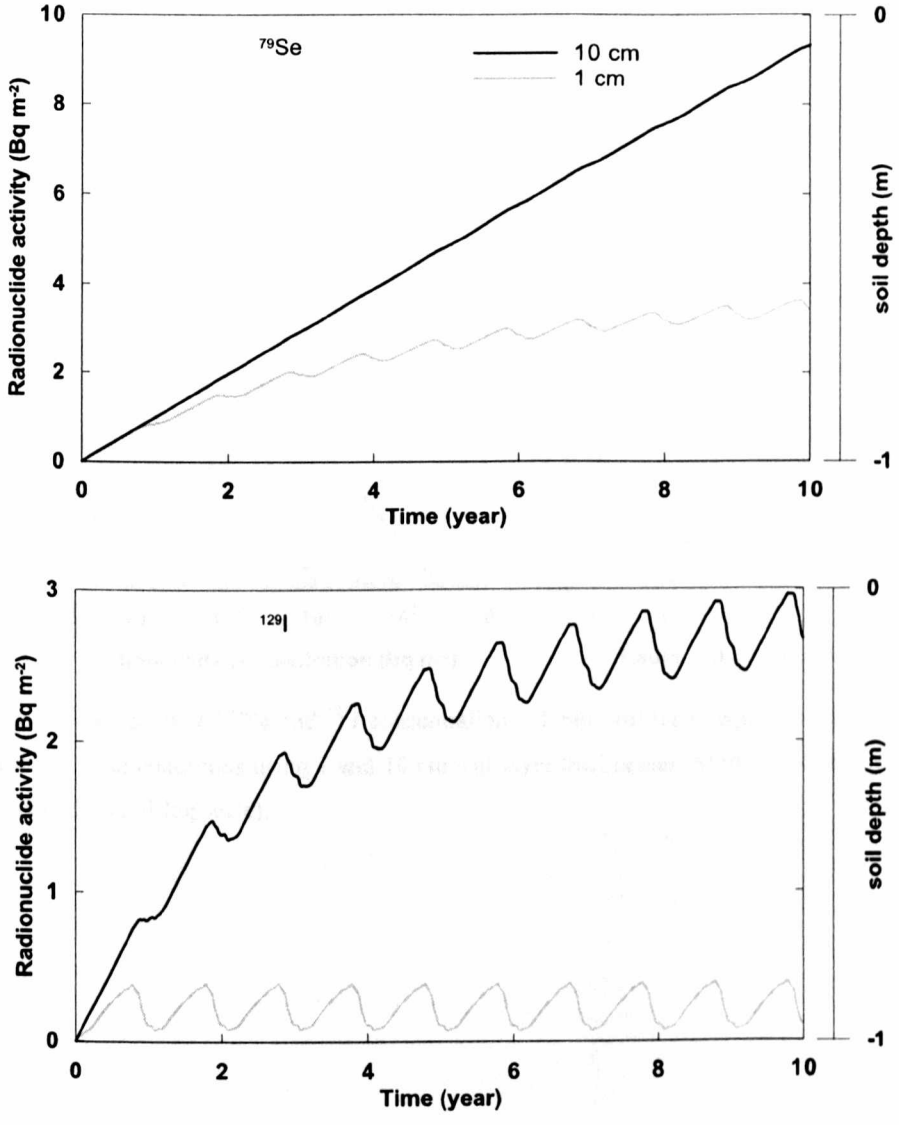

Fig. 4-10 Predictions of ^{79}Se and ^{129}I accumulation (total activity) within a 1 m bare soil column over a 10 years period using 1 and 10 cm soil layer thicknesses. Model time step was fixed at 1 day.

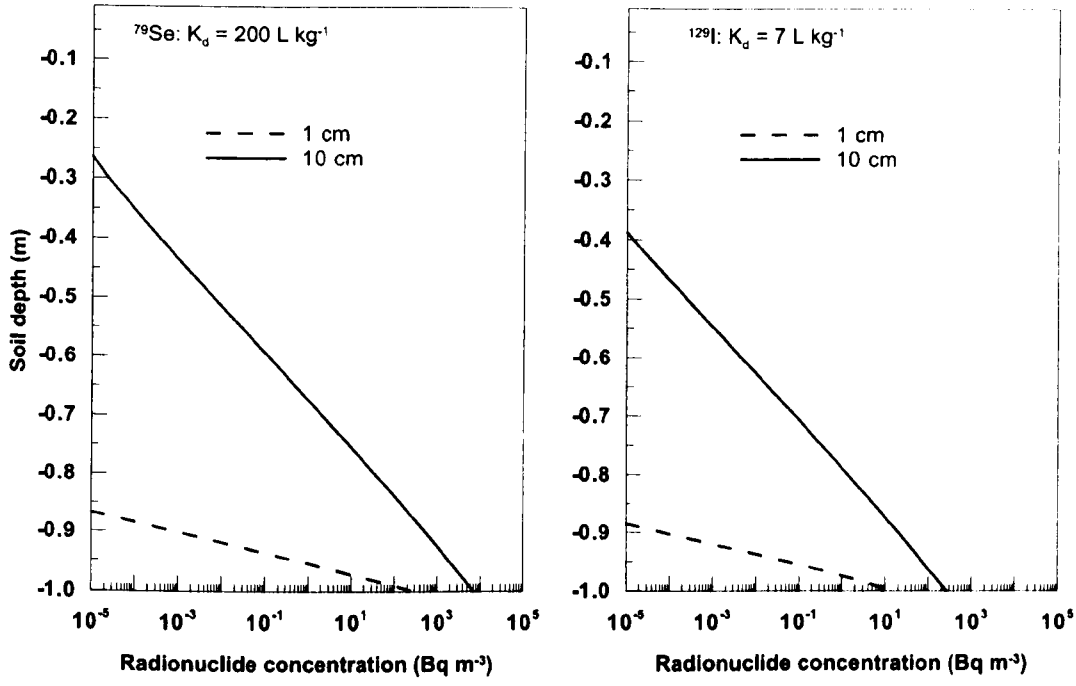

Fig. 4-11 Predictions of ^{79}Se and ^{129}I concentration - depth profiles at equilibrium (annual average) under bare land conditions using 1 and 10 cm soil layer thicknesses. Model time step was fixed at 1 day (note the semi-log scale).

4.6. Overview of the RIGEMA approach

RIGEMA is a physically-calibrated compartmental modelling approach to assess vertical migration and accumulation of radionuclides in the soil column and surface soil. The method was developed by integrating the physically-based Richards model of water flow in soil and the ecological modelling approach commonly used in radioecological modelling. This combined approach is generic and capable of simulating radionuclide migration and distribution within various terrestrial ecosystems.

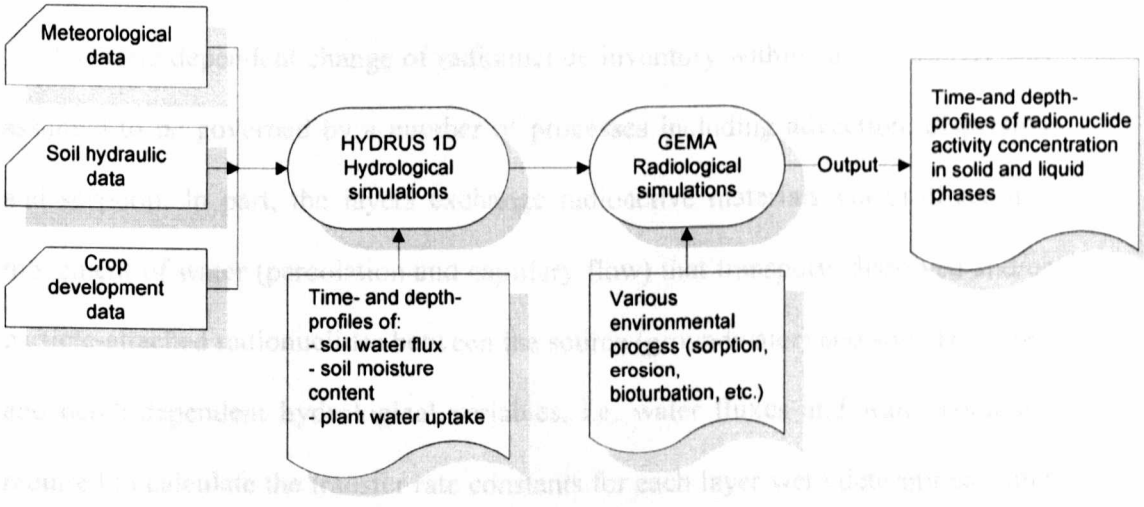

Fig. 4-12 A diagram demonstrating the structure of RIGEMA and how it is implemented. The diagram shows the connections between the model input data, HYDRUS-1D hydrological simulator and GEMA radiological model.

The RIGEMA approach was used to simulate the migration and vertical distribution of an annual hypothetical release of 1 Bq of a radionuclide into a 100 cm soil column bounded by the soil surface and the groundwater table. The variably saturated soil was equally divided into a number of 1 cm thick layers with

the number of layers being dictated by physical considerations. The 1 cm thickness is sufficiently small reliably to simulate soil water dynamics, a key driver of radionuclide migration in the soil, using Richards model. This discretisation scheme maintained the magnitude of the numerical dispersion component of the model (D_{num}) in accordance with the actual effective dispersion (D).

The RIGEMA approach functions on a daily time step. Hydrological as well as radiological simulations were run using daily values of the model inputs (e.g. rainfall, evapotranspiration, water flow, etc.). This short time step ensures the long-term effects of the intra-annual variability of soil water and radionuclide dynamics are represented in the model.

The time dependent change of radionuclide inventory within each soil layer was assumed to be governed by a number of processes including advection, dispersion and sorption. In part, the layers exchange radioactive materials via bi-directional movement of water (percolation and capillary flow) that transports dissolved and/or particle-attached radionuclides between the source (groundwater) and soil. The time- and depth-dependent hydrological variables, i.e. water fluxes and water contents, required to calculate the transfer rate constants for each layer were determined using the HYDRUS-1D code. The values of these variables were then used to calculate the transfer rate constants used in RIGEMA. Effective dispersion was modeled explicitly following the method of Xu et al. (2007).

RIGEMA incorporates the major processes responsible for the migration and accumulation of radioactivity in soils. Ecosystem-specific processes such as plant root uptake and bioturbation can be accounted for by translating their effect into transfer rate constants which add linearly into the overall transfer rate constant of each layer. RIGEMA makes use of the solid-liquid distribution coefficient, K_d, as a

combined measure of instantaneous sorption and desorption. Variants of K_d can be readily incorporated into the transfer rate constant expression including constant and parametric K_d models as described in the next chapter.

Chapter 5 Simulating the migration of radionuclides in soils

5.1. Introduction

This chapter describes the results of simulations undertaken to investigate the transport of radioselenium (^{79}Se) and radioiodine (^{129}I) through a soil column. ^{79}Se and ^{129}I are fission products encountered in the radioactive wastes and are of a particular interest in terms of their radio-ecological behaviour (Pröhl et al., 2005; Kłos and Albrecht, 2005; BIOPROTA, 2005). Mobility of ^{79}Se is enhanced under oxic conditions; in contrast, ^{129}I becomes less mobile under these conditions.

Vertical transport and accumulation of ^{79}Se and ^{129}I, within the soil under different land uses were simulated. The simulations were designed to explore cycling of ^{79}Se and ^{129}I in the soil under land management scenarios commonly considered in the context of geological disposal safety assessments. In particular, the influence of factors such as variation in atmospheric conditions, presence and growth of vegetation, irrigation with contaminated groundwater and K_d on the long-term radionuclide distribution in the soil was evaluated.

The arable land at Sutton Bonington site was assumed to receive an annual input of 1 Bq of ^{79}Se and ^{129}I to the subsoil. The environmental settings, including climatic conditions and land use in addition to the simulation scenarios, are described in the following sections.

5.2. Materials and methods

5.2.1. Site description

Sutton Bonington is characterised by a temperate climate with mild winters and warm summers Table 5-1. Mean annual precipitation is 622 mm with April and August being the driest and rainiest months, respectively. The groundwater table at the site is rather shallow in winter and drops to ~ 1 m below surface in summer.

Table 5-1 Meteorological data (averages over the period from 2006 to 2010) used for the hydrological and radiological simulations. Data was obtained from the local automatic meteorological station at Sutton Bonington site.

Month	Min Temp °C	Max Temp °C	Rainfall (mm)
January	2.28	7.24	50
February	1.24	7.38	40
March	2.25	10.31	42
April	4.46	14.11	31
May	7.18	16.47	50
June	9.90	20.05	64
July	12.29	22.34	70
August	11.95	21.16	73
September	10.26	19.37	42
October	7.91	15.33	48
November	4.07	10.74	59
December	2.46	7.58	55

The land at Sutton Bonington site is primarily under arable cultivation (winter wheat and barley). The soil types range from sandy loam to alluvial. Details of the soil properties were given earlier (Chapter 3).

5.3. Soil water flow modelling (HYDRUS-1D)

Following the approach described in the previous chapter, one-dimensional soil water flow was simulated using HYDRUS-1D (Šimůnek et al., 2009). Soil parameters necessary for the simulation process are summarised in Table 5-2.

Table 5-2 Soil hydraulic data for a generic sandy loam soil obtained from HYDRUS-1D database for the hydrological simulations.

Parameters	**Value**
van Genuchten-Mualem (1980) model:	
saturated soil-water content: θ_s	0.41
residual soil-water content: θ_r	0.065
retention curve shape parameters: α and n	7.5 m^{-1} and 1.89
saturated hydraulic conductivity: K_s	1.061 m day^{-1}
tortuosity and pore connectivity parameter: ℓ	0.5
Feddes (1978) water stress reduction model:	
h_1	0 m
h_2	-5 m
h_3	-9 m
h_4	-160 m
critical stress index: ω_c[5]	0

Atmospheric conditions (precipitation and Penman-Monteith ET_0) were used as an upper boundary condition. A constant pressure head (h = 0 m) corresponding to the depth of the groundwater table (-1 m) was used as a bottom boundary condition.

[5] threshold value above which root water is uptake reduced in stressed parts of the root zone is fully compensated by increased uptake from other parts

5.4. Sorption modelling

Although regression models were derived from experimental data (Section 3.3.6) that relate K_d of different elements to pH, dissolved organic carbon and iron concentrations in soil solution, K_d values calculated using these models were not used to represent the sorption/desorption processes in RIGEMA models. These models calculate K_d from soil solution characteristics (i.e. pH, dissolved organic carbon and soluble iron) the measurement of which is not commonly part of site characterisation procedures for potential sites of underground waste repositories. Alternatively, parameteric models that relate K_d to basic, readily available soil data (i.e. soil pH, solid phase organic matter and mineral contents) reported in the literature (Sheppard, 2011; Sheppard et al., 2009; Sheppard et al., 2007) were used to represent radionuclide sorption/desorption in soils. This also extends the applicability of RIGEMA to model change in sorption behaviour in response to environmental change as for example the change in soil characterstics due to land management change.

5.4.1. Generic K_d

For this approach, sorption was parameterised and quantified using a constant K_d - i.e. sorption was not affected by the change in physical and chemical properties between different soil layers. K_d data reported in the recent IAEA (2009) compendium was used in these simulation runs (Table 5-3).

Table 5-3 K_d values used in RIGEMA model for ^{79}Se and ^{129}I as reported in the IAEA (2009) compendium for a generic soil type.

Element	K_d[6] (L kg^{-1})			
	Min	**GM**	**GSD**	**Max**
^{79}Se	4	200	3	2100
^{129}I	0.01	7	5	580

5.4.2. Parametric K_d approach

In this case sorption was expressed as a function of soil physicochemical properties. K_ds of ^{79}Se and ^{129}I were estimated using the parametric (empirical) models of Sheppard et al. (2009) which relate the K_ds to soil pH, clay and organic matter content (OM). K_ds of ^{79}Se and ^{129}I for Sutton Bonington arable soils calculated using Sheppard et al (2009) models are presented in Table 5-4.

Table 5-4 Measured (mean of K_ds determined from 0.1, 0.22 and 0.45μm porewater filtrates) and calculated (from parametric models of Sheppard et al. (2007)) ^{79}Se[7] and ^{129}I[8] K_d (L kg^{-1}) values for SB arable top and subsoils. Only calculated K_ds were used in the numerical simulations.

Element	Selenium		Iodine	
Method	**Measured**	**Calculated**	**Measured**	**Calculated**
SB-AT	200 ± 10	440	95 ± 20	166
SB-AS	115 ± 15	390	25 ± 2	160

[6] Soil types include: sandy, loamy, clayey and organic

[7] Log (Se-K_d) = 1.79 + 0.133*pH – 0.00163*clay*pH

[8] Log(I-K_d) = 2.13 + 0.00297*OM + 0.00181*clay*pH

5.5. Simulation scenarios

The 100 cm soil column was modeled using 2 compartments (solid and liquid phases) and 100 layers (justification of the choice of soil layer thickness in the model was discussed in Chapter 4). With respect to modeling timescale and model time step, preliminary calculations showed that a period of 1000 years was sufficient for ^{79}Se and ^{129}I to attain steady-state under the simulation conditions considered in this study. Thus, all simulations were run for 1000 years (1 ka) using a daily time step. The different simulation scenarios are described below.

5.5.1. Bare soil

This is the reference (control) scenario for this study. An annual discharge of 1 Bq of ^{79}Se and ^{129}I into the base of the soil column was assumed. This assumption is consistent with the definition of a source term in the context of long-term radiological assessment of geological disposal adopted by several studies (Klos, 2010; Xu et al., 2008; Klos, 2008; Agüero et al., 2008). The primary objective of this assumption is to facilitate model-model comparisons. The main processes considered in these simulations were advection, dispersion and sorption. Sorption was represented using generic K_ds (Section 5.4.1).

5.5.2. Non-irrigated vegetated soil

To investigate the effect of root uptake on the dynamics and long-term distribution of radionuclides within the soil, a vegetation compartment (winter wheat) was added to the bare soil model. A fraction of the soil radionuclide inventory was assumed to be taken up by wheat plants via their roots, and hence

transferred into the vegetation compartment. The activity concentration in the wheat was calculated by assuming passive uptake from the transpiration stream and a uniform distribution of radioactivity within wheat biomass.

Winter wheat growing season extends from early September to mid-July; no irrigation was considered. Crop data necessary for running the model (e.g. root depth, leaf area index and crop biomass) were calculated using the Sirius wheat simulation model (Jamieson et al., 1998). Harvest (assumed to be during late July) was treated as a discrete (i.e. once only) process, and was simulated following the approach of Whicker and Kirchner (1987). Residual wheat biomass (roots and stalks) of 0.1 kg m^{-2} was assumed. The remnant radionuclide activity in the residual wheat biomass was homogeneously incorporated into the topsoil (0-20 cm) by ploughing.

5.5.3. Irrigated vegetated soil

This is an extension of the non-irrigated scenario above. Irrigation was simulated as a discrete process (i.e. applied as a series of smaller discrete applications between May and July). A total amount of 0.2 m^3 of contaminated irrigation water (with an activity of 1 Bq m^{-3}) was applied between May and July (25 mm/application). In all other respects, the scenario was as described in Section 5.5.2.

5.6. Results

5.6.1. ^{79}Se and ^{129}I dynamics in soil

The annual mean activity concentrations of ^{79}Se and ^{129}I within the uppermost and lowermost 20 cm of the vegetated, non-irrigated and irrigated soil column over the entire simulation period (1 ka) are shown in Fig. 5-1. The activity concentration of ^{129}I attained steady-state in both parts of the soil column more quickly than ^{79}Se. Activity concentrations of ^{79}Se and ^{129}I attained steady-state earlier, and were, respectively, two and one order of magnitude higher within the lower part of the soil column than the upper part. The steady-state activity concentrations of ^{79}Se within the upper and lower 20 cm of the soil column were higher than their ^{129}I counterparts by 1 and 2 orders of magnitude, respectively.

Time trends of ^{79}Se and ^{129}I activity concentrations within upper and lower parts of the soil column when irrigation was practiced remained similar to the non-irrigated scenario. Irrigating with contaminated water resulted in an increase in ^{129}I activity concentrations in the upper (1.5 orders of magnitude) and the lower (by a factor of 4) parts of the column. ^{79}Se activity concentration in the upper 20 cm of the soil column also increased by 2 orders of magnitude due to irrigation which seems to have a counter-effect (slight decrease) on ^{79}Se concentration in the lower 20 cm of the column.

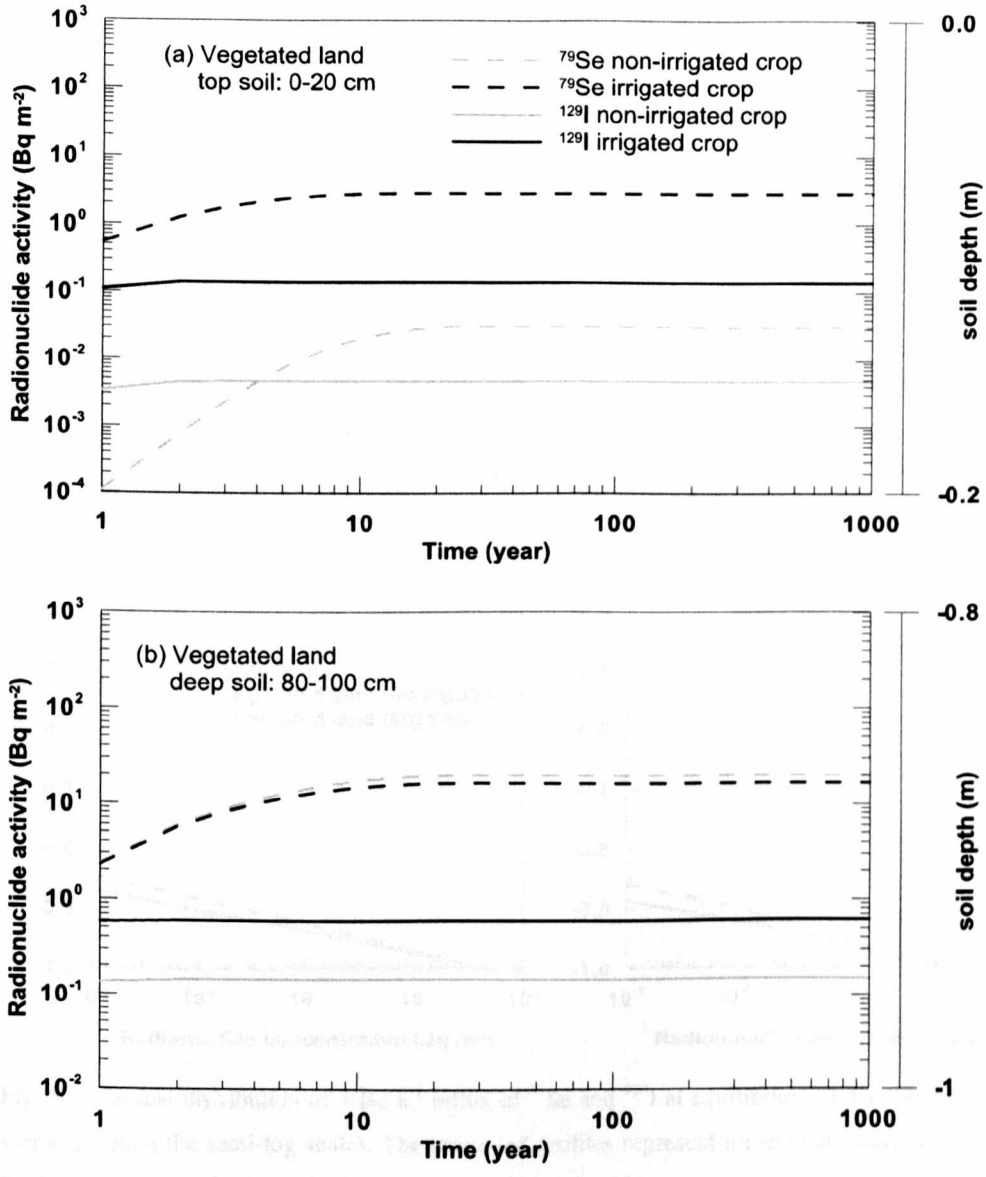

Fig. 5-1 Predictions of ^{79}Se and ^{129}I accumulation (total activity) within the top (0-20 cm) and subsoil (80-100 cm) of a soil column cropped with winter wheat. The graphs show the effect of irrigation with contaminated groundwater (note the log-log scale).

5.6.2. Vertical distributions of ^{79}Se and ^{129}I within the soil

Predicted depth profiles of ^{79}Se and ^{129}I at equilibrium for different land use scenarios are shown in Fig. 5-2.

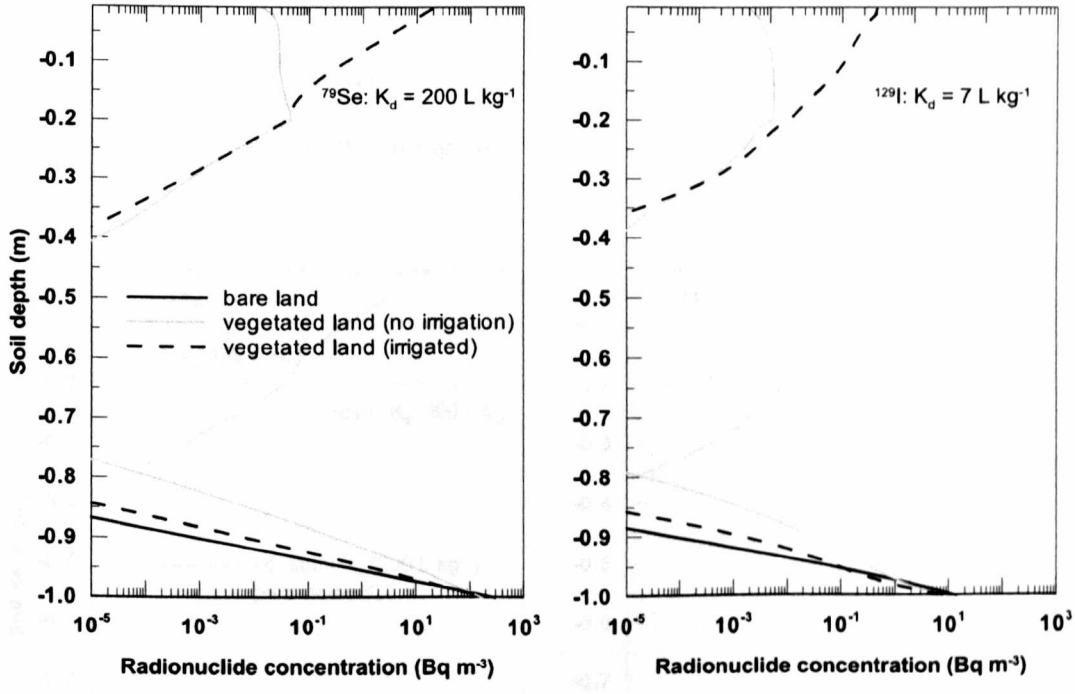

Fig. 5-2 Vertical distribution of 1 Bq a^{-1} influx of ^{79}Se and ^{129}I at equilibrium under different land use scenarios (note the semi-log scale). The presented profiles represent mean of the daily profiles of the final year when equilibrium was reached.

For all scenarios considered in this study, ^{79}Se migrated further away from the contaminated groundwater than ^{129}I. Nevertheless, considerable contamination levels ($\geq 10^{-5}$ Bq m^{-3}) were confined to the lowermost 20 cm of the bare soil column. By adding a crop compartment into the model (the vegetated soil scenarios) ^{79}Se (and ^{129}I) contamination levels greater than 10^{-3} Bq m^{-3} (and 10^{-5} Bq m^{-3}) were predicted within the uppermost 20 cm of the soil column. Furthermore, practicing irrigation with contaminated water resulted in enrichment of the topsoil with ^{79}Se

and ^{129}I and leaching of these radionuclides from the lowermost part of the soil column.

The effect of vertical variation of sorption characteristics (the chemical zonation) on the vertical distribution of ^{79}Se and ^{129}I was investigated by allowing K_ds to vary as a function of soil pH, clay and organic matter content using Sheppard et al. (2009) parametric models (see Section 3.3.6). Equilibrium concentration depth profiles of ^{79}Se and ^{129}I under non-irrigated and irrigated vegetated soil for constant and parametric K_ds are shown in Fig. 5-3.

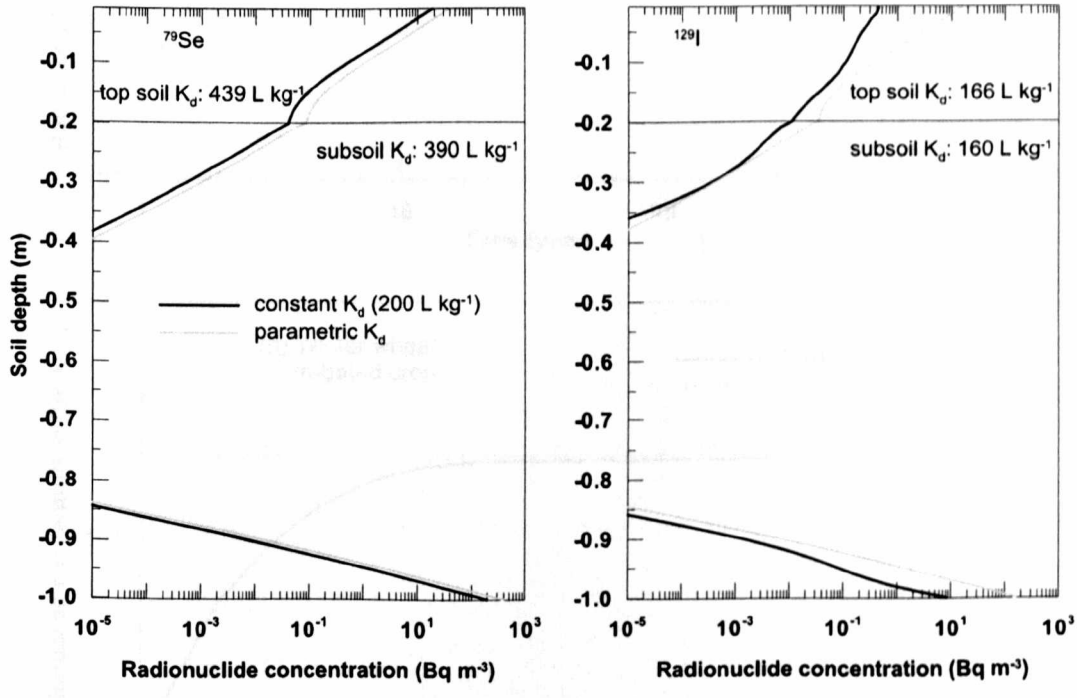

Fig. 5-3 Vertical distribution of 1 Bq a^{-1} influx of ^{79}Se and ^{129}I at equilibrium under vegetated land (with irrigation) predicted using constant and parametric K_ds (note the semi-log scale). The presented profiles represent mean of the daily profiles of the final year when equilibrium was reached.

5.6.3. ^{79}Se and ^{129}I in wheat

Accumulation of ^{79}Se and ^{129}I activity in wheat biomass under two land uses over the simulation period is shown in Fig. 5-4.

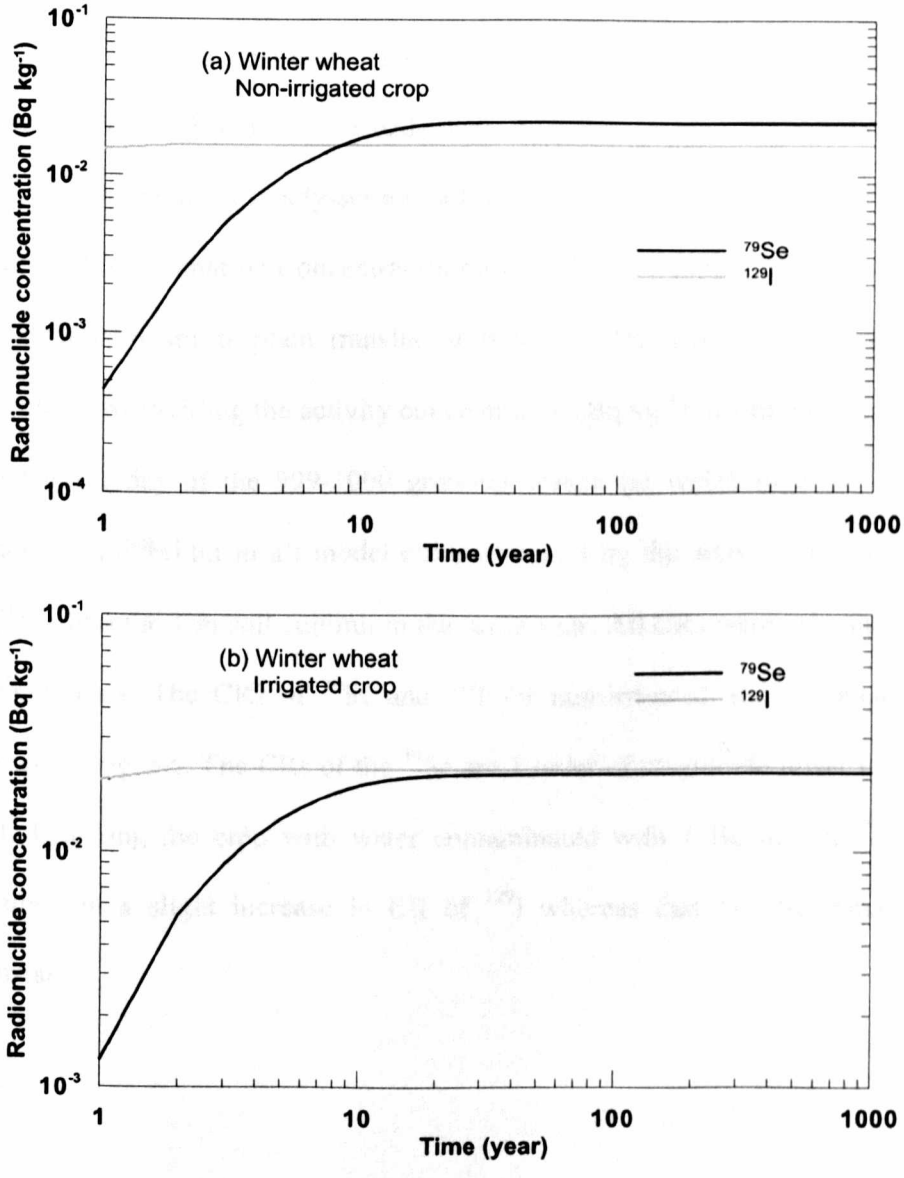

Fig. 5-4 Accumulation of ^{79}Se and ^{129}I activity in wheat biomass (dw) as a function of time predicted for non-irrigated and irrigated wheat crops. Values represent activity concentration in biomass on the day of harvest (note the log-log scale).

Under the non-irrigated wheat scenario, the equilibrium concentration of ^{79}Se in the wheat biomass (dry weight) was slightly higher than that of ^{129}I. In contrast, the equilibrium activity concentration of ^{129}I in wheat biomass exceeded that of ^{79}Se when irrigation was practiced. Overall, irrigation resulted in a slight decrease in ^{79}Se and a slight increase in ^{129}I activity concentration in the wheat. A significant difference between ^{79}Se and ^{129}I is the timescale to equilibrium concentrations in wheat. While ^{129}I attained a steady-state in a few years, ^{79}Se accumulated more slowly and attained a steady-state in a few decades. This behaviour was common to both land use scenarios Concentration ratios (CRs) are simple measures to quantify the degree of soil-to-plant transfer of radionuclides. CRs of ^{79}Se and ^{129}I were calculated by dividing the activity concentration (Bq kg^{-1}) incorporated in the crop at the harvest day of the 999-1000 growing season (at which time the activity has reached equilibrium in all model compartments) by the activity concentration (Bq kg^{-1}) within the 1 m soil column in the same year. All CRs were calculated on a dry weight basis. The CRs of ^{79}Se and ^{129}I for non-irrigated and irrigated crops are shown in Fig. 5-5. The CRs of the ^{79}Se are 1 order of magnitude lower than those of ^{129}I. Irrigating the crop with water contaminated with 1 Bq m^{-3} of ^{79}Se and ^{129}I resulted in a slight increase in CR of ^{129}I whereas that of ^{79}Se remained fairly constant.

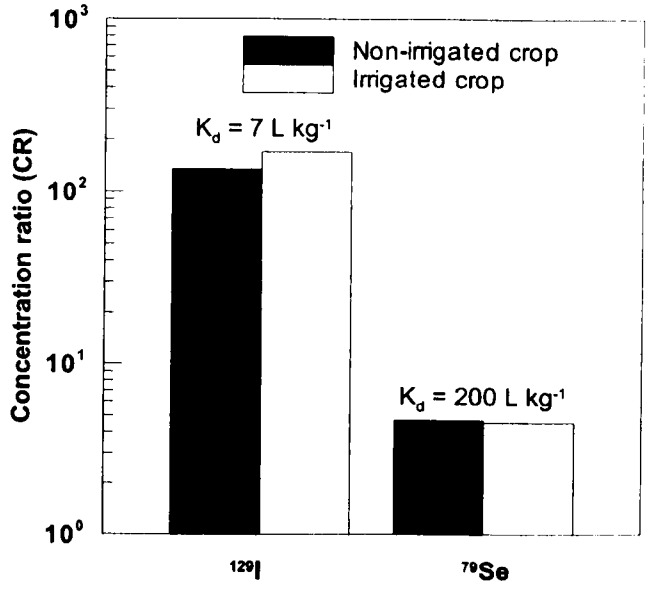

Fig. 5-5 Concentration ratios (Bq kg^{-1} biomass dw/Bq kg^{-1} soil) of ^{79}Se and ^{129}I for non-irrigated and irrigated wheat crops at equilibrium (note the log scale).

5.7. Discussion

Simulation results revealed a strong correlation between local hydrological conditions and the dynamics of ^{79}Se and ^{129}I activity concentration in the soil column. This influence was clearly manifested in temporal patterns of ^{79}Se and ^{129}I activity concentrations that followed seasonal variability of soil hydrological conditions. During wet periods (winter), precipitation exceeded evapotranspiration, the bulk movement of soil water was downward and leaching became the dominant transport mechanism. In contrast, high evaporation (for bare soil) and evapotranspiration (for vegetated soil) rates during summer time resulted in upward movement (capillary rise) of contaminated groundwater. As a result, ^{79}Se and ^{129}I activity concentrations in the soil column decreased and increased during wet and dry seasons, respectively. This climate-driven dynamics of radioactivity would be expected to have significant implications on long-term redistribution of radionuclides within the biosphere. A greater migration potential, in particular for strongly sorbing radionuclides such as ^{79}Se, would be expected in dry environments (e.g. arid) than under wet ones (e.g. temperate). Aspects of seasonal variation in radioactivity dynamics in soils are rarely addressed in long-term radiological assessments (Klos, 2010; Xu et al., 2008; Klos, 2008; Avila, 2006b). The influence of seasonal variation in soil water flow on the assessment results becomes more apparent should the source term definition be coupled to local hydrological conditions. The current representation of the source term assumes a constant input of 1 Bq a^{-1} to the base of the soil column. Although this assumption facilitates comparison of different biosphere model formulations, it overlooks the influence of seasonal variability of local hydrology on radionuclide influx into the soil column.

Therefore, unless there is evidence to support such an assumption, e.g. data from hydrological modeling, coupling the model source term to local hydrological patterns (e.g. inflowing groundwater by capillary rise) would make a more realistic assumption.

The concentration - depth profiles of ^{79}Se and ^{129}I at equilibrium indicated that for non-vegetated soil contamination inventories greater than 10^{-5} Bq m^{-3} were limited to the bottom 20 cm of the soil column and that the radionuclides remained close to the source. Activity concentration depth profiles calculated in the context of this modelling work again highlight the importance of accurate description and simulation of local hydrological conditions. Klos (2010) performed similar calculations and predicted distribution profiles of a suite of radionuclides in a 5-meter thick Quaternary deposit (QD) overlying bedrock in Forsmark, Sweden assuming constant and uniform hydrological conditions (fully saturated QD and constant water flow throughout the column). The author found that the higher the water flow (Darcy velocity) the more uniform the depth profile. These constant hydrological conditions assumed by Klos (2010) contrast with the assumptions made here regarding soil water content and through-flow. The activity concentration depth profiles presented here (Fig. 5-2 and Fig. 5-3) reflect the temporal and depth variability in local hydrology in response to climatic forcing. Therefore, the non-uniform ^{79}Se and ^{129}I distributions predicted in this work are not surprising.

Changing land use and growing deeply-rooted crops such as wheat would have important implications for long-term vertical distribution of ^{79}Se and ^{129}I. As wheat roots had access to deeper, contaminated soil layers, the contamination could reach the topsoil. When wheat was harvested, remnant ^{79}Se and ^{129}I in residual biomass (straw and roots) were deposited and mixed by ploughing within the upper 20 cm of

the soil. In addition, this "biological pumping" mechanism enhanced the upward migration of the ^{79}Se and ^{129}I from deeper parts of the soil column. As the comparison between the hydrological variables for the various land uses suggests (Fig. 5-6), root uptake depleted soil moisture and stimulated upward capillary flux from contaminated groundwater. The comparison shows a maximum capillary flux for the vegetated, non-irrigated scenario. Contamination levels within the mid-zone of the soil profile were below 10^{-5} Bq m^{-3} for all scenarios. This mid-zone was relatively remote from discharge point (i.e. the base of the soil column), hydrologically isolated and at field capacity for most of the year. Water fluxes (percolative and capillary) within this zone were relatively small compared to fluxes near the column boundaries. Consequently, diffusion dominated over advection in this zone leading to relatively low activity concentrations of ^{79}Se and ^{129}I.

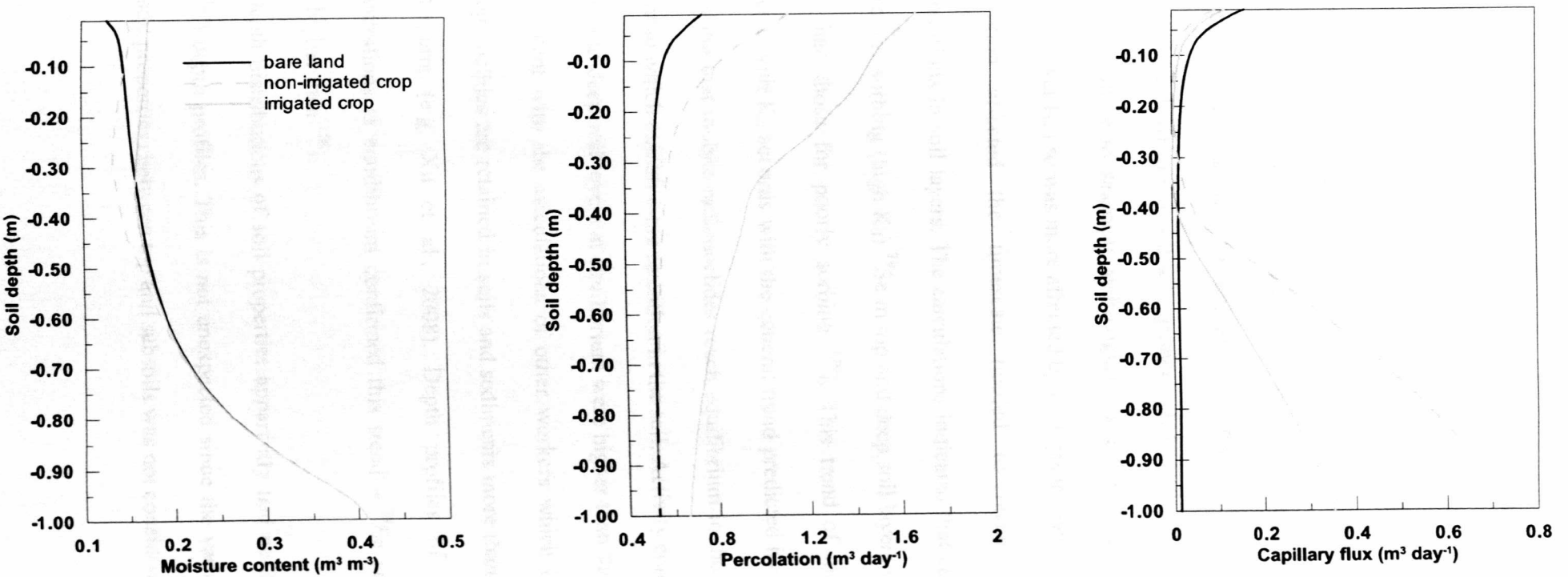

Fig. 5-6 Mean profiles of soil moisture content, percolation and capillary flux under different land uses predicted by HYDRUS-1D (using a daily time step and 1 cm grid cell length) for SB site.

As the results suggest, sorption, represented by K_d, was a key parameter controlling ^{79}Se and ^{129}I dynamics. Temporal variation in activity concentrations of these nuclides appeared to be responsive to seasonal variation of soil hydrology (i.e. moisture content and water fluxes). The magnitude of this response, however, was depended on K_d. Seasonal fluctuation of the local hydrology impacted the dissolved fraction of the radionuclide total activity concentration. ^{79}Se, which had a high K_d, was bound (sorbed) to the soil to a greater extent so prevented from leaching and was less sensitive to seasonal hydrological variation. In contrast, ^{129}I was more mobile (a lower K_d) so was more affected by changes in water fluxes and leaching.

Sorption affected the timescale needed to reach equilibrium activity concentrations in soil layers. The calculations indicated that equilibrium timescales for strongly sorbing (high K_d) ^{79}Se in top and deep soil layers were longer (by c. 10 years) than those for poorly sorbing ^{129}I. This trend of increasing equilibrium timescale with K_d accords with the general trend predicted by Agüero et al. (2008) who found that mobile radionuclides reach equilibrium in the topsoil layers earlier than those which exhibit more retention in the soil. Activity concentrations of ^{79}Se in the top and deep soil layers at equilibrium were higher than those of ^{129}I. This trend is consistent with the calculations of other workers which indicate that strongly sorbing nuclides are retained in soils and sediments more than their weakly sorbing counterparts (e.g. Xu et al., 2008). Depth profiles of radionuclide activity concentrations at equilibrium confirmed this trend - ^{79}Se activity concentrations were higher than ^{129}I.

Depth distributions of soil properties apparently had no marked effect on ^{79}Se and ^{129}I depth profiles. This is not unexpected since the variation in K_d predictors (i.e. soil properties) between top and subsoils was not considerable and was reflected

in a marginal difference in K_d between the top and subsoils for both radionuclides. The abrupt increase in activity concentrations, particularly that of ^{79}Se, within the topsoil (above the dashed lines) can be attributed to incorporation and mixing of the radionuclide inventories within the residual wheat biomass remained after harvesting (roots and straws). The increase in concentration was more noticeable for ^{79}Se, with a higher K_d than ^{129}I, with a low one due to the higher fixation of the added radionuclide. Using K_ds predicted from the models of Sheppard et al. (2009) models substantially over-predicted the ^{129}I activity depth profile in comparison to the profile predicted using the generic K_d.

The models of Sheppard et al (2009) do not account for effects such as soil moisture content and redox status on K_d, in spite of the ample literature evidence of such effects (Ashworth et al., 2008; Ashworth and Shaw, 2006b). Redox gradients do exist within the soil, particularly around the groundwater table and affect chemical speciation of ^{79}Se and ^{129}I and hence their sorption properties. In addition to the literature, the results of the experiments undertaken in this study have demonstrated strong interactions between soil moisture content, redox status and K_d (Chapter 3). Soil flooding resulted in soil redox potential falling over time and the soil became anoxic. These changes stimulated dissolution of sorbing phases such as Fe oxyhydroxides and organic matter, releasing sorbed radionuclides and K_d changed accordingly.

Although not considered here, it should be noted that the sorbed fraction of the radionuclide is not strictly immobile. Mass fluxes of radionuclides bound to soil solid materials are still possible via bioturbation (i.e. transport of soil by burrowing animals). This process has been shown to be an important transport mechanism (Bunzl, 2002; Bunnenberg and Taeschner, 2000; Müller-Lemans and van Dorp,

1996) and has recently been accounted for in assessment models (Klos, 2008; Bergström et al., 1999).

Radionuclide uptake by vegetation is expected to be a function of activity distribution within the soil in relation to root distribution. ^{79}Se and ^{129}I activity concentrations in the wheat crop at harvest are the integration of uptake over the entire root depth through the growing season. As the simulation results suggest, ^{79}Se seemed to be less bioavailable to wheat than ^{129}I. Although total activity concentration (solid + liquid) of ^{79}Se at equilibrium, as depth profiles indicated, was higher than that of ^{129}I, the calculated CR of ^{79}Se for non-irrigated and irrigated crops were 1 order of magnitude smaller than those of ^{129}I. As sorption of ^{129}I was small it was, on the basis of the current model assumptions, more bioavailable to wheat roots system. In contrast, ^{79}Se was removed from the soil porewater by sorption making it less bioavailable for the crop. Dissolved ^{129}I activity concentration increased due to irrigation, and so did its uptake by the crop, leading to higher crop activity concentrations compared to the non-irrigated crop. In contrast, the crop could not exploit the small inputs of ^{79}Se in the irrigation water which sorbed onto the soil solid phase.

The current simulation results emphasise the need to distinguish between the total activity concentration and the bioavailable fraction of radionuclides in the soil. The results corroborate the findings of Ehlken and Kirchner (2002): it is the bioavailable fraction that controls biological uptake, not total soil activity concentration. Uptake is dictated by the radionuclide being in a readily available form for the plant roots. The results of this study imply that radionuclide mobility is an indicator of bioavailabilty. This finding is consistent with that reported by

Sheppard et al. (2010) who found a negative correlation between CR and K_d for a group of 40 elements.

In order to keep the complexity of RIGEMA to a manageable level it was assumed that all plant radionuclide uptake is passive, i.e. flow of radionuclides into plant roots is associated with flow of water supplying the plant transpiration demand. Mathematically, plant radionuclide uptake was simulated by multiplying root water uptake by dissolved radionuclide concentration in soil solution. Radionuclides were also assumed to be taken up, translocated and uniformly distributed between different parts of a plant indiscriminately. This representation of plant radionuclide uptake suffers a number of limitations. It implies that uptake is controlled by unrestricted convective mass flow of a radionuclide. In practice mass flow is restricted if plant nutrient requirement is fulfilled and nutrients (e.g. Ca^{2+} and Mg^{2+}) tend to accumulate (or even precipitate) at the root surface. A depletion zone may develop around the absorbing roots if root uptake rate exceeds mass flow rate, and passive uptake is reduced since diffusion of nutrients from bulk solution into root surface is slow (Ehlken and Kirchner, 2002). The effect of ion competition between a radionuclide (e.g. Cs^+) and a macronutrient (e.g. K^+) could also reduce radionuclide uptake (e.g. Shaw and Bell, 1991). Active plant uptake which embraces a wide range of energy-driven processes such as cation channel and element-specific membrane transport and commonly modelled using Michaelis-Menten kinetics (Šimůnek and Hopmans, 2009; Chen et al., 2008) was neglected in the current RIGEMA formulation. Moreover, Allocation of radionuclides taken up by plants is radionuclide- and plant-specific, and it has been shown that different radionulicdes tend to accumulate preferentially in different plant tissues (Hong et al., 2008; Zhu et al., 2004). Consequently, it is not surprising that CR predicted by RIGEMA differ

from empirically determined values. They are a few orders of magnitude higher, from those determined experimentally for I-wheat system (0.0001 – 0.11) (Kashparov et al., 2005; Shinonaga et al., 2001). Predicted CRs of ^{79}Se, however, fall within the range 0.06–11.0 and are similar to the mean value of 5.54 reported by Bitterli et al. (2010) for wheat (*Triticum aestivum*) grains.

5.8. Conclusions

The RIGEMA modelling approach, described in Chapter 4 and implemented in Chapter 5, was used to simulate the long-term dynamics and vertical distribution of ^{79}Se and ^{129}I, in soil columns under different hydrological and cropping regimes. The current assessment focused on three issues: (a) long-term dynamics of radionuclides in soil in relation to seasonal variation in climatic conditions; (b) influence of vegetation cover, in particular plant uptake, on vertical distribution patterns of radionuclides and (c) effects of sorption characteristics on both dynamics and vertical distribution of radionuclides in the soil. The results have highlighted the interactions between weather conditions, soil hydrology, vegetative cover and radionuclide sorption (K_ds).

Soil activity concentrations exhibited temporal variability in accordance with the seasonal variability of soil water flow, clearly driven by changes in precipitation and evapotranspiration rates. Activity concentrations of ^{79}Se and ^{129}I increased during dry periods and decreased during wet periods. This implies that higher radionuclide migration rates would be expected under drier climatic conditions, particularly for poorly sorbing nuclides. This conclusion may provide insights into the behaviour of long-lived radionuclides discharged from a radioactive waste repository into biospheres where different climatic conditions exist.

The results underscore the importance of vegetation as a component of the biosphere that contributes to the transfer of ^{79}Se and ^{129}I from the geosphere to the surface environment. In comparison to advective-dispersive transport, crop uptake serves as a fast pathway that facilitates transport of radionuclides, particularly of strongly sorbing ones such as ^{79}Se, from the contaminated deeper zone into the surface zone. This highlights the importance of properly representing this biological

pumping effect in radiological risk assessment models. The current approach to modelling plant uptake and translocation is, however, rather simplistic and does not account for mechanisms such as active uptake or dependency of radionuclide translocation and mobility within the plant or their identity. Clearly, further model refinements with respect to these mechanisms are required.

Sorption, parameterised using the K_d concept, governs many aspects of ^{79}Se and ^{129}I behaviour in the soil. K_d determines the influence of soil hydrology on radionuclide dynamics in the soil. The results suggest that soil activity concentrations of ^{129}I, an example of a mobile radionuclide with low K_d, is more responsive to seasonal variability of hydrology than ^{79}Se, a less mobile radionuclide with a high K_d. In contrast to the mobile ^{129}I that is leached out of the soil, ^{79}Se tends to accumulate particularly near to discharge points (sources). This implies that strongly sorbing radionuclides (high K_d) such as ^{79}Se may pose a greater risk to biota than their weakly sorbing (low K_d) counterparts such as ^{129}I given their tendency to accumulate over time.

Chapter 6 Summary of conclusions, recommendations and future work

6.1. Conclusions

Simulations undertaken using the RIGEMA modelling methodology (Section 5.6) illustrate the sensitivity of the long-term vertical distributions of ^{79}Se and ^{129}I in soils to variations in K_d, a parameter that quantifies the partitioning of a radionuclide between solid and liquid phases. Radionuclides with higher K_d will take a longer time to achieve steady state activity concentrations which will be higher than those achieved by radionuclides with lower K_ds (Table 6-1).

Table 6-1 Sensitivity to K_d of RIGEMA predictions of steady state activity concentrations in the topsoil (0-20) cm under two land use scenarios. Time step size and soil layer thickness were fixed at 1day and 1 cm, respectively.

Biosphere model	**K_d = 7 L kg^{-1} Conc. at steady state (Bq m^{-3})**	**K_d = 200 L kg^{-1} Conc. at steady state (Bq m^{-3})**
Vegetated land (no irrigation)	0.145	3.88
Vegetated land (with irrigation)	0.148	3.81

Variation in K_d may be attributed to differences in determination methods used to determine K_d values experimentally, spatial variability in soil characteristics and the dynamic behaviour of radionuclides in soils (time-varying processes). Differences in some aspects of measurement methods, such as incubation method, porewater separation and filtration techniques, resulted in a 10-fold variation in K_d (Section 3.3.4). This finding is in agreement with similar studies (Sheppard et al., 2007). For some elements (e.g. I), the variation in K_d may be up to 4 orders of magnitude (IAEA, 2009). Therefore, a standard K_d determination procedure seems appealing since it will reduce measurement-related variation in K_d. However, since K_d is an abstract term that encompasses different concepts, the appropriateness of a measurement method depends on the specific application. For example, a K_d determined by equilibrating a tracer with a sorbent, such as soil, represents short-term sorption, and therefore it is therefore applicable when assessing short-term behaviour of that tracer, or its analogues, in soils. In contrast, a K_d determined from desorption of naturally occurring elements in soil (i.e. the approach adopted in the experiments of this thesis) into the solution phase represents long-term fixation, and is more suitable for assessing long-term behaviour of these elements. As a result, the latter approach is appropriate for assessing the retardation of radionuclide releases from underground repositories into surface ecosystems given the long timescales typical of these assessments.

Overall, the relatively organic Sutton Bonington topsoils had higher sorption capacities than subsoils. This is manifested in high K_ds obtained for topsoils compared with those for subsoils. The observed variation in K_d between six Sutton Bonington soils was within one order of magnitude (Section 3.3.4, Fig. 3-10). This variation in K_d reflects the variability in the physicochemical characteristics, not

only between top and subsoils, but also among arable, grassland and woodland soils. In practice, landscapes considered in the context of post-closure safety assessments of geological repositories are much larger than the sampling area at Sutton Bonington; a landscape of ~10^4 m^2 (1 hectare) area and a few meters in depth would be typical (Klos, 2010; Klos, 2008). Such a landscape may encompass a range of ecosystems; therefore, the spatial variation in K_d may be comparable to that observed at Sutton Bonington (or even higher) for actual repository sites.

K_d changes with time in response to soil flooding and the trend and magnitude of this change are element specific. The maximum variation was observed for I whose K_d decreased by c. 2 orders of magnitude by the end of a 3 week incubation period (Section 3.3.2, Fig. 3-3). This variation may be attributed to a number of biogeochemical processes, the most important of which is solubilisation of soil iron and organic phases under anaerobic conditions. Therefore, dynamics of iron and organic carbon can be assumed to be important for predicting the mobility and fate of contaminants in anoxic, iron and organic matter rich soils.

The thickness of soil layers in compartmental models should be justified and should represent the physics of transport mechanisms in the system. The long-term simulation of vertical migration and distribution of ^{79}Se and ^{129}I shows considerable sensitivity to model predictions to time step size and soil layer thickness of the model (Section 4.5.2, Fig. 4-8). Reducing the soil layer thickness results in higher predictions of the migration potentials and the steady state concentrations of ^{79}Se and ^{129}I in soil profiles (Table 6-2). This behaviour is a direct consequence of the numerical dispersion effect, an artifact of the compartmental modelling approach. A dicretisation procedure that relies on the physics of soil water flow should provide a

useful frame of reference for discretisation of soil compartmental models (Section 4.5).

Table 6-2 Sensitivity to the soil layer thickness and time step of the bare land model predictions of steady state activity concentration (Bq m^{-3}) in the soil column.

	Time step	Soil layer thickness	
K_d = 7 L kg^{-1}		**1 cm**	**10 cm**
	1 day	0.2	3.8
	1 year	3.6	-
K_d = 200 L kg^{-1}		**1 cm**	**10 cm**
	1 day	4.2	75.6
	1 year	96	-

This procedure requires the soil column (the flow domain) to be vertically discretised to achieve convergence of the solution to the water flow (Richards) equation. Application of this dicretisation procedure to environmental conditions prevailing at Sutton Bonington site resulted in an optimum soil layer thickness of 1 cm (Section 4.5.2). This resolution scale is in agreement with previously reported scales.

Land management has a pronounced effect on long-term fate and distribution of ^{79}Se and ^{129}I in soil (Section 5.6.2, Fig. 5-2). Absence of vegetation restricts upward migration to zones adjacent to the contaminated groundwater table. In contrast, presence of vegetation enhances upward migration via root uptake. Absorption and subsequent translocation into various parts of the plant (roots, leaves, grains, etc.) facilitates upward migration of ^{79}Se and ^{129}I and results in enrichment of topsoil with ^{79}Se and ^{129}I.

6.2. Recommendations

Site-specific K_ds are advantageous when field measurements are feasible. Yet, modelers and risk assessors can still utilise the extensive available K_d data available within the literature provided that reasonably appropriate K_d values are selected for the assessments. For example, desorption K_ds of native, stable elements represent quasi-equilibrium conditions with respect to radionuclide sorption onto soils and therefore they are more appropriate for long-term assessments than short-term sorption K_ds obtained in laboratory batch experiments.

Modelers may need to assign different K_ds to different soil horizons to account for variability in sorption characteristics and K_d down the soil profile. For example, relatively organic topsoils have higher sorptive capacities than subsoils, and hence would be expected to have higher K_ds. Mobility of some radionuclides, such as I and Se, is redox-sensitive and gradients in redox potential do exist in natural soils (e.g. near the groundwater table). As a result, modelers should select the appropriate K_ds to represent this relationship between soil redox status and radionuclide mobility. Modelers may, for example, use different K_ds for soil horizons that differ in moisture contents and, thus, redox status. They also may avoid using K_ds determined from oversaturated batch tests when simulating radionuclide transport in oxic soils.

Vertical discretisation (layer thickness) and temporal resolution (time step size) of compartmental models of radionuclide transport in soils should be justified and should reflect the physical characteristics of transport processes. Spatial convergence studies can be undertaken to identify the proper resolution that accurately describes the solution to Richards equation with maximum computational efficiency. In other words, the thickness of the soil layer may be optimised by iteratively solving the water flow equation for increasingly thinner soil layers untill

convergence is achieved. The compartmental model is then discretised in accordance with the optimum layer thickness. Regarding the temporal resolution scale, using a daily time step enables the model to capture the intra-annual variation in hydrology and radionuclide dynamics and thus produce more detailed predictions.

Given the long time periods associated with radiological risk assessments of geological repositories, changes to land management seems a certainty. However, uncertainty regarding the nature of these changes and the general evolution of the present-day landscape represents remains one of the challenges to reliable and accurate long-term radioecological modeling. Therefore, in order to improve reliability and accuracy of assessment model predictions, available models need to address the phenomenon of landscape evolution. One approach is to postulate a set of future biospheres into which the present-day landscape is projected to evolve. The state of the landscape is changed at certain points in time, and the fate of radionuclides is simulated accordingly after adjusting the initial conditions to account for radioactivity present in the previous biosphere.

6.3. Future work

The models constructed using the RIGEMA approach are meant to be as generic as possible and they therefore involve a great deal of simplification. Nevertheless, the simulations presented in this thesis provide valuable information on radionuclide behaviour in soils under various environmental conditions. The future work will focus on building models that incorporate a wider range of processes. For example, only mass flow in the liquid phase is considered and radionuclide transport is solely driven by advection and diffusion. Bioturbation, can also mobilise solid-borne radionuclides by mixing top and subsoils. In fact, this mechanism may be more important and effective in displacing and redistributing soil radionuclides in some soils as advection and diffusion mechanisms.

Improving the RIGEMA method to account for preferential flow of radionuclides in soils is a task set for future work. The standard Richards equation adopted in the RIGEMA approach is adequate for simulating uniform water and solute flow in porous media but cannot simulate preferential flows. Preferential flow, caused by soil heterogeneity and the presence of macropores, leads to acceleration of water and solute movement as they travel through macropores, bypassing the soil matrix. Nevertheless, Richards equation can be modified to simulate preferential flow in soils by using a variety of approaches including dual porosity and dual permeability models.

Since chemical speciation and mobility of redox-sensitive radionuclides are dependent on soil redox potentials (E_h) it is important for the RIGEMA approach to account for these dependencies. E_h, however, is a notoriously difficult variable to measure and interpret so other variables which are intrinsically linked to E_h and which may be considered to be 'surrogates' of E_h, such as dissolved oxygen

concentration and moisture content, may be used. RIGEMA would benefit from an explicit representation of the relationship between E_h 'surrogates' and species-dependent K_ds (e.g. K_ds for iodate and iodide). Mathematical or statistical representation of these relationships needs more experimental investigations.

The assumption of invariant environmental conditions (climate, depth of groundwater table, land use, soil characteristics, etc.) during 1000 years cannot be justified since environmental change is almost a certainty on such timescales which are typical of safety assessments of geological repositories. Thus, one area identified for further research is extending the RIGEMA approach to handle environmental change scenarios. A classical approach has been to build models for the projected succession of present-day landscape, i.e. radioecological models of ecosystems projected to occur in the future. This approach has a number of limitations since assumptions have to be made regarding the characteristics of these ecosystems and the time of transformation between different ecosystem states. For example, future ecosystem characteristics are assumed to be invariant for a certain period of time before abrupt shifts between different ecosystem states occur. Besides, both future ecosystem characteristics and time of ecosystem transformation are assumed to be known. Clearly, these assumptions are oversimplifications for many reasons. Extreme events such as floods that change many ecological attributes compromise the assumption of invariant environmental conditions. Also, not all changes to ecosystems are abrupt, especially when the change is natural and not enforced by human intervention. A very important consideration for future modelling studies will be the exploration of the relative consequences of gradual environmental change versus punctuated, possibly catastrophic, natural events on radionuclide

distribution and impacts in the biosphere. Therefore, much research is needed in this area.

Bibliography

Agüero, A., Pinedo, P., Simón, I., Cancio, D., Moraleda, M., Trueba, C. & Pérez-Sánchez, D. 2008. Application of the Spanish methodological approach for biosphere assessment to a generic high-level waste disposal site. *Science of The Total Environment,* 403, 34-58.

Allen, R. G., Pereira, L. S., Raes, D. & Smith, M. 1998. *Crop Evapotranspiration. Guidelines for Computing Crop Water Requirements - FAO Irrigation and drainage Paper No. 56.* FAO, Rome.

Anschutz, P., Zhong, S. J., Sundby, B., Mucci, A. & Gobeil, C. 1998. Burial efficiency of phosphorus and the geochemistry of iron in continental margin sediments. *Limnology and Oceanography,* 43, 53-64.

Appelo, C. A. J. & Postma, D. 2005. *Georchemsitry, groundwater and pollution,* Balkema, Amesterdam, pp.635.

Ashworth, D. J., Moore, J. & Shaw, G. 2008. Effects of soil type, moisture content, redox potential and methyl bromide fumigation on K-d values of radio-selenium in soil. *Journal of Environmental Radioactivity,* 99, 1136-1142.

Ashworth, D. J. & Shaw, G. 2005. Soil migration and plant uptake of technetium from a fluctuating water table. *Journal of Environmental Radioactivity,* 81, 155-171.

Ashworth, D. J. & Shaw, G. 2006a. A comparison of the soil migration and plant uptake of radioactive chlorine and iodine from contaminated groundwater. *Journal of Environmental Radioactivity,* 89, 61-80.

Ashworth, D. J. & Shaw, G. 2006b. Effects of moisture content and redox potential on in situ K-d values for radioiodine in soil. *Science of the Total Environment,* 359, 244-254.

Ashworth, D. J. & Shaw, G. 2006c. Soil migration, plant uptake and volatilisation of radio-selenium from a contaminated water table. *Science of The Total Environment,* 370, 506-514.

Ashworth, D. J., Shaw, G., Butler, A. P. & Ciciani, L. 2003. Soil transport and plant uptake of radio-iodine from near-surface groundwater. *Journal of Environmental Radioactivity,* 70, 99-114.

Avila, R. 2006a. *The ecosystem models used for dose assessments in SR-Can.* Technical and Social Science Report No.R-06-81, Swedish Nuclear Fuel and Waste Management Co., Stockholm. Available from: www.skb.se/upload/publications/pdf/R-06-81webb.pdf [Accessed May 2008].

Avila, R. 2006b. *Model of the long-term transfer of radionuclides in forests.* Technical Report No.TR-06-08, Swedish Nuclear Fuel and Waste Management Co., Stockholm. Available from: www.skb.se/upload/publications/pdf/TR-06-08webb.pdf [Accessed October 2008].

Avila, R. M., Kautsky, U. & Ekström, P. A. 2006. Modeling the long-term transport and accumulation of radionuclides in the landscape for derivation of dose conversion factors. *Ambio,* 35, 513-523.

Balistrieri, L. S. & Chao, T. T. 1990. Adsorption of selenium by amorphous iron oxyhydroxide and manganese dioxide. *Geochimica et Cosmochimica Acta,* 54, 739-751.

Bar-Yosef, B. & Meek, D. 1987. Selenium Sorption By Kaolinite and Montmorillonite. *Soil Science,* 144, 11-19.

Barnett, M. O., Jardine, P. M., Brooks, S. C. & Selim, H. M. 2000. Adsorption and transport of uranium (VI) in subsurface media. *Soil Science Society of America Journal,* 64, 908-917.

Bednar, A. J., Medina, V. F., Ulmer-Scholle, D. S., Frey, B. A., Johnson, B. L., Brostoff, W. N. & Larson, S. L. 2007. Effects of organic matter on the distribution of uranium in soil and plant matrices. *Chemosphere,* 70, 237-247.

Bergström, U., Nordlinder, S. & Aggeryd, I. 1999. *Models for dose assessments Modules for various biosphere types.* Technical Report No.TR-99-14, Swedish Nuclear Fuel and Waste Management Co., Stockholm. Available from: www.skb.se/upload/publications/pdf/TR99-14webb.pdf [Accessed April 2008].

BIOPROTA 2005. *Model intercomparison with focus on accumulation in soil. A report prepared within the International Collaborative Project BIOPROTA: Key Issues in Biosphere Aspects of Assessment of the Long-term Impact of Contaminant Releases Associated with Radioactive Waste Management.* Theme 2, Task 4 ANDRA (Agence nationale pour la gestion des dechets radioactifs), Chatenay-Malabry, France. Available from: www.bioprota.com [Accessed March 2008].

Bitterli, C., Bañuelos, G. S. & Schulin, R. 2010. Use of transfer factors to characterize uptake of selenium by plants. *Journal of Geochemical Exploration,* 107, 206-216.

Bohn, H. L., McNeal, B. L. & O'Connor, G. A. 2001. *Soil Chemistry,* John Wiley & Sons, Inc., New York, pp.307.

Boone, F. W., Kantelo, M. V., Mayer, P. G. & Palms, J. M. 1985. Residence Half-times of 129I in Undisturbed Surface Soils Based on Measured Soil Concentration Profiles. *Health Physics,* 48, 401-413.

Brookins, D. G. 1988. *Eh-pH diagrams for geochemistry,* Springer-Verlag, Berlin, pp.176.

Brooks, R. H. & Corey, A. T. 1964. Hydraulic properties of porous media. Hydrology paper no.3. Civil Engineering Dep, Colorado State University, Fort Collins, Colorado

Bunnenberg, C. & Taeschner, M. 2000. Soil fauna transport versus radionuclide migration. *Radiation Protection Dosimetry,* 92, 35-38.

Bunzl, K. 2002. Transport of fallout radiocesium in the soil by bioturbation: a random walk model and application to a forest soil with a high abundance of earthworms. *Science of The Total Environment,* 293, 191-200.

Butler, A. P., Chen, J., Aguero, A., Edlund, O., Elert, M., Kirchner, G., Raskob, W. & Sheppard, M. 1999. Performance assessment studies of models for water flow and radionuclide transport in vegetated soils using lysimeter data. *Journal of Environmental Radioactivity,* 42, 271-288.

Chappaz, A., Gobeil, C. & Tessier, A. 2008. Sequestration mechanisms and anthropogenic inputs of rhenium in sediments from Eastern Canada lakes. *Geochimica et Cosmochimica Acta,* 72, 6027-6036.

Chen, W., Li, L., Chang, A. C., Wu, L., Kwon, S.-I. & Bottoms, R. 2008. Modeling uptake kinetics of cadmium by field-grown lettuce. *Environmental Pollution,* 152, 147-152.

Darcheville, O., Février, L., Haichar, F. Z., Berge, O., Martin-Garin, A. & Renault, P. 2008. Aqueous, solid and gaseous partitioning of selenium in an oxic sandy soil under different microbiological states. *Journal of Environmental Radioactivity,* 99, 981-992.

Dhillon, S. K. & Dhillon, K. S. 2000. Selenium adsorption in soils as influenced by different anions. *Journal of Plant Nutrition and Soil Science,* 163, 577-582.

Di Bonito, M. 2005. *Trace elements in soil porewater: a comparison of sampling methods.* PhD Thesis, University of Nottingham.

Dolor, M. K., Gilmour, C. C. & Helz, G. R. 2009. Distinct Microbial Behavior of Re Compared to Tc: Evidence Against Microbial Re Fixation in Aquatic Sediments. *Geomicrobiology Journal,* 26, 470 - 483.

Doorenbos, J. & Pruitt, W. O. 1977. *Guidelines for predicting crop water requirements.* Irrigation and drainage paper, 24 Food and Agriculture Organization of the United Nations, Rome, pp.144.

Dripps, W. & Bradbury, K. 2007. A simple daily soil–water balance model for estimating the spatial and temporal distribution of groundwater recharge in temperate humid areas. *Hydrogeology Journal,* 15, 433-444.

Duc, M., Lefevre, G., Fedoroff, M., Jeanjean, J., Rouchaud, J. C., Monteil-Rivera, F., Dumonceau, J. & Milonjic, S. 2003. Sorption of selenium anionic species on apatites and iron oxides from aqueous solutions. *Journal of Environmental Radioactivity,* 70, 61-72.

Duff, M. C. & Amrhein, C. 1996. Uranium(VI) adsorption on goethite and soil in carbonate solutions. *Soil Science Society of America Journal,* 60, 1393-1400.

Echevarria, G., Sheppard, M. I. & Morel, J. 2001. Effect of pH on the sorption of uranium in soils. *Journal of Environmental Radioactivity,* 53, 257-264.

Ehlken, S. & Kirchner, G. 2002. Environmental processes affecting plant root uptake of radioactive trace elements and variability of transfer factor data: a review. *Journal of Environmental Radioactivity,* 58, 97-112.

Feddes, R. A., Kowalik, P. J. & Zaradny, H. 1978. *Simulation of Field Water Use and Crop Yield,* John Wiley & Sons, New York, NY, pp.188.

Fernández-Martínez, A. & Charlet, L. 2009. Selenium environmental cycling and bioavailability: a structural chemist point of view. *Reviews in Environmental Science and Biotechnology,* 8, 81-110.

Février, L., Martin-Garin, A. & Leclerc, E. 2007. Variation of the distribution coefficient (Kd) of selenium in soils under various microbial states. *Journal of Environmental Radioactivity,* 97, 189-205.

Fiedler, S., Vepraskas, M. J. & Richardson, J. L. 2007. Soil Redox Potential: Importance, Field Measurements, and Observations. *In:* Donald, L. S. (ed.) *Advances in Agronomy.* Academic Press, p.1-54.

Gerla, P. J., Sharif, M. U. & Korom, S. F. 2011. Geochemical processes controlling the spatial distribution of selenium in soil and water, west central South Dakota, USA. *Environmental Earth Sciences,* 62, 1551-1560.

Gil-García, C., Tagami, K., Uchida, S., Rigol, A. & Vidal, M. 2009. New best estimates for radionuclide solid-liquid distribution coefficients in soils. Part 3: miscellany of radionuclides (Cd, Co, Ni, Zn, I, Se, Sb, Pu, Am, and others). *Journal of Environmental Radioactivity,* 100, 704-715.

Graham, M. C., Oliver, I. W., MacKenzie, A. B., Ellam, R. M. & Farmer, J. G. 2008. An integrated colloid fractionation approach applied to the characterisation of porewater uranium-humic interactions at a depleted uranium contaminated site. *Science of The Total Environment,* 404, 207-217.

Grybos, M., Davranche, M., Gruau, G., Petitjean, P. & Pédrot, M. 2009. Increasing pH drives organic matter solubilization from wetland soils under reducing conditions. *Geoderma,* 154, 13-19.

Gu, B. H., Yan, H., Zhou, P., Watson, D. B., Park, M. & Istok, J. 2005. Natural humics impact uranium bioreduction and oxidation. *Environmental Science & Technology,* 39, 5268-5275.

Gustafsson, J. P. & Johnsson, L. 1994. The association between selenium and humic substances in forested ecosystems - laboratory evidence. *Applied Organometallic Chemistry,* 8, 141-147.

Heckman, K., Welty-Bernard, A., Rasmussen, C. & Schwartz, E. 2009. Geologic controls of soil carbon cycling and microbial dynamics in temperate conifer forests. *Chemical Geology,* 267, 12-23.

Hong, C. L., Weng, H. X., Qin, Y. C., Yan, A. L. & Xie, L. L. 2008. Transfer of iodine from soil to vegetables by applying exogenous iodine. *Agronomy for Sustainable Development,* 28, 575-583.

Hooda, P. S. (ed.) 2010. *Trace elements in soils,* Chichester: John Wiley & Sons Ltd, pp.616.

Hou, X. 2004. Application of 129I as an environmental tracer. *Journal of Radioanalytical and Nuclear Chemistry,* 262, 67-75.

Hou, X., Dahlgaard, H. & Nielsen, S. P. 2001. Chemical speciation analysis of 129I in seawater and a preliminary investigation to use it as a tracer for geochemical cycle study of stable iodine. *Marine Chemistry,* 74, 145-155.

Hou, X., Hansen, V., Aldahan, A., Possnert, G. r., Lind, O. C. & Lujaniene, G. 2009. A review on speciation of iodine-129 in the environmental and biological samples. *Analytica Chimica Acta,* 632, 181-196.

Hou, X. L., Fogh, C. L., Kucera, J., Andersson, K. G., Dahlgaard, H. & Nielsen, S. P. 2003. Iodine-129 and Caesium-137 in Chernobyl contaminated soil and their chemical fractionation. *The Science of The Total Environment,* 308, 97-109.

Hu, Q. H., Rose, T. P., Zavarin, M., Smith, D. K., Moran, J. E. & Zhao, P. H. 2008. Assessing field-scale migration of radionuclides at the Nevada Test Site: "mobile" species. *Journal of Environmental Radioactivity,* 99, 1617-1630.

IAEA 2003. *"Reference Biospheres" for solid radioactive waste disposal, Report of BIOMASS Theme 1 of the BIOsphere Modelling and ASSessment (BIOMASS) Programme.* International Atomic Energy Agency, Vienna, pp.560. Available from: www.pub.iaea.org [Accessed November 2008].

IAEA 2009. *Quantification of radionuclide transfer in terrestrial and freshwater environments for radiological assessments.* International atomic energy agency, Vienna. Technical document 1616. Available at: www.iaea.org.

Icenhower, J. P., Qafoku, N. P., Zachara, J. M. & Martin, W. J. 2010. The biogeochemistry of technetium: a review of the behavior of an artificial element in the natural environment. *American Journal of Science,* 310, 721-752.

Ishikawa, N. K., Uchida, S. & Tagami, K. 2010. Iodine sorption and its chemical form in the soil–soil solution system in Japanese agricultural fields. *19th World Congress of Soil Science, Soil Solutions for a Changing World.* Brisbane, Australia.

Jamieson, P. D., Semenov, M. A., Brooking, I. R. & Francis, G. S. 1998. Sirius: a mechanistic model of wheat response to environmental variation. *Eur. J. Agron.*, 8, 161-179.

John, P., Margaret, M., Lynne, H. & Fred, M. 2007. *Radiological and chemical fact sheets to support health risk analyses for contaminated areas.* Argonne National Laboratory.

Kaiser, K. & Guggenberger, G. 2000. The role of DOM sorption to mineral surfaces in the preservation of organic matter in soils. *Organic Geochemistry,* 31, 711-725.

Kalbitz, K., Solinger, S., Park, J.-H., Michalzik, B. & Matzner, E. 2000. Controls on the Dynamics of Dissolved Organic Matter in Soils: A Review. *Soil Science,* 165, 277-304.

Kamei-Ishikawa, N., Nakamaru, Y., Tagami, K. & Uchida, S. 2008. Sorption behavior of selenium on humic acid under increasing selenium concentration or increasing solid/liquid ratio. *Journal of Environmental Radioactivity,* 99, 993-1002.

Karlsson, S., Bergström, U., Meili, M. & Studsvik Eco and Safety AB 2001. *Models for dose assessments Models adapted to the SFR-area.* Technical Report No.TR-01-04, Swedish Nuclear Fuel and Waste Management Co., Stockholm. Available from: www.skb.se/upload/publications/pdf/tr-01-04webb.pdf [Accessed June 2008].

Kashparov, V., Colle, C., Zvarich, S., Yoschenko, V., Levchuk, S. & Lundin, S. 2005. Soil-to-plant halogens transfer studies: 1. Root uptake of radioiodine by plants. *Journal of Environmental Radioactivity,* 79, 187-204.

Kendy, E., Gérard-Marchant, P., Todd Walter, M., Zhang, Y., Liu, C. & Steenhuis, T. S. 2003. A soil-water-balance approach to quantify groundwater recharge from irrigated cropland in the North China Plain. *Hydrological Processes,* 17, 2011-2031.

Kim, E., Benedetti, M. F. & Boulègue, J. 2004. Removal of dissolved rhenium by sorption onto organic polymers: study of rhenium as an analogue of radioactive technetium. *Water Research,* 38, 448-454.

Kim, E. & Boulègue, J. 2003. Chemistry of rhenium as an analogue of technetium: Experimental studies of the dissolution of rhenium oxides in aqueous solutions. *Radiochimica Acta,* 91, 211-216.

Kirchner, G. 1998. Applicability of compartmental models for simulating the transport of radionuclides in soil. *Journal of Environmental Radioactivity,* 38, 339-352.

Kirchner, G., Strebl, F., Bossew, P., Ehlken, S. & Gerzabek, M. H. 2009. Vertical migration of radionuclides in undisturbed grassland soils. *Journal of Environmental Radioactivity,* 100, 716-720.

Klos, R. 2008. *The Generalised Ecosystem Modelling Approach in Radiological Assessment.* SSI Rapport No.2008:09, Swedish Radiation Protection Authority, Stockholm. Available from: www.stralsakerhetsmyndigheten.se/Publikationer/Rapport/.../200809/ [Accessed July 2008].

Klos, R. 2010. *GEMA3D – landscape modelling for dose assessments.* SSM Research Report No.2010:28, Swedish Radiation Safety Authority, Stockholm. Available from: www.stralsakerhetsmyndigheten.se [Accessed October 2010].

Kłos, R. & Albrecht, A. 2005. The significance of agricultural vs. natural ecosystem pathways in temperate climates in assessments of long-term radiological impact. *Journal of Environmental Radioactivity,* 83, 137-169.

Kłos, R. & Wilmot, R. 2002. *Review of Project SAFE: Comments on biosphere conceptual model description and risk assessment methodology*. SSI Rapport No.2002:17, Swedish Radiation Protection Authority, Stockholm. Available from: www.stralsakerhetsmyndigheten.se/Publikationer/Rapport/.../200217/ [Accessed April 2008].

Kögel-Knabner, I., Amelung, W., Cao, Z., Fiedler, S., Frenzel, P., Jahn, R., Kalbitz, K., Kölbl, A. & Schloter, M. 2010. Biogeochemistry of paddy soils. *Geoderma*, 157, 1-14.

Kohler, M., Curtis, G. P., Meece, D. E. & Davis, J. A. 2003. Methods for Estimating Adsorbed Uranium(VI) and Distribution Coefficients of Contaminated Sediments. *Environmental Science & Technology*, 38, 240-247.

Langmuir, D. 1978. Uranium solution-mineral equilibria at low temperatures with applications to sedimentary ore deposits. *Geochimica et Cosmochimica Acta*, 42, 547-569.

Liu, Y., Pereira, L. S. & Fernando, R. M. 2006. Fluxes through the bottom boundary of the root zone in silty soils: Parametric approaches to estimate groundwater contribution and percolation. *Agricultural Water Management*, 84, 27-40.

Luo, W. & Gu, B. 2009. Dissolution and Mobilization of Uranium in a Reduced Sediment by Natural Humic Substances under Anaerobic Conditions. *Environmental Science & Technology*, 43, 152-156.

M.J. Watts & Mitchell, C. J. 2008. A pilot study on iodine in soils of Greater Kabul and Nangarhar provinces of Afghanistan. *Environ Geochem Health. DOI 10.1007/s10653-008-9202-9.*

Maillant, S., Sheppard, M. I., Echevarria, G., Denys, S., Villemin, G., Tekely, P., Leclerc-Cessac, E. & Morel, J. L. 2007. Aged anthropogenic iodine in a boreal peat bog. *Applied Geochemistry*, 22, 873-887.

Marklund, L., Worman, A., Geier, J., Simic, E. & Dverstorp, B. Impact of landscape topography and quaternary overburden on the performance of a geological repository of nuclear waste. Proceedings of International High-Level Radioactive Waste Management Conference, Apr 30-May 04, 2006, Las Vegas, NV: Amer Nuclear Soc p.165-179.

Maset, E. R., Sidhu, S. H., Fisher, A., Heydon, A., Worsfold, P. J., Cartwright, A. J. & Keith-Roach, M. J. 2006. Effect of organic co-contaminants on technetium and rhenium speciation and solubility under reducing conditions. *Environmental Science & Technology,* 40, 5472-5477.

Masscheleyn, P. H., Delaune, R. D. & Patrick, W. H., Jr. 1991. Arsenic and Selenium Chemistry as Affected by Sediment Redox Potential and pH. *J Environ Qual,* 20, 522-527.

Mathias, S. A., Butler, A. P. & Wheater, H. S. 2008. Modelling radioiodine transport across a capillary fringe. *Journal of Environmental Radioactivity,* 99, 716-729.

Millward, G. E. & Liu, Y. P. 2003. Modelling metal desorption kinetics in estuaries. *Science of The Total Environment,* 314–316, 613-623.

Morris, K., Livens, F. R., Charnock, J. M., Burke, I. T., McBeth, J. M., Begg, J. D. C., Boothman, C. & Lloyd, J. R. 2008. An X-ray absorption study of the fate of technetium in reduced and reoxidised sediments and mineral phases. *Applied Geochemistry,* 23, 603-617.

Mualem, Y. 1976. A new model for predicting the hydraulic conductivity of unsaturated porous media. *Water Resour. Res.,* 12, 513-522.

Müller-Lemans, H. & van Dorp, F. 1996. Bioturbation as a mechanism for radionuclide transport in soil: Relevance of earthworms. *Journal of Environmental Radioactivity,* 31, 7-20.

Muramatsu, Y. & Yoshida, S. 1999. Effects of microorganisms on the fate of iodine in the soil environment. *Geomicrobiology Journal,* 16, 85-93.

Muramatsu, Y., Yoshida, S., Uchida, S. & Hasebe, A. 1996. Iodine desorption from rice paddy soil. *Water, Air, & Soil Pollution,* 86, 359-371.

Nagata, T. & Fukushi, K. 2010. Prediction of iodate adsorption and surface speciation on oxides by surface complexation modeling. *Geochimica et Cosmochimica Acta,* 74, 6000-6013.

Nagata, T., Fukushi, K. & Takahashi, Y. 2009. Prediction of iodide adsorption on oxides by surface complexation modeling with spectroscopic confirmation. *Journal of Colloid and Interface Science,* 332, 309-316.

Nakamaru, Y., Tagami, K. & Uchida, S. 2005. Distribution coefficient of selenium in Japanese agricultural soils. *Chemosphere,* 58, 1347-1354.

Nash, J. E. & Sutcliffe, J. V. 1970. River flow forecasting through conceptual models part I - A discussion of principles. *Journal of Hydrology,* 10, 282-290.

NDA 2011. *The 2010 UK Radioactive Waste Inventory: Main Report.* Nuclear Decommissioning Authority, Cumbria, pp.130. Available from: www.nda.gov.uk/ukinventory [Accessed December 2011].

Nierop, K. G. J. J., Jansen, B. & Verstraten, J. M. 2002. Dissolved organic matter, aluminium and iron interactions: precipitation induced by metal/carbon ratio, pH and competition. *The Science of The Total Environment,* 300, 201-211.

Pabalan, R. & Turner, D. 1996. Uranium(6+) sorption on montmorillonite: Experimental and surface complexation modeling study. *Aquatic Geochemistry,* 2, 203-226.

Pédrot, M., Boudec, A. L., Davranche, M., Dia, A. & Henin, O. 2011. How does organic matter constrain the nature, size and availability of Fe nanoparticles for biological reduction? *Journal of Colloid and Interface Science,* 359, 75-85.

Pokrovsky, O. S., Schott, J. & Dupre, B. 2006. Trace element fractionation and transport in boreal rivers and soil porewaters of permafrost-dominated basaltic terrain in Central Siberia. *Geochimica et Cosmochimica Acta,* 70, 3239-3260.

Ponnamperuma, F. N. 1972. The chemistry of submerged soils. *Advances in Agronomy,* 24, 29–96.

Posiva 2010. *Interim Summary Report of the Safety Case 2009.* No.2010-02, Posiva Oy, Eurajoki, pp.174. Available from: http://www.posiva.fi/en/databank/posiva_reports/interim_summary_report_of_the_safety_case_2009.429.xhtml?cd_order=name&cd_offset=10 [Accessed December 2011].

Pröhl, G., Olyslaegers, G., Kanyar, B., Pinedo, P., Bergström, U., Mobbs, S., Eged, K., Katona, T., Simón, I., Hallberg, U. B., Chen, Q., Kowe & Zeevaert, T. 2005. Development and comparison of five site-specific biosphere models for safety assessment of radioactive waste disposal. *Journal of Radiological Protection,* 25, 343-373.

Rädlinger, G. & Heumann, K. G. 2000. Transformation of Iodide in Natural and Wastewater Systems by Fixation on Humic Substances. *Environmental Science & Technology,* 34, 3932-3936.

Rausch, R., Schäfer, W., Therrien, R. & Wagner, C. 2005. *Solute Transport Modelling: An Introduction to Models and Solution Strategies,* Gebr. Borntraeger Verlagsbuchhandlung, Science Publishers, Stuttgart.

Richards, L. A. 1931. Cpillary Conduction of Liquids Through Porous Mediums. *Physics,* 1, 318-333.

Rovira, M., Giménez, J., Martinez, M., Martinez-Lladó, X., de Pablo, J., Martí, V. & Duro, L. 2008. Sorption of selenium(IV) and selenium(VI) onto natural iron oxides: Goethite and hematite. *Journal of Hazardous Materials,* 150, 279-284.

Santschi, P. H. & Schwehr, K. A. 2004. 129I/127I as a new environmental tracer or geochronometer for biogeochemical or hydrodynamic processes in the hydrosphere and geosphere: the central role of organo-iodine. *Science of The Total Environment,* 321, 257-271.

Schwehr, K. A., Santschi, P. H., Kaplan, D. I., Yeager, C. M. & Brinkmeyer, R. 2009. Organo-Iodine Formation in Soils and Aquifer Sediments at Ambient Concentrations. *Environmental Science & Technology,* 43, 7258-7264.

Séby, F., Potin-Gautier, M., Giffaut, E., Borge, G. & Donard, O. F. X. 2001. A critical review of thermodynamic data for selenium species at 25°C. *Chemical Geology,* 171, 173-194.

Séby, F., Potin-Gautier, M., Giffaut, E. & Donard, O., F.X. 1998. Assessing the speciation and the biogeochemical processes affecting the mobility of selenium from a geological repository of radioactive wastesto the biosphere. *Analusis,* 26, 193-198.

Shaw, G. & Ashworth, D. 2006. Selenium: Radionuclides. *Encyclopedia of Inorganic Chemistry.* John Wiley & Sons, Ltd.

Shaw, G. & Bell, J. N. B. 1991. Competitive effects of potassium and ammonium on caesium uptake kinetics in wheat. *Journal of Environmental Radioactivity,* 13, 283-296.

Sheppard, M. I., Sheppared, S. C. & Grant, C. A. 2007. Solid/liquid partition coefficients to model trace element critical loads for agricultural soils in Canada. *Canadian Journal of Soil Science,* 87, 189-201.

Sheppard, M. I. & Thibault, D. H. 1992. Chemical behaviour of iodine in organic and mineral soils. *Applied Geochemistry,* 7, 265-272.

Sheppard, M. I., Thibault, D. H., McMurry, J. & Smith, P. A. 1995. Factors affecting the soil sorption of iodine. *Water, Air, & Soil Pollution,* 83, 51-67.

Sheppard, S., Long, J., Sanipelli, B. & Sohlenius, G. 2009. *Solid/liquid partition coefficients (Kd) for selected soils and sediments at Forsmark and Laxemar-Simpevarp.* Technical and Social Science Report No.R-09-27, Swedish Nuclear Fuel and Waste Management Co., Stockholm. Available from: www.skb.se/upload/publications/pdf/R-09-27webb.pdf [Accessed Jan 2010].

Sheppard, S. C. 2003. Interpolation of solid/liquid partition coefficients, Kd, for iodine in soils. *Journal of Environmental Radioactivity,* 70, 21-27.

Sheppard, S. C. 2011. Robust Prediction of Kd from Soil Properties for Environmental Assessment. *Human and Ecological Risk Assessment,* 17, 263-279.

Sheppard, S. C., Long, J. M. & Sanipelli, B. 2010. Plant/soil concentration ratios for paired field and garden crops, with emphasis on iodine and the role of soil adhesion. *Journal of Environmental Radioactivity,* 101, 1032-1037.

Shimamoto, Y. S., Takahashi, Y. & Terada, Y. 2011. Formation of Organic Iodine Supplied as Iodide in a Soil-Water System in Chiba, Japan. *Environmental Science & Technology,* 45, 2086-2092.

Shinonaga, T., Gerzabek, M. H., Strebl, F. & Muramatsu, Y. 2001. Transfer of iodine from soil to cereal grains in agricultural areas of Austria. *The Science of The Total Environment,* 267, 33-40.

Shotbolt, L. 2008. Pore water sampling from lake and estuary sediments using Rhizon samplers. *Journal of Paleolimnology.*

Šimůnek, J. & Hopmans, J. W. 2009. Modeling compensated root water and nutrient uptake. *Ecological Modelling,* 220, 505-521.

Šimůnek, J., Šejna, M., Saito, H., Sakai, M. & van Genuchten, M. T. 2009. *The HYDRUS-1D Software Package for Simulating the One-Dimensional Movement of Water, Heat, and Multiple Solutes in Variably-Saturated Media. Version 4.08.* Department of environmental sciences, University of California Riverside, Riverside, California.

Šimůnek, J., van Genuchten, M. T. & Sejna, M. 2008. Development and Applications of the HYDRUS and STANMOD Software Packages and Related Codes. *Vadose Zone Journal,* 7, 587-600.

Singhal, R. K., Kumar, A., Karpe, P. J. R., Datta, M. & Hegde, A. G. 2005. Association of uranium with colloids of natural organic matter in subsurface aquatic environment. *Journal of Radioanalytical and Nuclear Chemistry,* 265, 405-408.

SKB 2010. *RD&D Programme 2010. Programme for research, development and demonstration of methods for the management and disposal of nuclear waste.* Technical Report No.TR-10-63, Swedish Nuclear Fuel and Waste Management Co., Stockholm. Available from: http://www.skb.se/Templates/Standard___17139.aspx [Accessed December 2011].

Smith, J. T. & Elder, D. G. 1999. A comparison of models for characterizing the distribution of radionuclides with depth in soils. *European Journal of Soil Science,* 50, 295-307.

Sparks, D. L. 2003. *Environmental Soil Chemistry,* Academic Perss, pp.352.

Sposito, G. 2008. *The Chemistry of Soils,* Oxford University Press, Inc, New York.

Stumm, W. & Morgan, J. J. 1996. *Aquatic chemistry: chemical equilibria and rates in natural waters,* John Wiley & Sons, Inc., New York, pp.1040.

Tagami, K. & Uchida, S. 2008. Determination of bioavailable rhenium fraction in agricultural soils. *Journal of Environmental Radioactivity,* 99, 973-980.

Takeno, N. 2005. *Atlas of Eh-pH diagrams: Intercomparison of thermodynamic databases.* Geological Survey of Japan Open File Report No.419 National Institute of Advanced Industrial Science and Technology, Research Center for Deep Geological Environments.

Tipping, E. 1998. Humic Ion-Binding Model VI: An Improved Description of the Interactions of Protons and Metal Ions with Humic Substances. *Aquatic Geochemistry,* 4, 3-47.

Tolu, J., Le Hécho, I., Bueno, M., Thiry, Y. & Potin-Gautier, M. 2011. Selenium speciation analysis at trace level in soils. *Analytica Chimica Acta,* 684, 126-133.

Um, W., Serne, R. J., Brown, C. F. & Last, G. V. 2007. U(VI) adsorption on aquifer sediments at the Hanford Site. *Journal of Contaminant Hydrology,* 93, 255-269.

van Dam, J. C. & Feddes, R. A. 2000. Numerical simulation of infiltration, evaporation and shallow groundwater levels with the Richards equation. *Journal of Hydrology,* 233, 72-85.

van Dam, J. C., Huygen, J., Wesseling, J. G., Feddes, R. A., Kabat, P., van Walsum, P. E. V., Groenendijk, P. & van Diepen, C. A. 1997. *Theory of SWAP Version 2.0.* No.71, Department of Water Resources, Wageningen Agricultural University, pp.167.

van Genuchten, M. T. 1980. A closed-form equation for predicting the hydraulic conductivity of unsaturated soils. *Soil Sci. Soc. Am. J.,* 44, 892-898.

Vanclooster, M., Viaene, P., Christiaens, K. & Ducheyne, S. 1996. *WAVE, Release 2.1: Instruction Manual Institute for Land and Water Manegement.* Katholeke Universiteit Leuven, Leuve, Belgium.

Vandenhove, H., Gil-García, C., Rigol, A. & Vidal, M. 2009a. New best estimates for radionuclide solid-liquid distribution coefficients in soils. Part 2. Naturally occurring radionuclides. *Journal of Environmental Radioactivity,* 100, 697-703.

Vandenhove, H., Van Hees, M., Olyslaegers, G. & Vidal, M. 2009b. Proposal for new best estimates for the soil solid-liquid distribution coefficient and soil-to-plant transfer of nickel. *Journal of Environmental Radioactivity,* 100, 342-347.

Vandenhove, H., Van Hees, M., Wouters, K. & Wannijn, J. 2007. Can we predict uranium bioavailability based on soil parameters? Part 1: Effect of soil parameters on soil solution uranium concentration. *Environmental Pollution*, 145, 587-595.

Wang, Z. & Gao, Y. 2001. Biogeochemical cycling of selenium in Chinese environments. *Applied Geochemistry*, 16, 1345-1351.

Wegehenkel, M. 2005. Validation of a soil water balance model using soil water content and pressure head data. *Hydrological Processes*, 19, 1139-1164.

Weng, L. P., Vega, F. A., Supriatin, S., Bussink, W. & Van Riemsdijk, W. H. 2011. Speciation of Se and DOC in Soil Solution and Their Relation to Se Bioavailability. *Environmental Science & Technology*, 45, 262-267.

Wharton, M. J., Atkins, B., Charnock, J. M., Livens, F. R., Pattrick, R. A. D. & Collison, D. 2000. An X-ray absorption spectroscopy study of the coprecipitation of Tc and Re with mackinawite (FeS). *Applied Geochemistry*, 15, 347-354.

Wheater, H. S., Bell, J. N. B., Butler, A. P., Jackson, B. M., Ciciani, L., Ashworth, D. J. & Shaw, G. G. 2007. *Biosphere Implications of Deep Disposal of Nuclear Waste: The Upward Migration of Radionuclides in Vegetated Soils*, Imperial College Press, London.

Whicker, F. W. & Kirchner, T. B. 1987. PATHWAY: a dynamic food-chain model to predict radionuclide ingestion after fallout deposition. *Health Physics*, 52, 717-737.

Whitehead, D. C. 1973. Studies on iodine in British soils. *European Journal of Soil Science*, 24, 260-270.

Whitehead, D. C. 1974. The sorption of iodide by soil components. *Journal of the Science of Food and Agriculture*, 25, 73-79.

Whitehead, D. C. 1984. The distribution and transformations of iodine in the environment. *Environment International*, 10, 321-339.

Xu, S., Wörman, A., Dverstorp, B., Kłos, R., Shaw, G. & Marklund, O. L. 2008. *SSI's independent consequence calculations in support of the regulatory review of the SR-Can safety assessment.* No.2008:08, Swedish Radiation Protection Authority, Stockholm. Available from: www.stralsakerhetsmyndigheten.se/Publikationer/Rapport/.../200808/.

Xu, S. L., Worman, A. & Dverstorp, B. 2007. Criteria for resolution-scales and parameterisation of compartmental models of hydrological and ecological mass flows. *Journal of Hydrology,* 335, 364-373.

Yamada, H., Kang, Y. M., Aso, T., Uesugi, H., Fujimura, T. & Yonebayashi, K. 1998. Chemical forms and stability of selenium in soil *Soil Sci. Plant Nutr.*, 44 385– 391

Yamaguchi, N., Nakano, M., Takamatsu, R. & Tanida, H. 2010. Inorganic iodine incorporation into soil organic matter: evidence from iodine K-edge X-ray absorption near-edge structure. *Journal of Environmental Radioactivity,* 101, 451-457.

Yamaguchi, N., Nakano, M., Tanida, H., Fujiwara, H. & Kihou, N. 2006. Redox reaction of iodine in paddy soil investigated by field observation and the I K-Edge XANES fingerprinting method. *Journal of Environmental Radioactivity,* 86, 212-226.

Yamashita, Y., Takahashi, Y., Haba, H., Enomoto, S. & Shimizu, H. 2007. Comparison of reductive accumulation of Re and Os in seawater - sediment systems. *Geochimica et Cosmochimica Acta,* 71, 3458-3475.

Yoshida, S., Muramatsu, Y., Katou, S. & Sekimoto, H. 2007. Determination of the chemical forms of iodine with IC-ICP-MS and its application to environmental samples. *Journal of Radioanalytical and Nuclear Chemistry,* 273, 211-214.

Zhang, Moore, J. N. & Frankenberger, W. T. 1999. Speciation of Soluble Selenium in Agricultural Drainage Waters and Aqueous Soil-Sediment Extracts Using Hydride Generation Atomic Absorption Spectrometry. *Environmental Science & Technology,* 33, 1652-1656.

Zhang, Y. & Moore, J. N. 1996. Selenium Fractionation and Speciation in a Wetland System. *Environmental Science & Technology,* 30, 2613-2619.

Zhang, Y. & Moore, J. N. 1997a. Interaction of selenate with a wetland sediment. *Applied Geochemistry,* 12, 685-691.

Zhang, Y. & Moore, J. N. 1997b. Reduction Potential of Selenate in Wetland Sediment. *J Environ Qual,* 26, 910-916.

Zhang, Y., Zahir, Z. A. & Frankenberger, W. T., Jr. 2004. Fate of Colloidal-Particulate Elemental Selenium in Aquatic Systems. *J Environ Qual,* 33, 559-564.

Zhou, P. & Gu, B. H. 2005. Extraction of oxidized and reduced forms of uranium from contaminated soils: Effects of carbonate concentration and pH. *Environmental Science & Technology,* 39, 4435-4440.

Zhu, Y. G., Huang, Y., Hu, Y., Liu, Y. & Christie, P. 2004. Interactions between selenium and iodine uptake by spinach (Spinacia oleracea L.) in solution culture. *Plant and Soil,* 261, 99-105.

Appendix 1 Elemental concentrations in porewater samples collected from microcosms

Elemental concentrations in porewater samples collected from mini column microcosms. Sample ID code: sampling day-soil type-replicate No.

Sample ID	Fe $\mu g\ L^{-1}$	Se $\mu g\ L^{-1}$	I $\mu g\ L^{-1}$	Re $ng\ L^{-1}$	U $\mu g\ L^{-1}$
d1-SB-ATS-1	104.19	1.12	36.85	26.94	0.54
d1-SB-ATS-2	95.95	1.10	36.13	17.73	0.45
d1-SB-ATS-3	no sample	1.04	34.29	27.58	no sample
d2-SB-ATS-1	175.73	1.14	50.73	16.88	0.75
d2-SB-ATS-2	135.93	1.08	53.10	14.51	0.70
d2-SB-ATS-3	181.73	1.09	48.11	16.77	0.20
d3-SB-ATS-1	255.46	0.97	72.12	12.94	0.92
d3-SB-ATS-2	314.56	0.87	85.12	11.43	0.83
d3-SB-ATS-3	291.06	0.88	55.62	13.83	0.89
d4-SB-ATS-1	605.06	0.90	98.18	7.40	1.03
d4-SB-ATS-2	339.76	0.79	111.28	8.15	0.94
d4-SB-ATS-3	378.16	0.70	108.28	6.78	0.82
d5-SB-ATS-1	706.66	0.91	119.18	7.95	1.01
d5-SB-ATS-2	801.96	0.85	165.08	6.51	1.09
d5-SB-ATS-3	619.06	0.83	131.18	7.17	1.05
d6-SB-ATS-1	1346.76	0.87	177.28	6.43	1.10
d6-SB-ATS-2	1312.76	0.79	137.18	6.37	1.14
d6-SB-ATS-3	1307.76	0.81	136.28	6.34	1.04
d7-SB-ATS-1	1945.76	0.81	147.68	6.71	0.98
d7-SB-ATS-2	1761.76	0.77	183.88	5.95	0.94

Sample ID	Fe	Se	I	Re	U
	$\mu g\ L^{-1}$	$\mu g\ L^{-1}$	$\mu g\ L^{-1}$	$ng\ L^{-1}$	$\mu g\ L^{-1}$
d7-SB-ATS-3	2055.76	0.82	159.18	5.80	1.01
d10-SB-ATS-1	5336.00	1.16	337.82	9.47	0.77
d10-SB-ATS-2	6140.00	0.95	402.52	8.63	1.41
d10-SB-ATS-3	9566.00	0.99	376.72	7.84	1.32
d14-SB-ATS-1	13030.00	1.40	538.42	9.60	0.85
d14-SB-ATS-2	12760.00	1.13	718.62	11.29	1.84
d14-SB-ATS-3	14950.00	1.05	693.12	7.90	1.20
d17-SB-ATS-1	20700.00	1.77	711.12	11.30	0.56
d17-SB-ATS-2	22000.00	1.33	909.02	11.13	1.38
d17-SB-ATS-3	22730.00	1.20	700.12	8.08	0.83
d22-SB-ATS-1	19129.95	1.30	901.76	7.09	1.04
d22-SB-ATS-2	17089.95	1.34	1097.16	10.31	2.30
d22-SB-ATS-3	19619.95	1.33	1080.16	8.51	0.97
d1-SB-ASS-1	177.59	2.05	55.07	57.58	0.20
d1-SB-ASS-2	179.39	2.04	55.17	61.29	0.21
d1-SB-ASS-3	185.89	2.08	55.49	61.62	0.21
d2-SB-ASS-1	122.33	1.79	52.76	25.10	0.16
d2-SB-ASS-2	128.53	1.91	57.93	32.83	0.20
d2-SB-ASS-3	143.53	1.89	60.30	31.12	0.20
d3-SB-ASS-1	180.86	1.37	72.36	12.50	0.17
d3-SB-ASS-2	145.76	1.44	81.59	14.45	0.20
d3-SB-ASS-3	104.06	1.43	87.98	12.98	0.50
d4-SB-ASS-1	249.56	1.16	75.87	11.02	0.23
d4-SB-ASS-2	412.36	1.23	88.34	10.54	0.20
d4-SB-ASS-3	519.36	1.26	92.38	11.77	0.21
d5-SB-ASS-1	422.56	1.09	70.51	9.90	0.24
d5-SB-ASS-2	511.16	1.13	97.68	10.80	0.22
d5-SB-ASS-3	625.56	0.82	105.38	8.06	0.17
d6-SB-ASS-1	762.16	1.02	90.28	10.76	0.23
d6-SB-ASS-2	514.56	1.05	107.58	9.16	0.20

Sample ID	Fe	Se	I	Re	U
	µg L^{-1}	µg L^{-1}	µg L^{-1}	ng L^{-1}	µg L^{-1}
d6-SB-ASS-3	892.16	1.07	117.78	10.10	0.21
d7-SB-ASS-1	1164.76	0.90	100.68	7.59	0.23
d7-SB-ASS-2	1007.76	1.01	117.38	9.22	0.21
d7-SB-ASS-3	1142.76	1.02	122.58	9.59	0.21
d10-SB-ASS-1	4148.00	1.02	238.62	9.35	0.21
d10-SB-ASS-2	3148.00	1.10	290.12	10.39	0.24
d10-SB-ASS-3	4778.00	1.13	262.32	10.64	0.22
d14-SB-ASS-1	7074.00	1.20	441.52	11.54	0.28
d14-SB-ASS-2	5339.00	1.19	403.82	11.41	0.29
d14-SB-ASS-3	6958.00	1.13	380.82	10.51	0.20
d17-SB-ASS-1	12810.00	1.27	466.72	9.49	0.16
d17-SB-ASS-2	11540.00	1.28	539.72	10.30	0.28
d17-SB-ASS-3	12280.00	1.26	557.82	10.46	0.25
d22-SB-ASS-1	11799.95	1.43	841.36	10.24	0.67
d22-SB-ASS-2	11169.95	1.46	799.26	9.67	0.72
d22-SB-ASS-3	11719.95	1.41	700.16	9.22	0.38
d1-SB-WTS-1	6413.69	5.80	73.91	55.10	0.29
d1-SB-WTS-2	6297.69	6.15	75.82	70.13	0.29
d1-SB-WTS-3	6764.69	6.17	72.23	68.11	0.31
d2-SB-WTS-1	5522.73	5.46	69.06	50.84	0.25
d2-SB-WTS-2	6031.73	6.06	74.23	59.57	0.27
d2-SB-WTS-3	5529.73	7.10	71.41	71.24	0.25
d3-SB-WTS-1	4925.76	5.43	78.08	51.80	0.22
d3-SB-WTS-2	6000.76	6.11	70.46	58.16	0.26
d3-SB-WTS-3	5917.76	7.96	75.96	75.80	0.26
d4-SB-WTS-1	5679.76	6.05	83.45	53.48	0.24
d4-SB-WTS-2	6166.76	6.02	84.52	56.92	0.25
d4-SB-WTS-3	6609.76	7.30	82.04	66.15	0.27
d5-SB-WTS-1	5342.76	5.88	92.78	53.56	0.21
d5-SB-WTS-2	5860.76	5.58	107.38	54.68	0.23

Sample ID	Fe	Se	I	Re	U
	µg L^{-1}	µg L^{-1}	µg L^{-1}	ng L^{-1}	µg L^{-1}
d5-SB-WTS-3	5883.76	6.32	276.08	57.45	0.24
d6-SB-WTS-1	6377.76	6.07	110.62	56.12	0.25
d6-SB-WTS-2	6300.76	5.73	88.36	54.28	0.23
d6-SB-WTS-3	6222.76	5.88	87.29	56.38	0.22
d7-SB-WTS-1	7214.76	5.85	107.08	50.84	0.26
d7-SB-WTS-2	6117.76	5.20	94.38	48.21	0.21
d7-SB-WTS-3	no sample	0.00	102.78	0.00	no sample
d10-SB-WTS-1	21580.00	8.78	201.32	65.17	0.32
d10-SB-WTS-2	13770.00	7.63	152.12	61.21	0.28
d10-SB-WTS-3	22450.00	10.42	199.02	73.80	0.38
d14-SB-WTS-1	54530.00	12.95	332.72	95.06	0.44
d14-SB-WTS-2	40520.00	12.04	285.82	88.42	0.38
d14-SB-WTS-3	54730.00	14.20	351.12	95.89	0.47
d17-SB-WTS-1	87420.00	14.59	510.22	127.50	0.52
d17-SB-WTS-2	68420.00	13.94	466.82	114.40	0.44
d17-SB-WTS-3	77500.00	15.22	531.02	119.70	0.51
d22-SB-WTS-1	73870	16.98	943.9	181.7	2.07
d22-SB-WTS-2	63250	16.75	797.5	170.3	1.83
d22-SB-WTS-3	65370	17.21	864	153.8	2.04

Elemental concentrations in porewater samples collected from sacrificial microcosms. Sample ID code: sampling day-soil type-filter size-replicate No.

Sample ID	Fe	Se	I	Re	U
	$\mu g\ L^{-1}$	$\mu g\ L^{-1}$	$\mu g\ L^{-1}$	$ng\ L^{-1}$	$\mu g\ L^{-1}$
d7-SB-ATS-0.1-1	78.94	1.471	28.01	0.041	0.282
d7-SB-ATS-0.1-2	63.85	1.154	27.73	0.031	0.4
d7-SB-ATS-0.22-1	74.64	0.994	62.54	0.035	0.471
d7-SB-ATS-0.22-2	616.9	1.413	35.81	0.026	0.33
d7-SB-ATS-0.45-1	342.5	1.409	36.66	0.027	0.546
d7-SB-ATS-0.45-2	234.5	1.172	37.95	0.031	0.322
d15-SB-ATS-0.45-1	301.6	2	136.73	0.058	0.677
d15-SB-ATS-0.45-2	213.4	1.064	107.53	0.011	3.527
d21-SB-ATS-0.45-1	5951	2.42	728.12	0.021	10.02
d21-SB-ATS-0.45-2	4033	2.203	591.62	0.018	8.608
d30-SB-ATS-0.45-1	679.7	1.253	55.54	0.009	0.818
d30-SB-ATS-0.45-2	11570	1.874	950.02	0.022	11.19
d7-SB-ASS-0.1-1	90.69	3.881	155.43	0.085	0.285
d7-SB-ASS-0.1-2	58.15	1.701	78.51	0.133	0.04
d7-SB-ASS-0.22-1	405.8	1.928	93.41	0.125	0.146
d7-SB-ASS-0.22-2	252.8	1.858	89.83	0.125	0.081
d7-SB-ASS-0.45-1	520.3	1.914	81.57	0.112	0.104
d7-SB-ASS-0.45-2	570	1.813	99.77	0.133	0.118
d15-SB-ASS-0.45-1	293.8	2.111	158.23	0.057	0.605
d15-SB-ASS-0.45-2	1098	1.368	247.63	0.012	5.841
d21-SB-ASS-0.45-1	252.9	2.484	129.82	0.101	0.173
d21-SB-ASS-0.45-2	424.3	2.401	96.65	0.109	0.07
d30-SB-ASS-0.45-1	688.8	1.455	72.92	0.112	0.095
d30-SB-ASS-0.45-2	425.6	1.358	72.38	0.126	0.133
d7-SB-GTS-0.1-1	184.1	2.04	34.91	0.063	0.155
d7-SB-GTS-0.1-2	189.6	1.348	28.54	0.071	0.077
d7-SB-GTS-0.22-1	383	1.243	37.72	0.063	0.218
d7-SB-GTS-0.22-2	243.7	1.151	47.24	0.079	0.161

Sample ID	Fe	Se	I	Re	U
	$\mu g\ L^{-1}$	$\mu g\ L^{-1}$	$\mu g\ L^{-1}$	$ng\ L^{-1}$	$\mu g\ L^{-1}$
d7-SB-GTS-0.45-1	415.9	1.173	32.61	0.077	0.121
d7-SB-GTS-0.45-2	490.9	1.066	39.48	0.074	0.12
d15-SB-GTS-0.45-1	1564	1.409	192.43	0.023	1.239
d15-SB-GTS-0.45-2	1609	1.207	105.73	0.017	0.633
d21-SB-GTS-0.45-1	487.3	1.363	30.21	0.026	0.125
d21-SB-GTS-0.45-2	1293	1.371	22.59	0.042	0.129
d30-SB-GTS-0.45-1	1025	0.901	21.39	0.017	0.139
d30-SB-GTS-0.45-2	1287	0.902	20.14	0.014	0.175
d7-SB-GSS-0.1-1	72.62	2.52	70.35	0.16	0.075
d7-SB-GSS-0.1-2	157.8	2.013	79.30	0.146	0.106
d7-SB-GSS-0.22-1	406.1	2.101	195.63	0.139	0.543
d7-SB-GSS-0.45-1	634.5	2.122	69.02	0.156	0.171
d7-SB-GSS-0.45-2	569.5	2.063	64.56	0.139	0.193
d15-SB-GSS-0.45-1	717	1.066	90.46	0.091	0.129
d15-SB-GSS-0.45-2	1526	1.606	58.92	0.112	0.176
d21-SB-GSS-0.45-1	725.8	1.796	74.42	0.15	0.16
d21-SB-GSS-0.45-2	379.3	1.221	51.16	0.168	0.087
d30-SB-GSS-0.45-1	161.6	1.127	48.53	0.157	0.058
d30-SB-GSS-0.45-2	357.4	1.387	46.83	0.139	0.098
d7-SB-WTS-0.1-1	854.7	1.029	16.69	0.143	0.098
d7-SB-WTS-0.1-2	1958	1.782	182.93	0.138	0.215
d7-SB-WTS-0.22-1	732.4	0.773	15.68	0.137	0.114
d7-SB-WTS-0.22-2	11070	3.892	244.93	0.107	1.154
d7-SB-WTS-0.45-1	5298	2.896	88.32	0.11	0.917
d7-SB-WTS-0.45-2	1938	1.315	24.35	0.135	0.257
d15-SB-WTS-0.45-1	11040	5.076	173.23	0.069	1.378
d15-SB-WTS-0.45-2	14150	5.09	281.33	0.046	1.321
d21-SB-WTS-0.45-1	57170	6.768	1165.02	0.121	1.685
d21-SB-WTS-0.45-2	43200	6.648	845.42	0.12	1.735
d30-SB-WTS-0.45-1	21970	4.415	717.12	0.09	1.185

Sample ID	Fe	Se	I	Re	U
	µg L^{-1}	µg L^{-1}	µg L^{-1}	ng L^{-1}	µg L^{-1}
d30-SB-WTS-0.45-2	88830	6.463	808.22	0.112	1.721
d7-SB-WSS-0.1-1	1081	2.119	133.63	0.056	0.287
d7-SB-WSS-0.1-2	998.6	1.981	119.73	0.06	0.28
d7-SB-WSS-0.22-1	1728	2.138	116.23	0.063	0.435
d7-SB-WSS-0.22-2	1371	2.132	119.03	0.067	0.393
d7-SB-WSS-0.45-1	2467	2.213	145.13	0.074	0.666
d7-SB-WSS-0.45-2	2382	2.462	145.53	0.057	0.671
d15-SB-WSS-0.45-1	3357	1.81	113.23	0.044	0.582
d15-SB-WSS-0.45-2	1794	1.833	108.43	0.045	0.45
d21-SB-WSS-0.45-1	1341	1.65	115.02	0.059	0.397
d21-SB-WSS-0.45-2	1599	1.711	133.92	0.071	0.515
d30-SB-WSS-0.45-1	2304	1.971	149.62	0.053	0.467
d30-SB-WSS-0.45-2	1213	1.762	113.42	0.063	0.399
d7-SB-WTS-0.1-1-new Rh	1382	1.273	21.00	0.107	0.156
d7-SB-WTS-0.1-1-new Rh	880.2	0.908	16.06	0.108	0.102